SÍLVIA DE NAZARÉ MONTEIRO YANAGI

ALBEDO DE UMA FLORESTA TROPICAL AMAZÔNICA: MEDIÇÕES DE CAMPO, SENSORIAMENTO REMOTO, MODELAGEM, E SUA INFLUÊNCIA NO CLIMA REGIONAL.

Tese apresentada à Universidade Federal de Viçosa, como parte das exigências do Programa de Pós-graduação em Meteorologia Agrícola, para obtenção do título de *Doctor Scientiae*.

VIÇOSA

MINAS GERAIS-BRASIL

2006

Ficha catalográfica preparada pela Seção de Catalogação e Classificação da Biblioteca Central da UFV

T
Y21a
2006

Yanagi, Sílvia de Nazaré Monteiro, 1973-
Albedo de uma floresta tropical Amazônica: medições de campo, sensoriamento remoto, modelagem e sua influência no clima regional / Sílvia de Nazaré Monteiro Yanagi. – Viçosa : UFV, 2006.
xxii, 128f. : il. ; 29cm.

Texto em inglês.
Orientador: Marcos Heil Costa.
Tese (doutorado) - Universidade Federal de Viçosa.
Referências bibliográficas: f. 116-128.

1. Climatologia agrícola. 2. Amazônia - Clima - Modelos matemáticos. 3. Desmatamento. 4. Sensoriamento remoto. 5. Microclimatologia florestal. I. Universidade Federal de Viçosa. II.Título.

CDD 22.ed. 630.2515

SÍLVIA DE NAZARÉ MONTEIRO YANAGI

ALBEDO DE UMA FLORESTA TROPICAL AMAZÔNICA: MEDIÇÕES DE CAMPO, SENSORIAMENTO REMOTO, MODELAGEM, E SUA INFLUÊNCIA NO CLIMA REGIONAL.

Tese apresentada à Universidade Federal de Viçosa, como parte das exigências do Programa de Pós-graduação em Meteorologia Agrícola, para obtenção do título de *Doctor Scientiae*.

APPROVADA: 31 de outubro de 2006

Dr. Yosio Edemir Shimabukuro
Co-Orientador

Prof. Gilberto C. Sediyama

Dra. Francisca Zenaide de Lima

Dr. Humberto Alves Barbosa

Prof. Marcos Heil Costa
(Orientador)

Este trabalho é dedicado à
meus pais José e Nazaré,
minha avó Francisca "*in memorian*",
meu marido Tadayuki
e minha sogra Conceição.

AGRADECIMENTOS

À Universidade Federal de Viçosa (UFV), especialmente ao Departamento de Engenharia Agrícola, pela oportunidade de realizar o curso.

À Coordenadoria de Aperfeiçoamento de Pessoal de Ensino Superior (CAPES) e ao Conselho Nacional de Desenvolvimento Científico e Tecnológico (CNPq), pela concessão de bolsa de estudo.

Aos meus pais José e Nazaré Albuquerque, pela educação nos princípios da verdade, pelos grandes incentivos, apoio e força para vencer as dificuldades encontradas durante a realização deste trabalho, por tudo.

Aos meus irmãos, tio e sobrinho: Patrícia, José Walter, Nivaldo e Matheus, especialmente, a minha avó Francisca Monteiro (*in memoriam*) pela grande força na continuidade da minha vida profissional.

Ao meu marido Tadayuki Yanagi Junior pelo grande apoio nas horas difíceis em que me encontrei, pelos incentivos profissionais, pelo amor, força e amizade e, acima de tudo pela compreensão dos dias em que a distancia física nos separou.

A minha sogra e amiga Conceição Yanagi, pelo carinho e cuidado durante as minhas horas de estudo, e principalmente pela compreensão de minha ausência.

Ao professor Dr. Marcos Heil Costa, pela orientação, amizade e apoio profissional.

Aos meus conselheiros professores Drs. Humberto Ribeiro da Rocha e Yosio Edemir Shimabukuro, pelas valiosas sugestões e contribuições.

Aos membros do comitê de minha banca de defesa de tese Dr. Yosio Edemir Shimabukuro, Prof. Gilberto Chohaku Sediyama, Dr. Humberto Alves Barbosa, e Dra. Francisca Zenaide de Lima, pelas valiosas contribuições para finalização deste trabalho.

Ao professor Dr. Antônio Carlos Lôla da Costa da Universidade Federal do Pará, pelos conselhos e incentivos profissionais.

A todos os Professores do curso de Meteorologia Agrícola, em especial aos professores Drs. Gilberto C. Sediyama, José Maria Nogueira da Costa, Sérgio Zolnier, Luiz Cláudio Costa e Everardo C. Mantovani, pelos valiosos conhecimentos, atenção e amizade.

Aos funcionários do Departamento de Engenharia Agrícola, pelo suporte, em especial Marcos, Galinari, "Tia Maria" e as secretárias Kelly e Edna, pelo carinho e dedicação.

Aos estudantes do Grupo de Pesquisa em Climatologia, Christiane, Varejão, Hewlley, Santiago, Lucía, Francisca, Clever, Tomé, Edson, Márcia, Fabrício e Luciana pelo coleguismo e pelas contribuições no desenvolvimento deste trabalho.

A todos os meus colegas da Área de Meteorologia, em especial Welliam, Raniére, José Luiz, Danilo Filho, Vanda, Hernani, Michelly, Rochane, Rosandro, José de Paula, Evandro, Raquel, Evaldo pela força e amizade.

Aos meus queridos amigos Marcos Paulo ("iuiu"), Kelly, Welliam e Adriane, Christiane e Raniére, Hewlley e Luizinho, Olívio e Tânia, Sandra e André, Bergson, Leila e Mauro, Gleidson e outros a minha eterna amizade.

Agradeço especialmente a minha amiga Christiane Leite, pelo apoio nas horas incertas e pela sua grande ajuda durante as minhas simulações, quando estava fora da cidade de Viçosa participando de uma Conferência Internacional.

A todos os demais professores, colegas e funcionários que, direta ou indiretamente, participaram da realização deste trabalho, o meu sincero agradecimento.

BIOGRAFIA

SÍLVIA DE NAZARÉ MONTEIRO YANAGI, filha de José C. Moraes de Albuquerque e Maria de Nazaré Monteiro de Albuquerque, nasceu em 06 de maio de 1973, na cidade de Belém-Pará-Brazil.

Em dezembro de 1997 concluiu o curso de graduação em Meteorologia pela Universidade Federal do Pará (UFPA).

Em julho de 1998 concluiu o curso de especialização em Sensoriamento Remoto pela Universidade Federal do Pará (UFPA).

Em junho de 2001 concluiu o curso de pós-graduação, em nível de mestrado, em Meteorologia Agrícola na Universidade Federal de Viçosa (UFV).

Em setembro de 2002 iniciou o curso de pós-graduação, em nível de doutorado, em Meteorologia Agrícola na Universidade Federal de Viçosa (UFV).

SUMÁRIO

LISTA DE FIGURAS..... ix
LISTA DE QUADROS..... xv
LISTA DE ABREVIATURAS..... xvii
RESUMO..... xix
ABSTRACT..... xxi
GENERAL INTRODUCTION..... 01
CHAPTER 1 – SOURCES OF VARIATION OF ALBEDO OF AMAZONIAN VEGETATION……. 04
1.1. INTRODUCTION…….. 04
1.2. Sites, instrumentation and data……... 07
1.3. Sources of variation of hourly albedo…… 11
1.4. Sources of variation of monthly albedo…….. 17
1.5 CONCLUSIONS……..... 21
1.6 NOMENCLATURE……... 23
CHAPTER 2 – MODELING RADIATIVE TRANSFER IN TROPICAL RAINFOREST CANOPIES: SENSITIVITY OF SIMULATED ALBEDO TO CANOPY ARCHITECTURAL AND OPTICAL PARAMETERS……... 24
2.1. INTRODUCTION……..... 24
2.2. MATERIALS AND METHODS……... 26

2.2.1. IBIS description…….. 26
2.2.2. Experimental site and data…….. 32
2.2.3. Sensitivity to canopy architectural and optical parameters……. 33
2.3. RESULTS AND DISCUSSION……. 34
2.4. SUMMARY AND CONCLUSIONS……. 38
2.5 NOMENCLATURE……. 39
CHAPTER 3 – SIMULATIONS OF TROPICAL RAINFOREST ALBEDO: IS CANOPY WETNESS IMPORTANT? …… 41
3.1. INTRODUCTION…….. 41
3.2. MATERIALS AND METHODS……... 43
3.2.1. Sites, instrumentation and data……... 43
3.2.2. Description of the IBIS model…… 45
3.2.3. Experiment design…….. 46
3.3. RESULTS AND DISCUSSION……. 49
3.4. SUMMARY AND CONCLUSIONS……. 57
3.5 NOMENCLATURE……... 58
CHAPTER 4 – COMPARISON OF SEASONAL AND SPATIAL VARIATIONS OF ALBEDO ESTIMATED BY A CLIMATE MODEL AND ALBEDO DERIVED FROM REMOTE SENSORS DATA FOR THE AMAZON TROPICAL RAINFOREST ……. 59
4.1. INTRODUCTION…….. 59
4.2. ALBEDO DATA…… 61
4.2.1. Land surface albedo simulations……. 61
4.2.2. Remote sensing albedos…….. 61
4.2.3. Field measurements albedo……. 66
4.3. RESULTS AND DISCUSSION……. 66
4.4. SUMMARY AND CONCLUSIONS……. 73
CHAPTER 5 – RADIATIVE PROCESSES OF THE PRECIPITATION CHANGE AFTER TROPICAL DEFORESTATION…….. 75
5.1. INTRODUCTION…….. 75
5.2. MATERIALS AND METHODS……..... 77
5.2.1. Description of the CCM3-IBIS model…… 77
5.2.2. Experiment design…….. 78

5.3 RESULTS……... 79
5.3.1. Precipitation dependence on surface radiation balance…….. 79
5.3.2. Clouds dependence on surface radiation balance and feedbacks on the incoming solar radiance……... 84
5.3.3. Convection dependence on surface radiation balance…… 89
5.4. DISCUSSION……. 99
5.5. CONCLUSIONS…… 106
5.6 NOMENCLATURE……... 107
CHAPTER 6 – GENERAL CONCLUSIONS…….. 108
6.1. OVERVIEW…….. 108
6.2. CONCLUSIONS……... 111
6.3. RECOMMENDATIONS FOR FUTURE RESEARCH…… 114
GENERAL REFERENCES..... 116

LISTA DE FIGURAS

Figure 1.1 – Orientation map……. 08

Figure 1.2 – Forest albedo as a function of solar zenith angle for four transmissivity ranges (0-25%, 25-50%, 50-75% e 75-100%) and for (a) dry canopy and (b) wet canopy…… 15

Figure 1.3 – Pasture albedo as a function of solar zenith angle for four transmissivity ranges (0-25%, 25-50%, 50-75% e 75-100%) and for (a) dry canopy and (b) wet canopy…… 16

Figure 1.4 – Average monthly variability of (a) surface albedo and (b) atmospheric transmissivity for tropical rainforest and pasture……. 19

Figure 1.5 – (a) Average monthly albedo for the forest and pasture ecosystems as a function of atmospheric transmissivity (τ), and regression equations; (b) residuals between the observed albedo and the albedo estimated by the regression equations in Figure 5a……... 20

Figure 1.6 – Average monthly variability of surface albedo for tropical rainforest and pasture and its difference, considering the canopy wetness, where $\alpha_{F\ wet}$ and $\alpha_{F\ dry}$ are the wet and dry forest albedos, respectively; $\alpha_{P\ wet}$ and $\alpha_{P\ dry}$ are the wet and dry pasture albedos; and $\alpha'_{P\text{-}F\ wet}$ and $\alpha'_{P\text{-}F\ dry}$ are the difference between surface albedos for

wet and dry pasture and forest canopy, respectively……. 21
Figure 2.1 – Schematic representation of the radiative transfer model in IBIS……. 28
Figure 2.2 – Simulated albedo as a function of $\rho_{NIR,up}$ and χ_{up}, for the Cuieiras Biological Reserve (K34)…….. 35
Figure 2.3 – Temporal variation of the albedo observed in the Cuieiras Biological Reserve (K34) and the albedo simulated by the IBIS model, according to the upper canopy element orientation parameter…….. 36
Figure 2.4 – Root Mean Square Error (RMSE) between the observed and simulated albedo as a function of the canopy optical parameters $\rho_{NIR,up}$ and χ_{up}, for the Cuieiras Biological Reserve (K34)……... 37
Figure 3.1 – Orientation map……. 44
Figure 3.2 – Diurnal variation of the simulated and observed surface albedo in the Cuieiras Reserve for selected days…… 52
Figure 3.3 – Diurnal variation of the simulated and observed surface albedo in the Ducke Reserve for selected days……... 53
Figure 3.4 – Diurnal variation of the simulated and observed surface albedo in the Jaru Reserve for selected days……... 54
Figure 3.5 – Monthly profile of the observed and simulated surface albedo, monthly precipitation and frequency of rainfall events, at three Amazon rainforest sites: (a) Cuieiras Reserve, from June 1999 to September 2000, (b) Ducke Reserve, from January to December of 1995 and (c) Jaru Reserve, from January to December of 1993…….. 56
Figure 4.1 – Spatial variability of the surface albedo simulated by the (a) CCM3 model and albedo from six remote sensing products for Amazon basin: (b) CG99, (c) ERBE, (d) SRB/ISLSCP2, (e) UMD, (f) MODIS Black-sky and (g) MODIS white-sky and it respective anomalies: (h) CCM3-CG99, (i) CCM3-ERBE, (j) CCM3-SRB/ISLSCP2, (k) CCM3-UMD, (l) CCM3-MODIS Black-sky and (m) CCM3-MODIS white-sky ……. 68
Figure 4.2 – Seasonal variability of the surface albedo simulated by the CCM3 model and albedo from six remote sensing products for Amazon basin, and measured at three study sites……. 70
Figure 4.3 – Seasonal variability of the surface albedo simulated by the CCM3

model and albedo from six remote sensing products for the pixels comprising the three study sites, and albedo measured at the (a) Manaus (Cuieiras and Ducke) and (b) Jaru sites……... 72

Figure 5.1 – Annual mean precipitation profile as a function of albedo changes for different climatic experiments……... 76

Figure 5.2 – Annual mean precipitation anomaly as a function of albedo anomaly (a) and net radiation anomaly (b), for different levels of pastureland and soybean cropland expansions……. 80

Figure 5.3 – Semester mean precipitation anomaly as a function of albedo anomaly for the dry semester (a), rainy semester (b), and both (c), and as a function of net radiation anomaly for the dry semester (d), rainy semester and both (f). White squares represent pastureland and gray squares represent soybean cropland…….. 82

Figure 5.4 – Trimester mean precipitation anomaly as a function of albedo anomaly for the January to March trimester (a), April to June trimester (b), July to September trimester (c), October to December trimester (d) and all trimesters (e), and as a function of net radiation anomaly for the January to March trimester (f), April to June trimester (g), July to September trimester (h), October to December trimester (i) and all trimesters (j). White squares represent pastureland and gray squares represent soybean cropland…… 83

Figure 5.5 – Annual mean total cloud anomaly as a function of albedo anomaly (a) and net radiation anomaly (b), for different levels of pastureland and soybean cropland expansions……. 84

Figure 5.6 – Semester mean total cloud anomaly as a function of albedo anomaly for the dry semester (a), rainy semester (b), and both (c), and as a function of net radiation anomaly for the dry semester (d), rainy semester and both (f). White squares represent pastureland and gray squares represent soybean cropland…….. 86

Figure 5.7 – Trimester mean total cloud anomaly as a function of albedo anomaly for the January to March trimester (a), April to June trimester (b), July to September trimester (c), October to December trimester (d) and all trimesters (e), and as a function of net radiation anomaly for

the January to March trimester (f), April to June trimester (g), July to Se89ptember trimester (h), October to December trimester (i) and all trimesters (j). White squares represent pastureland and gray squares represent soybean cropland……... 87

Figure 5.8 – Annual mean incoming solar radiation anomaly as a function of total cloud anomaly (a) for different levels of pastureland and soybean cropland expansions. Semester mean incoming solar radiation anomaly as a function of total cloud anomaly for the dry semester (a), rainy semester (b), and both (c). Trimester mean incoming solar radiation anomaly as a function of total cloud anomaly for the January to March trimester (a), April to June trimester (b), July to September trimester (c), October to December trimester (d) and all trimesters (e). White squares represent pastureland and gray squares represent soybean cropland……... 88

Figure 5.9 – Annual mean vertical velocity anomaly as a function of albedo anomaly (a) and net radiation anomaly (b), for different levels of pastureland and soybean cropland expansions…….. 90

Figure 5.10 – Semester mean vertical velocity anomaly as a function of albedo anomaly for the dry semester (a), rainy semester (b), and both (c), and as a function of net radiation anomaly for the dry semester (d), rainy semester and both (f). White squares represent pastureland and gray squares represent soybean cropland……..... 91

Figure 5.11 – Trimester mean vertical velocity anomaly as a function of albedo anomaly for the January to March trimester (a), April to June trimester (b), July to September trimester (c), October to December trimester (d) and all trimesters (e), and as a function of net radiation anomaly for the January to March trimester (f), April to June trimester (g), July to September trimester (h), October to December trimester (i) and all trimesters (j). White squares represent pastureland and gray squares represent soybean cropland…… 92

Figure 5.12 – Annual mean precipitation anomaly as a function of vertical velocity anomaly (a) for different levels of pastureland and soybean cropland expansions. Semester mean precipitation anomaly as a function of

vertical velocity anomaly for the dry semester (a), rainy semester (b), and both (c). Trimester mean precipitation anomaly as a function of vertical velocity anomaly for the January to March trimester (a), April to June trimester (b), July to September trimester (c), October to December trimester (d) and all trimesters (e). White squares represent pastureland and gray squares represent soybean cropland… 93

Figure 5.13 – Seasonal profile of vertical velocity at 500 hPa, in forest (F^{ab}) for the February to April trimester (rainy season) (a) for the June to August trimester (dry season) (b) for the vertical velocity anomalies in different levels of pastureland expansions: $P^{ab}_{25\%} - F^{ab}$ (c), $P^{ab}_{50\%} - F^{ab}$ (d) and $P^{ab}_{75\%} - F^{ab}$ (e) for the February to April trimester, respectively, and for the anomalies $P^{ab}_{25\%} - F^{ab}$ (c), $P^{ab}_{50\%} - F^{ab}$ (g) and $P^{ab}_{75\%} - F^{ab}$ (h) for the June to August trimester, respectively. Positive values are represented by solid line and indicate decrease in vertical motion and negative values are represented by dashed line and indicate increase in vertical motion……... 95

Figure 5.14 – Seasonal profile of vertical velocity at 500 hPa, in forest (F^{ab}) for the February to April trimester (rainy season) (a) for the June to August trimester (dry season) (b) for the vertical velocity anomalies in different levels of soybean cropland expansions: $S_{25\%} - F^{ab}$ (c), $S_{50\%} - F^{ab}$ (d) and $S_{75\%} - F^{ab}$ (e) for the February to April trimester, respectively, and for the anomalies $S_{25\%} - F^{ab}$ (c), $S_{50\%} - F^{ab}$ (g) and $S_{75\%} - F^{ab}$ (h) for the June to August trimester, respectively. Positive values are represented by solid line and indicate decrease in vertical motion and negative values are represented by dashed line and indicate increase in vertical motion……... 96

Figure 5.15 – Seasonal profile of precipitation at 500 hPa, in forest (F^{ab}) for the February to April trimester (rainy season) (a) for the June to August trimester (dry season) (b) for the precipitation anomalies in different levels of pastureland expansions: $P^{ab}_{25\%} - F^{ab}$ (c), $P^{ab}_{50\%} - F^{ab}$ (d) and

$P^{ab}_{75\%}$ - F^{ab} (e) for the February to April trimester, respectively, and for the anomalies $P^{ab}_{25\%}$ - F^{ab} (c), $P^{ab}_{50\%}$ -F^{ab} (g) and $P^{ab}_{75\%}$ - F^{ab} (h) for the June to August trimester, respectively. Negative values are represented by dashed line and indicate decrease in pasture precipitation and positive values are represented by solid line and indicate increase in pasture precipitation…….. 97

Figure 5.16 – Seasonal profile of precipitation at 500 hPa, in forest (F^{ab}) for the February to April trimester (rainy season) (a) for the June to August trimester (dry season) (b) for the precipitation anomalies in different levels of soybean cropland expansions: $S_{25\%}$ - F^{ab} (c), $S_{50\%}$ - F^{ab} (d) and $S_{75\%}$ - F^{ab} (e) for the February to April trimester, respectively, and for the anomalies $S_{25\%}$ - F^{ab} (c), $S_{50\%}$ - F^{ab} (g) and $S_{75\%}$ - F^{ab} (h) for the June to August trimester, respectively. Negative values are represented by dashed line and indicate decrease in pasture precipitation and positive values are represented by solid line and indicate increase in pasture precipitation…….. 98

Figure 5.17 – Diagram of anomalies of radiative processes…… 101

Figure 5.18 – Schematic representation of the precipitation changes with and without cloud feedbacks……... 102

LISTA DE TABELAS

Table 1.1 – Main characteristics of the remote sensing albedo products ……... 08

Table 1.2 – Covariance analysis for hourly albedo data……. 13

Table 1.3 – Albedo differences for forest and pasture for dry- and wet canopy condition……..… 14

Table 1.4 – Covariance analysis for monthly albedo data…….. 18

Table 2.1 – Parameters used by the model…….. 34

Table 3.1 – Optical parameters used by the DF99 calibration, and by the new calibrations using the dry-canopy (DC_i) and wet-canopy (WC_i) versions of the model, where i is equal to M for the Manaus-nearby sites (Ducke and Cuieiras Reserves) or J for the Jaru Reserve. $\chi_{leaf\text{-}up}$ is the upper canopy leaf orientation, $\chi_{leaf\text{-}lo}$ is the lower canopy leaf orientation, α_{VIS-lo}^{Leaf} is the lower canopy visible leaf reflectance, α_{VIS-up}^{Leaf} is the upper canopy visible leaf reflectance, α_{NIR-lo}^{Leaf} is the lower canopy NIR leaf reflectance, α_{NIR-up}^{Leaf} is the upper canopy NIR leaf reflectance, f_{wetmax} is maximum fraction of water cover on two-sided leaf, τ_{drip} is the decay time for intercepted liquid drip off and ν is the ratio of the scattering coefficients of the canopy surfaces wet by water and dry canopy surfaces, applied individually to leaves and stems. All values

are dimensionless, except for τ_{drip}, which is in seconds…….. 48

Table 3.2 – Statistics of observed and simulated surface albedo for the entire time series and for precipitation hours at three Amazon rainforest sites (Cuieiras, Ducke and Jaru reserves), for the simulations based on the DF99 calibration, for the new calibration using the dry-canopy (DC) and wet-canopy (WC) versions of the model. $\overline{X}$ is the average albedo, ε is the mean relative error and RMSE is the root mean square error…. 50

Table 4.1 – Main characteristics of the remote sensing albedo products…… 62

Table 5.1 – Annual mean of the variables and of some parameters: Rn (net radiation), Sin (downward solar radiation), Sout (upward solar radiation), Lin-Lout (longwave balance), P (precipitation), E (evaporation), LE (latent heat flux) and H (sensible heat flux) for the simulations F^{ab} (Forest, control run), $P^{ab}_{25\%}$ (75% forest and 25% pasture), $P^{ab}_{50\%}$ (50% forest and 50% pasture), $P^{ab}_{75\%}$ (25% forest and 75% pasture), S25% (75% forest and 25% soybean), S50% (50% forest and 50% soybean), S75% (25% forest and 75% soybean), P_{total} (extrapolating to 100% of forest replaced by pasture), S_{total} (extrapolating to 100% of forest replaced by soybean), P_{total} - F^{ab} (difference between pasture and forest) and S_{total} - F^{ab} (difference between soybean and forest)…… 100

Table 5.2 – Coefficient of determination (R^2) of the linear regression analysis between Rn' (surface net radiation), ω' (wind vertical velocity), C' (total cloud) and P' (precipitation) versus the variables in the left bar… 99

LISTA DE ABREVIATURAS

ABRACOS	–	Anglo Brazilian Amazonian Climate Observation Study
ADM	–	Angular distribution model
ANCOVA	–	Analysis of covariance
AVHRR	–	Advanced Very High Resolution Radiometer
BB	–	Blackbody
BRDF	–	Bidirectional Reflectance Distribution Function
CCM3	–	NCAR Community Climate Model
CG99	–	Csiszar and Gutman (1999)
COLA	–	Center for Ocean-Land Atmosphere Studies
ERBE	–	Earth Radiation Budget Experiment
GCM	–	General Circulation Model
GEMEX	–	Global Energy and Water Cycle Experiment
GOES	–	Geostationary Operational Environmental Satellite
IBIS	–	Integrated Biosphere Simulator
INPA	–	Instituto Nacional de Pesquisas da Amazônia
ISLSCP2	–	The International Satellite Land Surface Climatology Project
LBA	–	Large-Scale Biosphere-Atmosphere Experiment in Amazonia
METEOSAT	–	Meteorological satellite
MODIS	–	Moderate Resolution Imaging Spectroradiometer

NASA	–	National Aeronautics and Space Administration
NIR	–	Near-infrared band
NOAA	–	National Oceanic and Atmospheric Administration
RMSE	–	Root mean square error
SD	–	Solar Diffuser
SDSM	–	Solar Diffuser Stability Monitor
SRB	–	Surface Radiative Budget
SRCA	–	Spectroradiometric Calibration Assembly
TOA	–	Top-of-the atmosphere
UMD	–	University of Maryland
VIS	–	Visible band

RESUMO

YANAGI, Sílvia de Nazaré Monteiro, D.Sc., Universidade Federal de Viçosa, outubro de 2006. **Albedo de uma floresta tropical Amazônica: medições de campo, sensoriamento remoto, modelagem, e sua influência no clima regional**. Orientador: Marcos Heil Costa. Co-Orientadores: Humberto Ribeiro da Rocha e Yosio Edemir Shimabukuro.

O albedo é definido como a razão entre a radiação solar refletida e a radiação solar incidente em uma superfície. É o principal fator que afeta o balanço de radiação terrestre e tem sido freqüentemente considerado em estudos do clima global e regional. A Amazônia é uma das regiões do planeta onde a resposta da circulação atmosférica regional a mudanças do albedo superficial é mais intensa. Estudos de simulação utilizando diversos modelos mostram que a conversão da floresta tropical em pastagem causa uma redução na precipitação local, a qual é principalmente dependente da mudança no albedo da superfície. O presente trabalho tem como objetivos investigar as fontes de variação espacial e temporal do albedo de uma floresta tropical amazônica, usando medições de campo, modelagem e produtos de sensoriamento remoto; e investigar o papel da mudança do albedo da superfície, após o desmatamento Amazônico, no clima regional. Neste trabalho foram utilizados dados de albedo observados em quatro áreas florestais (Reservas Florestais de

Caxiuanã, Cuieiras, Ducke e Jaru) e duas pastagens (Dimona e Nossa Senhora Aparecida) pertencentes aos Projetos LBA (Experimento de Grande Escala da Biosfera-Atmosfera na Amazônia) e ABRACOS (Estudos de Observação do Clima na Amazônia Anglo-Brasileira). Também foram utilizados seis produtos de sensoriamento remoto: CG99, ERBE, SRB/ISLSCP2, UMD e MODIS céu-claro e MODIS céu-escuro. Para a simulação do albedo em floresta tropical amazônica foi utilizado o modelo IBIS (Integrated Biosphere Simulator) em duas versões: pontual e acoplado ao modelo climático CCM3. Os resultados deste trabalho mostram que: as principais fontes de variação do albedo em escala horária e mensal são a cobertura vegetal e transmissividade atmosférica, e que o molhamento do dossel é uma importante fonte de variação em escala horária e deve ser incluída em modelos; que o albedo simulado mostrou uma forte sensibilidade aos parâmetros do dossel superior de orientação da folha e de refletância no infravermelho e nenhuma sensibilidade aos parâmetros do dossel inferior, consistente com a estrutura do dossel; que a incorporação do molhamento do dossel nos cálculos de transferência radiativa melhora os resultados de simulação em escala horária, diminuindo o albedo durante as horas de precipitação, mas não em escala sazonal, excluindo o molhamento do dossel como uma fonte principal da variabilidade sazonal do albedo em florestas tropicais; que os diferentes produtos de sensoriamento remoto apresentaram uma variação considerável em relação aos albedos observados em campo, incluindo grandes diferenças sazonais; que anomalias de precipitação podem ser explicadas por uma relação linear entre os processos radiativos, onde mudanças no albedo da superfície e na radiação líquida explicam aproximadamente 96% e 99% da variação anual da precipitação e que a substituição da floresta por soja afeta mais o clima regional que a conversão em pastagem, provavelmente devido ao alto valor do albedo das áreas de soja.

ABSTRACT

YANAGI, Sílvia de Nazaré Monteiro, D.Sc., Universidade Federal de Viçosa, October of 2006. **Albedo of an Amazon tropical rainforest: field measurements, remote sensing, modeling, and its influence on the regional climate**. Adviser: Marcos Heil Costa. Co-Advisers: Humberto Ribeiro da Rocha and Yosio Edemir Shimabukuro.

Albedo is defined as a ratio between reflected solar radiation and incoming solar radiation over a surface. It is a main factor that affects the terrestrial radiation balance and has been frequently considered in the global and regional climate studies. Amazon is one of planet's regions where the response of regional atmospheric circulation is more intense. Simulation studies using several models show that a conversion of tropical rainforest in pasturelands causes reduction in the local precipitation, which is mainly dependent of surface albedo changes. The objective of present work is to investigate the sources of spatial and temporal variation of an Amazon tropical rainforest surface albedo, using field measurements, modeling and satellite products; and to investigate the role of surface albedo changes, after Amazon tropical deforestation, in the regional climate. In this work it was used observed data from four forests (Caxiuanã, Cuieiras, Ducke and Jaru Reserves) and

two pastures (Dimona and Nossa Senhora Aparecida) belonging to LBA (Large-Scale Biosphere-Atmosphere Experiment in Amazonia) and ABRACOS (Anglo Brazilian Amazonian Climate Observation Study) projects. It was also used six different satellite systems: CG99, ERBE, SRB/ISLSCP2, UMD and MODIS white-sky and MODIS black-sky. For the simulation of Amazon tropical rainforest surface albedo the point IBIS (Integrated Biosphere Simulator) model and it coupled to CCM3 climate model was used. The results of this work show that: the main sources of variation of albedo in hourly and monthly scale are the vegetation cover and atmospheric transmissivity, and that the canopy wetness is an important source of variation in hourly scale and should be included in the models; that the simulated albedo show strong sensitivity to superior canopy parameters of leaf orientation and infrared reflectance and no sensitivity was found for the lower canopy parameters, consistent with the canopy structure; that an incorporation of canopy wetness in the radiative transfer calculation improve the results in a hourly scale, reducing the albedo during the hours with precipitation, but not in a seasonal scale, excluding the canopy wetness as a main source of the seasonal variability in tropical rainforest; that the different satellite systems present a considerable variation related to the field measured albedos, including great seasonal differences; that the precipitation anomalies can be explained by a linear relationship between radiative processes, where the changes in surface albedo and net radiation explain approximately 96% and 99% of the annual variation of precipitation and that the replacement of forest by soybean cropland affects more the regional climate than the conversion in pasture, probably due to the high value of soybean cropland albedo.

GENERAL INTRODUCTION

Surface albedo, or shortwave reflection coefficient, is defined as the ratio between the total reflected solar radiation and the total incoming solar radiation at a surface. Land cover albedo is an important land physical parameter and has frequently been considered in studies of global and regional climate. It controls not only the amount of net radiation available for heating the ground and lower atmosphere and for evaporating water (Rowe, 1991), but also affects the regional climate.

In tropical areas climatic simulations have demonstrated that the climate is sensitive to changes in the surface albedo caused by natural and anthropogenic activities, such as desertification and tropical deforestation (Charney et al., 1977; Dorman and Sellers, 1989; Lean and Warrilow, 1989; Xue et al., 1990; Hahmann and Dickinson, 1997; Costa and Foley, 2000; Wei et al., 2001; Zao et al., 2001; Berbet and Costa, 2003). Amazonia is one of the planet regions where the response of regional atmospheric circulation to changes in surface albedo is more intense, because the rainfall in that region is mainly of convective origin. Simulation studies for Amazonian basin using several models show that the conversion of tropical rainforest to pasturelands causes a reduction in local precipitation, which is mainly dependent of changes in surface albedo. Dirmeyer and

Shukla (1994) showed, through simulations with the COLA (Center for Ocean-Land Atmosphere Studies) model, that the annual mean precipitation decreases when the increase of albedo is greater than 0.03, being linearly proportional to the increase of albedo. Until recently, researches have only concerned in the effects of conversion of tropical rainforest to pasture on the annual mean climate, without considering the eventual cropland expansions and the seasonal effects that these changes may cause on the regional climate (Nobre et al., 1991, Hahmann and Dickinson, 1997; Zeng et al., 1996). However, Berbet and Costa (2003) studied the effect of the seasonal variation of surface albedo associated to the substitution of tropical rain forest by pasture in the pattern of seasonal precipitation, observing that the seasonal variations of the reflected radiation difference are related to the fluctuations in seasonal scale of precipitation anomalies caused by deforestation.

A more realistic representation of albedo in climate models will significantly improve the accuracy of climate simulation and prediction, because land surface albedo is an important source of uncertainty related to General Circulation models (GCMs).

Some authors discussed the albedo of a tropical rainforest in the context of climatic models (Culf et al., 1995; Wright et al., 1996; Berbet and Costa, 2003), but only the latter discussed the spatial and seasonal variation of albedo of a tropical rainforest and a pasture. Berbet and Costa (2003) verified that 28% of variance in the change of precipitation after tropical rainforest deforestation is explained by the variance of the reflected radiation. The authors also observed that the surface model used (IBIS) does not correctly represent the surface albedo during part of rainy season, although it does during the dry season. Culf et al. (1995) suggested that the seasonal variation of a tropical rainforest albedo is mainly correlated to the soil moisture, but it is believed that in fact they were referring to leaf wetness, once the presence of liquid water on the leaves considerably alters its optical properties (the liquid water presents strong absorption in the near infrared and high reflectance in the blue and green bands) (Asner, 1998; Asner et al., 2000).

Validation of simulated albedo can be done in two ways, against field measurements or against satellite products. Field data have the advantage of using high frequency data to validate simulated albedo measurements. Surface albedo has been measured in Amazonian ecosystems at four forests and two pastures belonging to LBA (Large-Scale Biosphere-Atmosphere Experiment in Amazonia) and ABRACOS (Anglo Brazilian Amazonian Climate Observation Study) projects. On the other hand, satellite data allow evaluation the spatial and temporal variability of surface characteristics. However, the satellite systems present several problems, such as a single measurement per day, loss of data in cloud presence, aerosols contamination and incomplete cover of the solar spectrum. Land surface albedo has been retrieved from several space-based satellites such as AVHRR (Advanced Very High Resolution Radiometer), ERBE (Earth Radiation Budget Experiment), and MODIS (Moderate Resolution Imaging Spectroradiometer).

The objective of this dissertation is to investigate the sources of spatial and temporal variation of an Amazon tropical rainforest surface albedo, using field measurements, modeling and satellite products; and to investigate the role of surface albedo changes, after Amazon tropical deforestation, in the regional climate. It is organized as follows: Chapter 1 presents the investigation of the sources of variation of surface albedo of Amazonian vegetation. In Chapter 2, the radiative transfer in tropical rainforest canopies is modeled; analyzing the sensitivity of simulated albedo to canopy architectural and optical parameters. In Chapter 3, the importance of canopy on the tropical rainforest albedo is evaluated using modeling. In chapter 4, a comparison of seasonal and spatial variations of albedos by a climate model and six different satellite products for the Amazon tropical rainforest is presented; and in chapter 5 the radiative processes of the precipitation change after tropical deforestation is analyzed.

CHAPTER 1

SOURCES OF VARIATION OF ALBEDO OF AMAZONIAN VEGETATION

1.1. INTRODUCTION

Surface albedo is defined as the ratio of reflected to incident radiation in the total solar in a certain wavelength interval. It is the main factor that affects the land radiation balance and has frequently been considered in studies of global and regional climate. The main identified sources of variation of land surface albedo are land cover, solar elevation angle, canopy wetness, and cloud cover (Pinker et al., 1980; Bastable et al., 1993; Culf et al., 1995).

The albedo of different tropical land covers has been studied for over 30 years. In one of the first studies comparing forest and non-forest albedos in Nigeria, Oguntoyinbo (1970) found an average albedo of 12% for forest and varying from 15 to 21% for non-forested areas. Pinker et al. (1980) compared dry evergreen forest and pasture albedos in Thailand, finding, during the winter monsoon season, an average midday albedo of 10.6%

for the forest and 13.4% for the clearing, whereas, during the summer monsoon the authors found albedos of 12.0% and 14.6% for the forest and clearing, respectively. In this study, difference between forest and clearing for winter and summer were 2.8% and 2.6%, respectively. The first measurements in Amazonia, during ARME – Amazon Region Micrometeorological Experiment, indicated an average albedo of 12.3±0.2% for a tropical forest near Manaus, Brazil (Shuttleworth et al., 1984). Later, during ABRACOS – Anglo Brazilian Amazonian Climate Observation Study, Bastable et al. (1993) verified an average albedo of 13.1% for the same site and 16.3% for a nearby pasture, a difference of 3.2%. Synthesizing the measurements at three Amazonian forest sites and three pasture sites, Culf et al. (1996) found average albedos of 13.4% and 18%, respectively (4.6% difference).

Solar elevation, as well as variations in cloud cover, can also cause changes in surface albedo. Pinker et al. (1980) studied the diurnal variation of the average albedo over a tropical dry evergreen forest and a nearby clearing, finding a strong dependence of the albedo on the zenith angle, although this dependence is weaker during cloudy days. Shuttleworth et al. (1984) found a quadratic dependency of the tropical rainforest surface albedo to the solar elevation angle. Usually, surface albedo present higher values in the morning and afternoon, and the minimum value occur at solar noon. However, Song (1998) verified that wind may change the leaves inclination causing asymmetric variation between morning and afternoon albedos. Giambelluca et al. (1999) observed a strong diurnal and annual cycle of albedo associated to changes in the solar elevation angle. At high solar angles, sunlight can penetrate to greater depths within a forest canopy. This effect is overall considered to increase with vegetation height, giving forests the lowest albedo and grassland the highest of any type of vegetation. Diffuse sunlight more effectively

penetrates the incident radiation has a high proportion of diffuse sunlight (i.e., cloudy skies), the solar angle effect on albedo is less significant (Nouvellon et al., 2000).

Most of results reviewed before are derived from observations collected over a period of a few days, and explain the sources of variation of surface albedo at the hourly time scale. At the monthly time scale, however, the sources of variation may be different. Culf et al. (1995), for example, presented results of the seasonal variability of Amazonian vegetation albedo that are inconsistent with the hourly-scale results. They suggest that the seasonal variability of the monthly mean albedo of the Amazon forest is correlated with soil moisture and is not correlated with solar elevation angle. In addition, they did not find a clearly defined seasonal trend of albedo for the pasture sites. It is unclear, however, whether this seasonal variability is driven by soil moisture-correlated variables, as discussed by Berbet and Costa (2003), or whether it is driven by other sources of variation correlated with rainfall, like canopy wetness and fraction of direct and diffuse radiation.

Moreover, Berbet and Costa (2003) also verified that a complex, state-of-the-art, land surface model is unable to reproduce correctly the seasonal variability of surface albedo of forests and pastures, although it reproduces well the annual mean and some aspects of the seasonal variability. This indicates that there is still much to be learned – and incorporated into models – about the sources of variation of albedo at both the hourly and monthly time scale. This is also important because, in tropical areas, such as Amazon forest, climatic simulations have demonstrated that the climate is sensitive to the surface albedo variations due to the deforestation, desertification and anthropogenic activity. As a small change in the surface albedo results in significant climate change, it is extremely important that climate models represent the land surface with a very high accuracy, especially in a seasonal basis.

Here, I investigate the sources of variation of surface albedo of tropical vegetation, at both the hourly and monthly time scales, with the goal to provide the necessary knowledge that will be, later, incorporated in land surface models. In particular, I investigate the role of canopy wetness and cloud cover, in addition to the traditional sources of variation (land cover and zenith angle), as well as the interactions among the sources of variation.

This chapter is divided in three parts. The next section describes the sites, instrumentation and data used in the analysis. Then, using statistical techniques, I analyze and discuss the sources of variation of surface albedo of Amazonian vegetation, at both the hourly and monthly time scales. I conclude discussing the relevance of the processes involved to the remote sensing and modeling of surface albedo of Amazonian vegetation.

1.2. Sites, instrumentation and data

Field data used in this paper were measured in six experimental sites in the Amazon during the ABRACOS (Anglo Brazilian Amazonian Climate Observation Study) and LBA projects (Large-Scale Biosphere-Atmosphere Experiment in Amazonia). Four of the sites have primary tropical rainforest as main land cover (Reserva Caxiuanã, Reserva Cuieiras (K34), Reserva Ducke, and Reserva Jaru), whereas the other two are pasture sites (Fazenda Dimona and Fazenda Nossa Senhora Aparecida). Table 1.1 and Figure 1.1 show other (additional) information about the sites and their location.

Table 1.1. Description of the experimental sites.

Experimental site	Coordinates	Location	Measurement period (dd/mm/yy)
Reserva Caxiuanã	01º 42'S, 51º 31' W	Melgaço, PA	16/04/99 to 10/02/00
Reserva K34	02º 35'S, 60º 06' W	Manaus, AM	15/05/99 to 28/11/01
Reserva Ducke	02º 57'S, 59º 57' W	Manaus, AM	31/12/90 to 31/12/96
Reserva Jaru	10º 05'S, 61º 55"W	Ji-Paraná, RO	24/10/91 to 31/12/96
Fazenda Dimona	02º 19' S, 60º 19'W	Manaus, AM	01/10/90 to 31/12/96
Fazenda Nossa Senhora Aparecida	10º 45'S, 62º 22'W	Ji-Paraná, RO	04/10/91 to 031/12/96

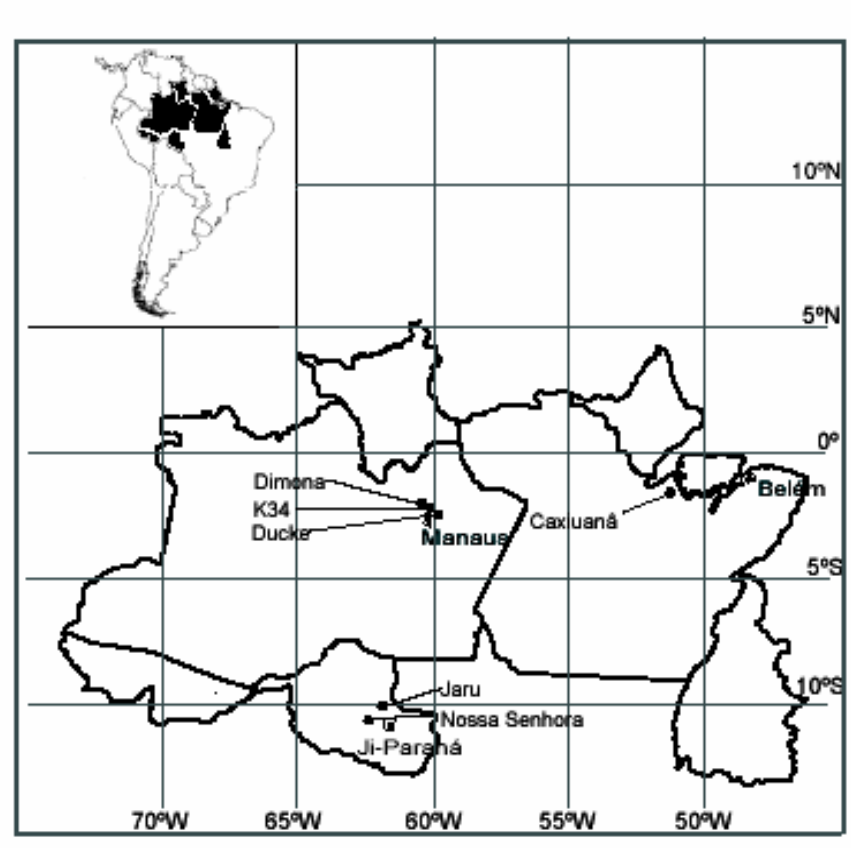

Figure 1.1. Orientation map.

Reserva Caxiuanã is an experimental area of primary tropical evergreen forest with approximately 330 km^2 and is located in Pará State about 400 km west of Belém. Reservas Ducke and Cuieiras (K34) are protected primary forest areas, located 25 km and 60 km north of Manaus, Amazonas State, respectively. These sites are surrounded by undisturbed forest for at least 5 km. Reserva Jaru is a forest reserve owned by the Brazilian Environmental Protection Agency (IBAMA) and is located about 80 km north of Ji-Paraná, in Rondônia State. Fazenda Dimona is cattle ranch with 10 km^2 of clearing, located about 100 km north of Manaus. There is little forest remaining in this area. Fazenda Nossa Senhora Aparecida is a ranch located 50 km northeast of Ji-Paraná and situated in a strip of cleared land about 4 km wide and several tens of kilometers long. The ranch is in the center of an area of about 50 km in radius, which has undergone large-scale clearing.

At Reserva Caxiuanã, incident and reflected solar radiation were measured with a net radiometer (Kipp & Zonen, Delft, Netherlands) mounted at 45.5 m on the top of a tower. Radiation data were measured every 10 s and averaged half-hourly and stored on a datalogger (21X, Campbell Scientific). At Reserva Cuieiras a piranometer (Kipp & Zonen CM 21, Delft, Netherlands), connected to a datalogger (CR10, Campbell Scientific, Shepshed, UK) was used to measure incident and reflected solar radiation each 30 seconds, storing the averages every 30 minutes. For the remaining sites, the incident and reflected solar radiation were measured using two solarimeters (Kipp and Zonen, Delft, the Netherlands). These instruments are part of an automatic weather station (Didcot Instruments, Abingdon, UK) connected to a datalogger (CR10, Campbell Scientific, Shepshed, UK) and hourly-averaged data were recorded.

Data of incident and reflected global solar radiation used in this study are available on-line through www.cptec.inpe.br/abracos/available.html and www.lba.cptec.inpe.be/beija-flor.

Data for the Reservas Jaru and Ducke, and Fazendas Dimona and Nossa Senhora Aparecida are the same used by Culf et al. (1995, 1996). Hourly averages of surface albedos are determined through the ratio between reflected and incident solar radiation. Hourly albedo data of six experimental sites (Table 1.1) are used to study both the hourly and monthly sources of variation of tropical rainforest and pasture albedo.

For the hourly-scale, I consider four possible sources of variation: type of land cover (forest, pasture), solar zenith angle (0º to 90º), canopy wetness (dry, wet) and atmospheric transmissivity (0 to 1), as an indicator of the partition of the incident radiation between direct and diffuse components. To avoid the undesirable effects of aerosols, common on this region, I considered only data collected a few days after a large storm (rainfall greater than 10 mm), when I assumed that the atmosphere would be clean of aerosols. With the help of hourly precipitation data, I also filtered the data to represent wet- and dry-canopy conditions: data collected between the beginning of a rain event and up to three hours after the end of a rain are used to represent wet-canopy conditions; data collected at least 24 hours after the end of a rain event are used to represent dry-canopy conditions; while data collected between three and 24 hours after a rain event are discarded from the analysis, as I am unsure about the canopy wetness status. Hourly atmospheric transmissivity is calculated as the ratio between incident solar radiation at the surface and calculated incident solar radiation at an horizontal surface at the top of the atmosphere.

For the monthly time scale, I considered three possible sources of variation: type of land cover, monthly-averaged solar zenith angle, and monthly-averaged atmospheric transmissivity. Data were not filtered for the presence of aerosols or for the canopy wetness conditions, except where noted.

Other possible sources of variation of land surface albedo are not included in this analysis, such as variation among sites that have the same land cover, and interannual variability due to changes in soil moisture or leaf area index.

1.3. Sources of variation of hourly albedo

An analysis of covariance (ANCOVA) evaluates and analyzes the effects of land cover, canopy wetness, atmospheric transmissivity and zenith angle on the surface albedo in Amazon region. I chose the analysis of covariance due to the combined effects of qualitative (vegetation and canopy wetness) and quantitative (transmissivity and solar zenith angle) factors on the albedo. Data were analyzed using the PROC GLM (SAS, 2001) with the model including a factorial combination of two levels of land cover, L, (forest and pasture), two levels of canopy wetness, ω, (dry and wet) and the fixed effects of two regression factors (atmospheric transmissivity, τ, and zenith angle, Z) on the analysis, as follows:

$$\alpha_{ijkl} = \mu + L_i + \omega_j + L\cdot\omega_{ij} + a\cdot\tau_{ijk} + b\cdot Z_{ijk} + \tau\cdot Z_{ijk} + \tau\cdot L_{ijk} + \tau\cdot\omega_{ijk} + Z\cdot L_{ijk} + Z\cdot\omega_{ijk} + \tau\cdot L\cdot\omega_{ijk} + Z\cdot L\cdot\omega_{ijk} + \tau\cdot Z\cdot L_{ijk} + \tau\cdot Z\cdot\omega_{ijk} + \tau\cdot Z\cdot L\cdot\omega_{ij} + \varepsilon_{ijkl} \quad (1)$$

where α_{ijkl} is the estimated albedo; μ is the overall mean; L_i is the effect of the *i*th level of factor L; ω_j is the effect of the *j*th level of factor ω; a is the true common slope of the covariate τ_{ijk}; τ_{ijk} is the overall average of the covariate τ for the observations in the study; b is the true common slope of the covariate Z_{ijk}; Z_{ijk} is the overall average of the covariate Z for the observations in the study; the products of the sources of variation represent the effect of the interaction between them (e.g. $L\cdot\omega_{ij}$, etc.); ε_{ijkl} is the random effect due to sampling, normally and independently distributed with mean zero and variance σ^2 $\left[\varepsilon_{ijkl}\ \mathrm{NID}\left(0,\sigma^2\right)\right]$.

In Table 1.2, I present results of the ANCOVA based on the type I error (Cochran and Cox, 1992). I chose the type I error because it quantifies the contribution of each factor and its interactions for the model, adjusted to the previous factors. At the hourly-scale, land cover (forest or pasture) explains 43.99% of the variance of the albedo. The addition of canopy wetness (ω) to the model increases the explanation of the variance by 3.42%. Further inclusion of the factors τ and Z, adjusted to the previous factors; improve the variance explained by the model by 6.77% and 0.06%, respectively. Overall, the model explains 57.08% of the variance of the albedo. The sources of variation L, ω, τ and Z, and the interactions τ·Z and τ·ω explain 56.25% of the total variance of the model, while the rest of the interactions explain only 0.83% (Table 1.2). Below, I discuss the effect of these main sources of variation and interactions.

As expected, tropical rainforest albedo is significantly different from pasture albedo, $P<10^{-10}$ (Table 1.2), with average values of 12.1% and 16.7%, respectively. These results are in agreement with previous publications by Oguntoyinbo (1970), Shuttleworth et al. (1984), Bastable et al. (1993) and Culf et al. (1996).

Table 1.2. Covariance analysis for hourly albedo data.

Source of variation	Degrees of Freedom	Mean Square	F Value	Probability F*	Variance explained (%)
Model	15	0.2573	490.47	$< 10^{-10}$	–
Land cover (L)	1	2.9744	5670.77	$< 10^{-10}$	43.99
Canopy wetness (ω)	1	0.2313	441.07	$< 10^{-10}$	3.42
L·ω	1	0.0004	0.72	0.3962	0.01
Atmospheric transmissivity (τ)	1	0.4577	872.59	$< 10^{-10}$	6.77
Zenith angle (Z)	1	0.0043	8.25	0.0041	0.06
τ·Z	1	0.0279	53.26	$< 10^{-10}$	0.41
τ·L	1	0.0002	0.43	0.5120	0.003
τ·ω	1	0.1084	206.66	$< 10^{-10}$	1.60
Z·L	1	0.0064	12.11	0.0005	0.09
Z·ω	1	0.0198	37.68	$< 10^{-10}$	0.29
τ·L·ω	1	0.0014	2.71	0.0998	0.02
Z·L·ω	1	0.0006	1.06	0.3033	0.01
τ·Z·L	1	0.0208	39.60	$< 10^{-10}$	0.31
τ·Z·ω	1	0.0051	9.66	0.0019	0.07
τ·Z·L·ω	1	0.0003	0.53	0.4666	0.004
Error	5533	0.0005	–	–	–
Total variance explained					57.08%
CV = 17.23					

* Indicates significance at the specified level of probability.

Albedos determined for wet and dry canopies are significantly different ($P<10^{-10}$) independent of vegetation type. The average difference between albedos for dry and wet canopy is 0.4% (Table 1.3), while there is no significant interaction (P~0.4) between the factors land cover and canopy wetness. Overall, reflectance of a wet canopy is smaller than

the reflectance of a dry canopy for both ecosystems, forest and pasture, because water has a very high absortance, especially in the near infrared band. The same difference between pasture albedo and forest albedo (0.046) is found when only dry canopy or only wet canopy albedos are analyzed, which confirms the non-significant interaction between land cover (L) and canopy wetness (ω).

Table 1.3. Albedo differences for forest and pasture for dry- and wet canopy condition.

Vegetation	All	Dry	Wet	Difference (Dry – Wet)
Forest	0.121	0.123	0.119	0.004
Pasture	0.167	0.169	0.165	0.004
Difference (Pasture – Forest)	0.046	0.046	0.046	-

Surface albedo is also influenced by zenith angle and by the interaction between τ and Z as verified in previous studies (Pinker et al., 1980; Shuttleworth et al., 1984; McCaughey, 1987; Giambelluca et al., 1999). Surface albedo only depends on zenith angle when direct solar radiation is predominant, which explains why the effect of the zenith angle ($P = 0.0041$) is less significant than the effect of the interaction between τ and Z ($P<10^{-10}$, Table 1.2).

Figure 1.2 and Figure 1.3 show the albedo of a tropical rainforest and pasture, respectively, for four transmissivity ranges (0-25%, 25-50%, 50-75% e 75-100%) as a function of solar zenith angle for dry- (Figure 1.2a and 1.3a) and wet-canopy (Figure 1.2b and 1.3b) conditions. The 0-25% transmissivity interval characterizes overcast sky condition with diffuse solar radiation predominance, whereas the 75-100% transmissivity interval indicates clear sky condition with predominance of direct solar radiation. Overall,

forest and pasture dry albedos under clear sky tend to increase with increasing solar zenith angle as observed by other authors (Pinker et al., 1980; McCaughey, 1987), while albedo is independent of solar zenith angle under overcast conditions, as also observed by Eck and Deering (1992) and Bégué et al. (1996).

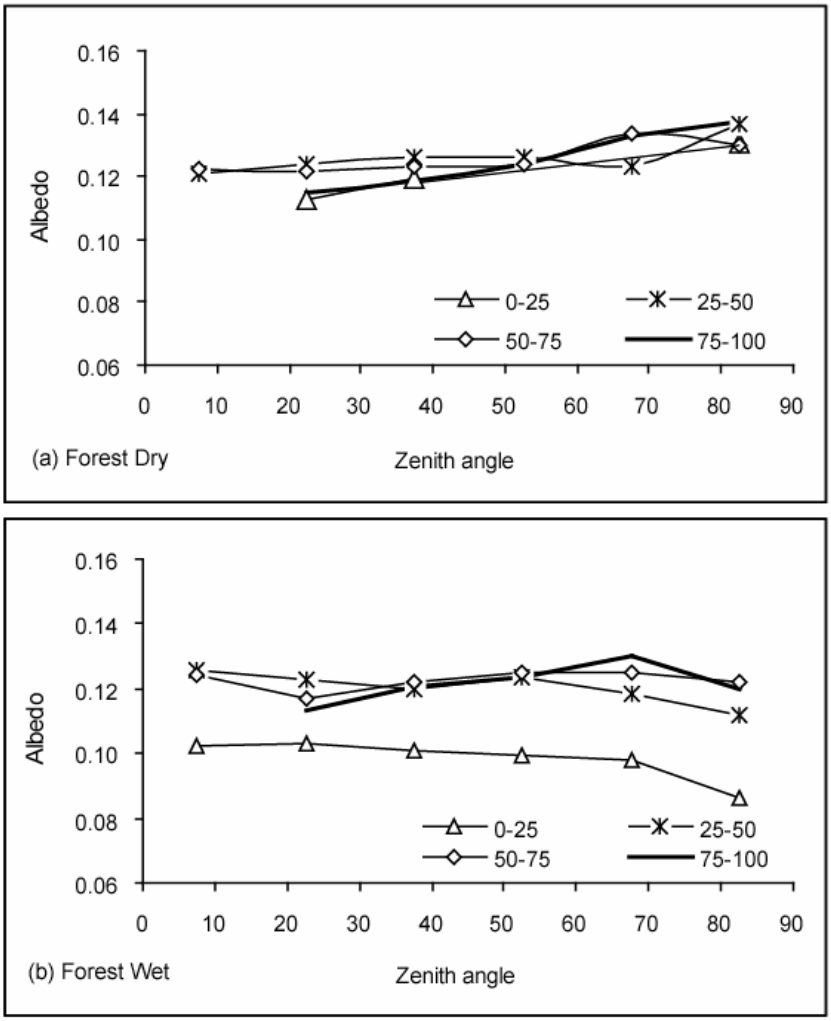

Figure 1.2. Forest albedo as a function of solar zenith angle for four transmissivity ranges (0-25%, 25-50%, 50-75% e 75-100%) for (a) dry forest canopy and (b) wet forest canopy.

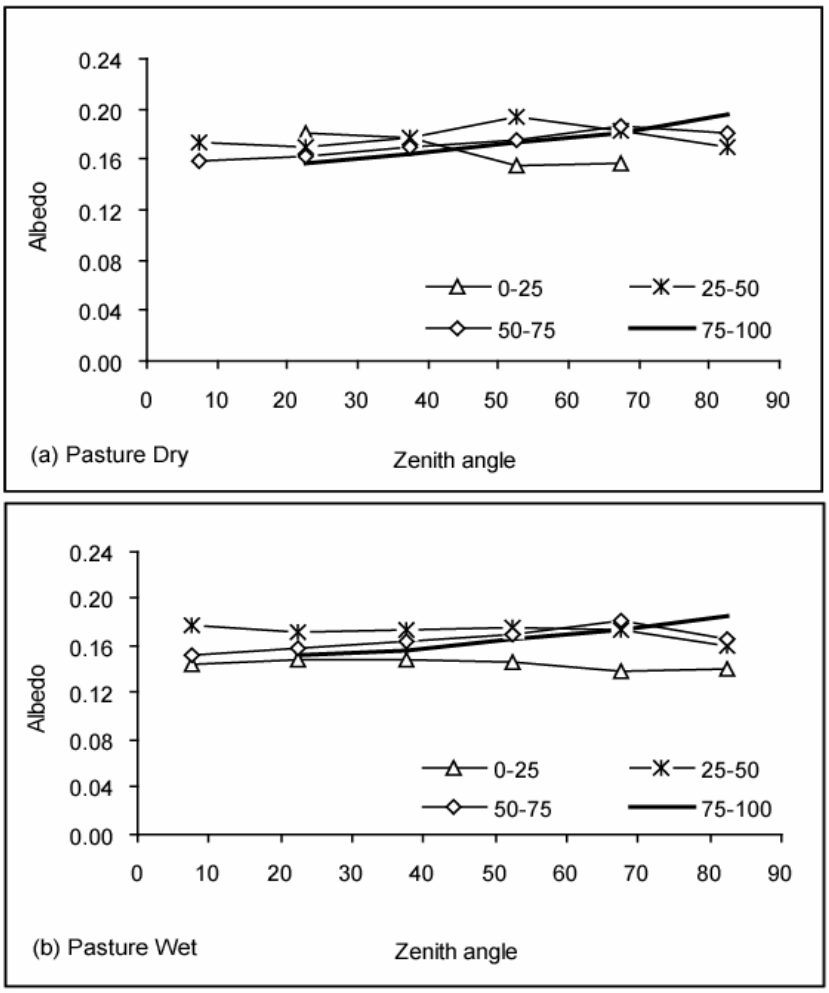

Figure 1.3. Pasture albedo as a function of solar zenith angle for four transmissivity ranges (0-25%, 25-50%, 50-75% e 75-100%) for (a) dry pasture canopy and (b) wet pasture canopy.

Figures 1.2 and 1.3 also confirm that atmospheric transmissivity affects surface albedo independently of land cover type ($P<10^{-10}$, Table 1.2). For example, lower values of albedo for wet-canopy are observed for 0-25% transmissivity interval (Figure 1.2b and 1.3b). Albedo tends to be approximately constant when diffuse irradiance predominates, because the diffuse light beams penetrate more deeply into the vegetation canopy and is more effectively absorbed (Nouvellon et al., 2000).

1.4. Sources of variation of monthly albedo

I also used an analysis of covariance (ANCOVA), through PROC GLM (SAS, 2001), to analyze the monthly albedo data via a factorial design. The factors land cover (L), atmospheric transmissivity (τ), zenith angle (Z) and the interactions τ·Z, τ·L, Z·L and τ·Z·L are considered, but the canopy wetness is not included. The statistical model tested by the ANCOVA is

$$\alpha_{ijkl} = \mu + L_i + a \cdot \tau_{ijk} + b \cdot Z_{ijk} + Z \cdot L_{ijk} + \tau \cdot Z_{ijk} + \tau \cdot L_{ijk} + \tau \cdot Z \cdot L_{ijk} + \varepsilon_{ijkl} \qquad (2)$$

Analogously to the previous section, I also used the type I error to compose the mean square for the monthly albedo analysis (Table 1.4). At the monthly-scale, land cover (L) explains 69.74% of the variance of the albedo. Addition of the effect of the atmospheric transmissivity (τ) to the model increases the explanation of the variance by 3.20%, while inclusion of the zenith angle (Z) adds an explanation of 0.91% of the variance. Overall, the model explains 76.91% of the variance of the model. The sources of variation L, τ and Z explain 73.85% of the total variance of the model, while the interactions among them explain only 3.06%.

Similar to the hourly scale analysis, forest and pasture albedos are significantly different ($P<10^{-10}$, Table 1.4), with average values of 12.3% and 17.4%, respectively. Atmospheric transmissivity and zenith angle also affect surface albedo ($P<10^{-10}$ and $P = 0.00094$, respectively) independently of land cover type.

Figure 1.4a shows the seasonal variability of albedo for forest and pasture ecosystems, showing also that the smaller difference of albedos occur between September and November, as also observed by Culf et al. (1995, 1996) and Wright et al. (1996). It is fundamental to understand what causes this variability. In particular, I discuss two possibilities raised in the introduction: seasonal changes in atmospheric transmissivity and seasonal changes in canopy wetness.

Table 1.4. Covariance analysis for monthly albedo data.

Source of variation	Degrees of Freedom	Mean Square	F Value	Probability F*	Variance explained (%)
Model	7	0.0291	135.65	$< 10^{-10}$	–
Land cover (L)	1	0.1846	860.90	$< 10^{-10}$	69.74
Atmospheric transmissivity (τ)	1	0.0085	39.57	$< 10^{-10}$	3.20
Zenith angle (Z)	1	0.0024	11.18	0.00094	0.91
Z·L	1	0.0017	7.99	0.00504	0.65
τ·Z	1	0.0019	8.79	0.00328	0.71
τ·L	1	0.0004	2.02	0.15633	0.16
τ·Z·L	1	0.0041	19.07	0.00002	1.54
Error	285	0.0002	–	–	–
Total variance explained					76.91%
CV = 10.26					

* Indicates significance at the specified level of probability.

The role of atmospheric transmissivity is demonstrated by Figures 1.4b and 1.5a. Figure 1.4b shows the variation of atmospheric transmissivity above each land cover type throughout the year. Atmospheric transmissivity over the forest sites is slightly greater (i.e. less cloudiness) than over the pasture sites during the dry season (June to November) and smaller during the wet season (December to May). The lower atmospheric transmissivity over the pasture sites during the dry season is probably related to the presence of aerosols (dust, soot, etc.) due to the constant fires this time of the year. During the dry season in Marabá County, Pará State, Fisch et al. (1994) found mean surface albedo of 0.19 and 0.08 during the days without and with burning occurrence, respectively. In addition, Cutrim et al. (1995) and Negri et al. (2004) verified an increase in shallow cumulus over deforested areas during the dry season in the Amazon. Figure 1.5a shows that α' ($\alpha' = \alpha_P - \alpha_F$,

difference between the pasture and forest albedos) decreases with the increase of τ. So, dry season (τ>0.45) albedos tend to be closer than rainy season (τ<0.45) albedos. The residuals between the observed albedo and the albedo estimated by the regression equations in Figure 1.5a are shown in Figure 1.5b. The seasonal variability of the residuals for the pasture is probably related to the seasonal variability of pasture leaf area index, as discussed by Wright et al. (1996). So far, I do not have an explanation for the seasonal variability of the residuals for the forest.

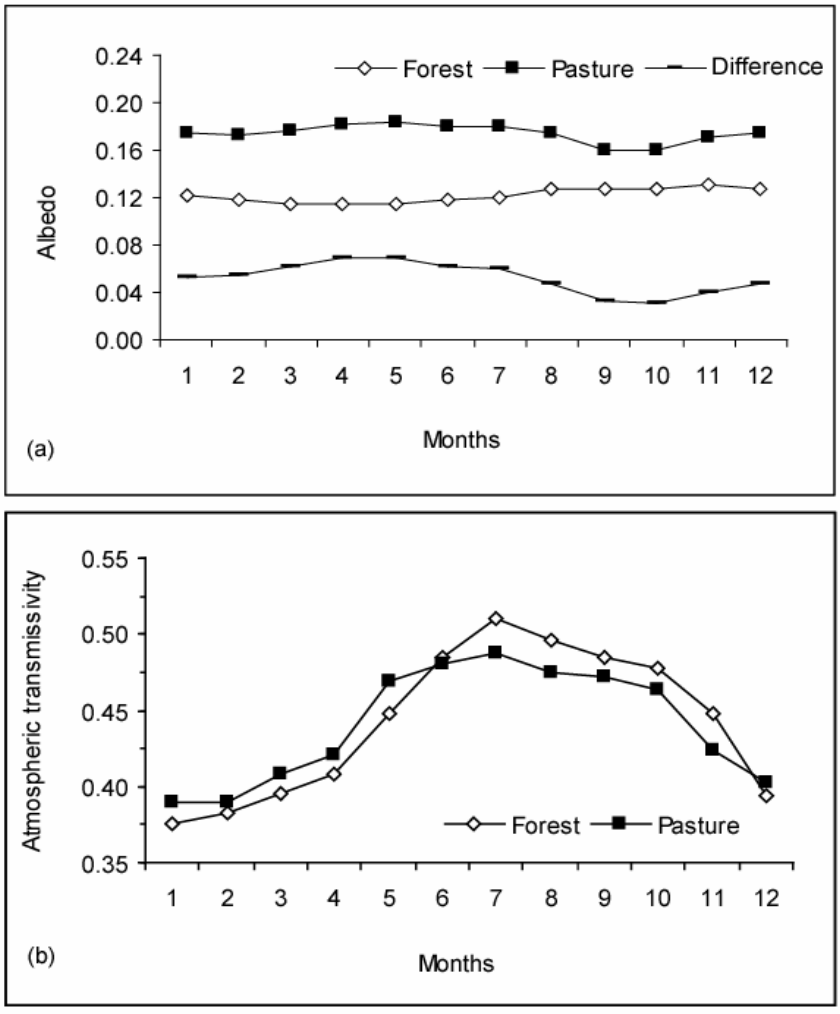

Figure 1.4. Average monthly variability of (a) surface albedo and (b) atmospheric transmissivity for tropical rainforest and pasture.

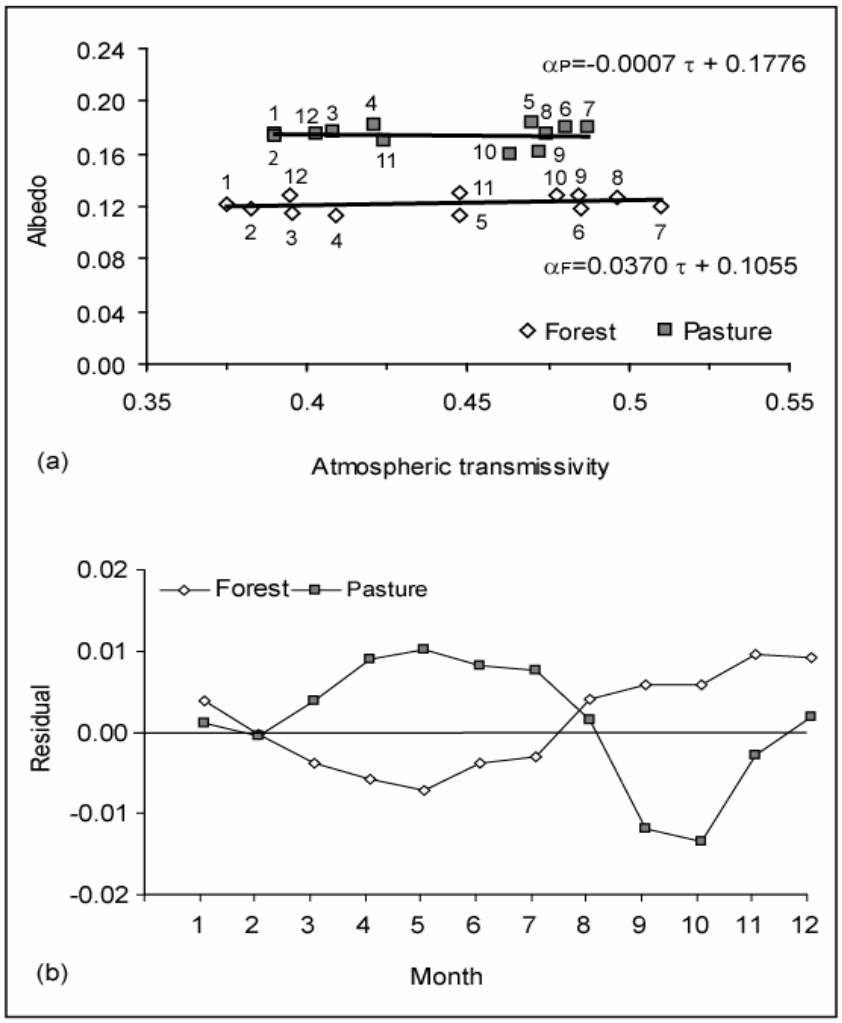

Figure 1.5. (a) Average monthly albedo for the forest and pasture ecosystems as a function of atmospheric transmissivity (τ), and regression equations; (b) residuals between the observed albedo and the albedo estimated by the regression equations in Figure 1.5a.

Using the dataset of the previous section, I also analyzed the effect of canopy wetness on the monthly variability of the surface albedo (Figure 1.6). At the monthly time scale, although the canopy wetness causes a small reduction in the albedo of both forest and pasture, its effect on the difference of albedo (α') is independent of the canopy wetness status.

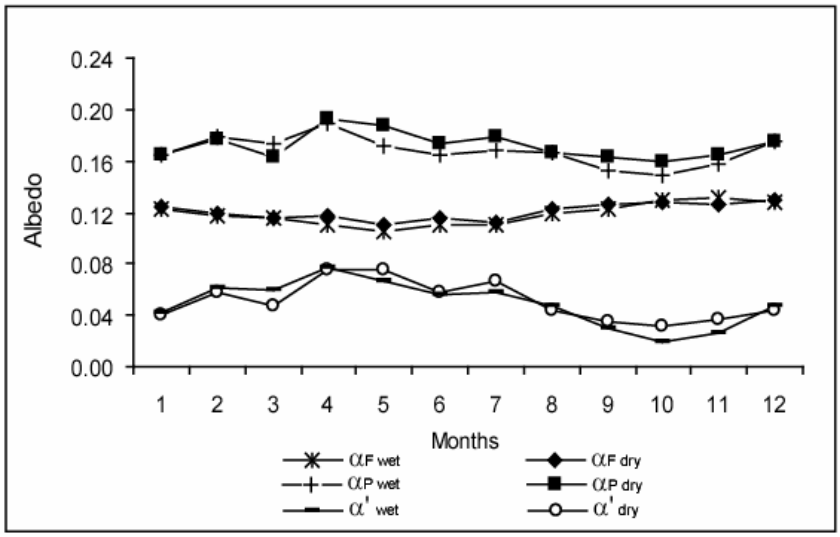

Figure 1.6. Average monthly variability of surface albedo for tropical rainforest and pasture and its difference, considering the canopy wetness, where $\alpha_{F\ wet}$ and $\alpha_{F\ dry}$ are the wet and dry forest albedos, respectively; $\alpha_{P\ wet}$ and $\alpha_{P\ dry}$ are the wet and dry pasture albedos; and $\alpha'_{P\text{-}F\ wet}$ and $\alpha'_{P\text{-}F\ dry}$ are the difference between surface albedos for wet and dry pasture and forest canopy, respectively.

1.5. CONCLUSIONS

Data from six experimental sites were used to analyze the sources of variation of hourly and monthly tropical vegetation albedo. At the hourly-scale data, land cover, atmospheric transmissivity and canopy wetness are the most important sources of variation; the effect of canopy wetness on the albedo is independent of land cover and reduces the albedo in 0.004 for both the forest and pasture ecosystems. The interactions $\tau \cdot Z$ and $\tau \cdot Z \cdot L$ are more important as drivers of variations on the albedo than the zenith angle by itself.

At the monthly time scale, land cover and atmospheric transmissivity are the major sources of variation. The results presented here let me conclude that, although the

difference in surface albedo (α') is partially dependent on τ (a consequence of the interaction $L \cdot \tau$), it is independent of the canopy wetness.

The classical paper of Sellers (1985), which provided the theoretical basis for most of the land surface models that simulate land surface albedo, assumes that the canopy reflectance is dependent mainly on land cover parameters, zenith angle, and fraction of direct and diffuse radiation. Such models usually incorporate only the reflectance effects of canopy snow, neglecting canopy wetness. The results of this study indicate that the canopy wetness is the third most important source of variation of hourly surface albedo, and can be included in such models. In addition, although the effect of direct and diffuse radiation is represented separately in such models, the partition between them from the incident solar radiation is usually poorly represented, and may be one of the main reasons why state-of-the-art land surface models are still unable to reproduce correctly most of existing variability in the data (Berbet and Costa, 2003).

It has been demonstrated that even a 0.03 change in tropical land surface albedo is sufficient to drive important large-scale changes in the regional atmospheric circulation (Dirmeyer and Shukla, 1994) and, hence, provoke climate change. This very small signal introduces a significant problem to our ability to correctly simulate the climate change after a tropical deforestation, because a hypothetical uncertainty of 0.01 in the simulated albedo would represent 1/3 of the climate change signal. In this context, considerable efforts are needed to improve the parameterizations for the tropical rainforest albedo and the land surface radiation balance, and reduce the uncertainty in the forcing of climate models. A rigorous incorporation of additional sources of variation in land surface models would improve the accuracy of land surface albedo simulations and would allow for more consistent experiments to evaluate the climate change after a tropical deforestation.

1.6. NOMENCLATURE

L	Land cover (pasture and forest)
Z	solar zenith angle (0º to 90º)
ω	canopy wetness (dry, wet)
τ	atmospheric transmissivity (0 to 1)
α_{ijkl}	estimated albedo
μ	overall mean
L_i	effect of the *i*th level of factor L
ω_j	effect of the *j*th level of factor ω
a	true common slope of the covariate τ_{ijk}
τ_{ijk}	overall average of the covariate τ
b	true common slope of the covariate Z_{ijk}
Z_{ijk}	overall average of the covariate Z
ε_{ijkl}	random effect due to sampling, normally and independently distributed with mean zero and variance σ^2
σ^2	Variance
α’	difference between the pasture and forest albedos
α_p	pasture albedos
α_f	forest albedos
$\alpha_{F\ wet}$	wet forest albedos
$\alpha_{F\ dry}$	dry forest albedos
$\alpha_{P\ wet}$	wet pasture albedos
$\alpha_{P\ dry}$	dry pasture albedos
$\alpha'_{P\text{-}F\ wet}$	difference between surface albedos for wet pasture and forest canopy
$\alpha'_{P\text{-}F\ dry}$	difference between surface albedos for dry pasture and forest canopy

CHAPTER 2

MODELING RADIATIVE TRANSFER IN TROPICAL RAINFOREST CANOPIES: SENSITIVITY OF SIMULATED ALBEDO TO CANOPY ARCHITECTURAL AND OPTICAL PARAMETERS

2.1. INTRODUCTION

Global climate models (GCMs) simulate the evolution of climate based on physical principles as well as initial and boundary conditions. To do so, these models must represent the exchanges of radiation, heat, momentum and mass between the atmosphere and the underlying surface, in particular terrestrial environments. Practical considerations, however, require that small scale processes be parameterized in terms of larger scale variables.

The parameterization of terrestrial surface processes in climate models is confined to modules implementing vertical exchange models. The radiation component of these modules relies on solutions derived from two-stream approaches (Dickinson, 1983;

Sellers, 1985), which follow developments made in the field of atmospheric physics (Coakley and Chylek, 1975; Meador and Weaver, 1980). Compared to the atmosphere analogue, the radiation transfer in plant canopies is rendered complex because the elementary scatterers – leaves and stems – are large compared to the typical wavelength of solar radiation, they can be oriented and clumped and they exhibit complex variable optical properties. The two-stream formulations thus have to be adapted to represent, at least in simplified forms, the effects of these complexities. Solutions have been developed for multiple possibilities of leaves and stems orientations, from strictly vertical (eroctophile) to strictly horizontal (planophile), including spherical and any other orientation in between, allowing a more realistic representation of vegetation canopies (Pinty et al., 2006).

Despite the several solutions available, model exercises usually do not take full advantage of the theoretical developments in canopy radiative transfer. For example, leaf orientation, an important architectural parameter, has usually been assumed to have a spherical orientation for broadleaf trees, and upright orientation for grasses, but the actual average orientation or its probability density function are generally not determined.

GCM-grade radiation transfer schemes are constrained by several limitations: they must be computer efficient and numerically stable, must use measurable or retrievable variables or parameters, must provide sufficiently accurate estimations of the radiant fluxes; and must respect energy conservation principles, which require that reflected, transmitted and absorbed fluxes sum up to the incident radiation, independent of the assumed canopy structure inside the domain. Radiation schemes should therefore be able to simulate accurately both the flux reflected from the top of the canopy, that is its albedo, and the flux transmitted to the ground underneath the vegetation layer. In this modeling context, the albedo is a prime candidate for validation exercises.

Here in this study I use the above canopy albedo as the main indicator of model performance, and evaluate the sensitivity of the simulated albedo of a tropical rainforest to a set of canopy architectural and optical parameters, with the goals of (a) understanding the response of the model to the several canopy optical parameters, and (b) obtaining the best set of parameters to be used in climate models, in particular leaf and stem orientation. I modeled the radiative transfer using the radiative transfer module of the Integrated Biosphere Simulator (IBIS), and I validate the simulations against albedo measurements taken at the tropical rainforest site at the Cuieiras Biological Reserve (K34).

2.2. MATERIALS AND METHODS

2.2.1. IBIS description

In this study a 0-D version of the Integrated Biosphere Simulator–IBIS (Foley et al., 1996) is used to model the radiative transfer in a tropical rainforest canopy. Although the model includes representations of several land surface processes (energy, water and momentum exchange between the soil-vegetation-atmosphere system, canopy physiology, vegetation phenology, vegetation dynamics, and terrestrial carbon balance), this study concerns only the solar radiation balance.

The albedo of a vegetation canopy layer (α) is defined as the ratio of the upwelling to the downwelling solar radiant fluxes at the top of the canopy, both depending on the location of the source, i.e., the cosine of the Sun zenith angle (μ) and type of illumination (normally both direct and diffuse). Representation of the albedo of such system requires the adoption of assumptions or simplifications. IBIS assumes that the surface albedo is approximated by a simple weighting of two distinct surface albedo types, each associated with an incident irradiance field: the directional hemispherical reflectance (α^d), associated with an incident irradiance field that is purely collimated (I_{in}^d) and the indirect

hemispherical reflectance (α^i), associated with an incident irradiance field that is purely isotropic (I_{in}^i). Both albedo types can be combined to approximate the surface albedo as follows (Kondratyev, 1972):

$$\alpha = \frac{I_{in}^d \alpha^d + I_{in}^i \alpha^i}{I_{in}^d + I_{in}^i} \tag{1}$$

In IBIS the exchange of solar radiation between the soil-vegetation-atmosphere system is calculated following the standard two-stream approximation, with separate calculations for direct and diffuse radiation in both visible and near-infrared bands. It solves the canonical radiative transfer problem of two-stream vegetation layer plus underlying surface of known albedo. Starting from the known soil albedo (α_g), the method is to first calculate the albedo of the combined lower canopy-ground system ($\alpha_{g\text{-}lo}$), then the albedo of the combined upper canopy-lower canopy-soil system ($\alpha_{lo\text{-}up}$).

As shown in Figure 2.1, effects of clumping and partial vegetation cover are also treated. When fluxes are passed between the upper and lower story, or between the lower story and the ground, the two-stream fluxes passing through the canopy are merged with the unmodified fluxes passing through the gaps (weighting with respect to the appropriate fractional cover f_{up} or f_{lo}). Assuming that there is no snow in the canopy, the albedo of each spectral band Λ is given by:

$$\alpha_{g-lo\Lambda}^d = \alpha_{g\Lambda}^d \cdot (1 - f_{lo}) + \alpha_{lo\Lambda}^d f_{lo} \tag{2}$$

$$\alpha_{g-lo\Lambda}^i = \alpha_{g\Lambda}^i \cdot (1 - f_{lo}) + \alpha_{lo\Lambda}^i f_{lo} \tag{3}$$

$$\alpha_{lo-up\Lambda}^d = \alpha_{g-lo\Lambda}^d \cdot (1 - f_{up}) + \alpha_{up\Lambda}^d f_{up} \tag{4}$$

$$\alpha_{lo-up\Lambda}^i = \alpha_{g-lo\Lambda}^i \cdot (1 - f_{up}) + \alpha_{up\Lambda}^i f_{up} \tag{5}$$

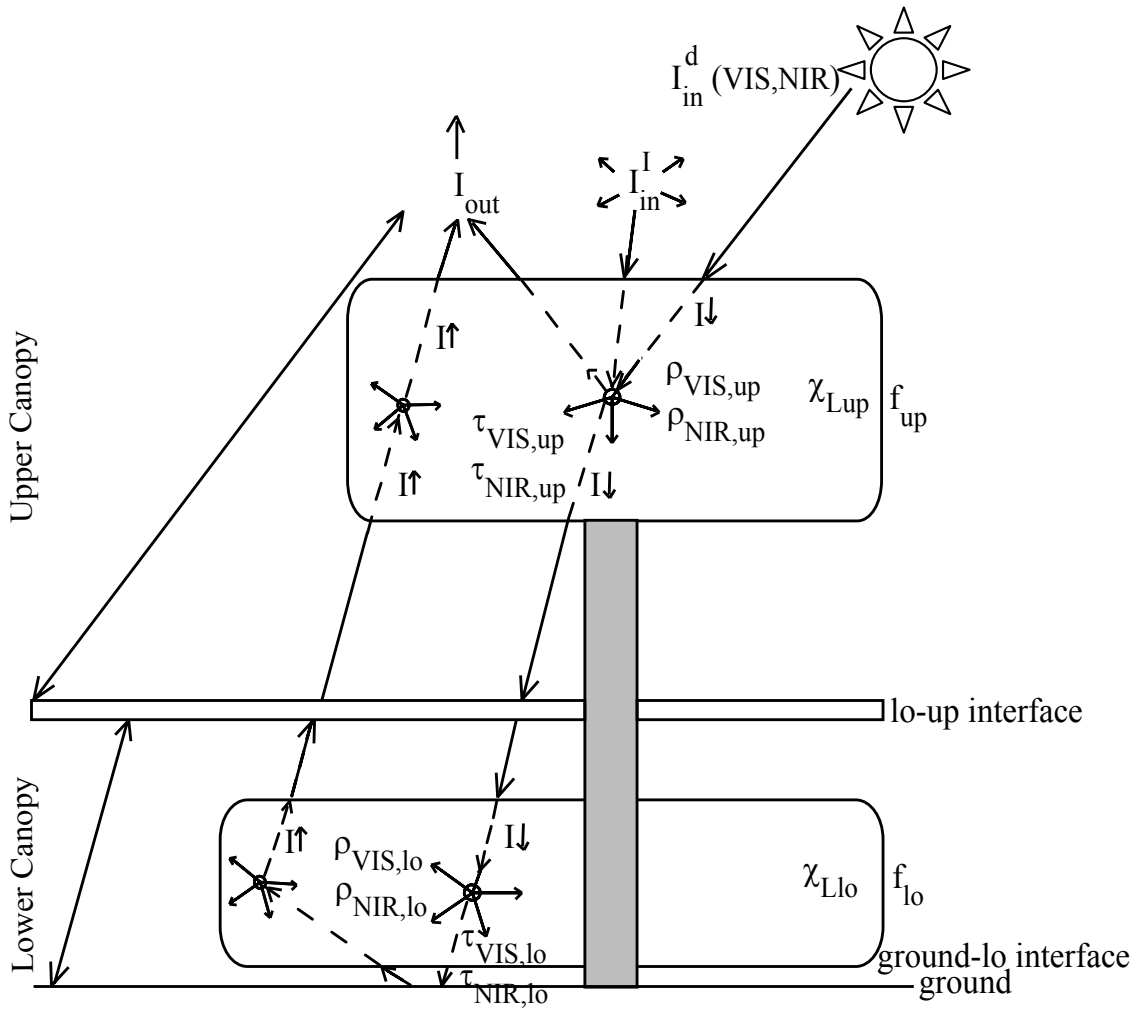

Figure 2.1. Schematic representation of the radiative transfer model in IBIS.

The two-stream algorithm uses several canopy architectural and optical parameters. The canopy architectural parameters include the upper and lower canopy element orientation (χ_{up} and χ_{lo}); fraction of ground area covered by lower and upper canopy (f_{lo} and f_{up}), leaf area index (L) and stem area index (S). The canopy optical parameters include the upper and lower canopy leaf reflectance by visible (VIS) and near-infrared (NIR) spectral band Λ (ρ_Λ: $\rho_{VIS,up}$,$\rho_{VIS,lo}$, $\rho_{NIR,up}$ and $\rho_{NIR,lo}$), and the upper and lower canopy leaf transmittance by visible (VIS) and near-infrared (NIR) spectral band Λ (τ_Λ: $\tau_{VIS,up}$,$\tau_{VIS,lo}$, $\tau_{NIR,up}$ and $\tau_{NIR,lo}$). The procedure below describes the major theoretical aspects of the two-stream approximation, and must be repeated for each vegetation layer.

Within each vegetation layer, the upward and downward diffuse fluxes obey

$$-\overline{\mu}\frac{dI^{\uparrow}}{d(L+S)}+\left[1-(1-\beta^{i})\omega\right]I^{\uparrow}-\omega\beta^{i}I_{\downarrow}=\omega\overline{\mu}K\beta^{d}e^{-K(L+S)} \tag{6}$$

$$-\overline{\mu}\frac{dI_{\downarrow}}{d(L+S)}+\left[1-(1-\beta^{i})\omega\right]I^{\downarrow}-\omega\beta^{i}I^{\uparrow}=\omega\overline{\mu}K(1-\beta^{d})\cdot e^{-K(L+S)} \tag{7}$$

where $I^{\uparrow}$ and $I^{\downarrow}$ are the upward and downward diffuse radiative fluxes per unit incident flux, $K = G(\mu)/\mu$ is the optical depth of direct beam per unit leaf and stem area, $G(\mu)$ is the relative projected area of leaf and stem elements in the direction $\cos^{-1}\mu$, $\overline{\mu}$ is the average inverse diffuse optical depth per unit leaf and stem area, ω is a scattering coefficient, β^{i} and β^{d} are upscatter parameters for indirect (diffuse) and direct beam radiation, respectively, L is the single-sided leaf area index, and S is the single-sided stem area index. Given the direct beam ground albedo $\alpha^{d}_{g,\Lambda}$ and diffuse ground albedo $\alpha^{i}_{g,\Lambda}$ for each spectral band Λ, these equations are solved to calculate the fluxes, per unit incident flux, absorbed by the vegetation, reflected by the vegetation, and transmitted through the vegetation for direct and diffuse radiation, for visible ($\Lambda < 0.7$ μm) and near-infrared ($\Lambda \geq 0.7$ μm) spectral bands.

Equations (6) and (7) are then solved analytically for a two-stream layer underlain by a non-specular surface of known albedo (i.e., the ground), with prescribed incoming downward direct and diffuse fluxes. This canonical solution (Equations 8 and 9) is applied first to the lower story underlain by soil to obtain the effective albedo of that system, then to the upper story underlain by the lower story and soil system, yielding the overall canopy albedo. The analytical solutions for the single scattering albedo of direct (α^{d}_{Λ}) and indirect (α^{i}_{Λ}) fluxes are

$$\alpha_{\Lambda}^{d} = \frac{h_1}{\sigma} + \frac{1}{d_1 e^{-h(L+S)}} \left\{ \left[\omega_{\Lambda} \bar{\mu} K \beta_{\Lambda}^{d} - \frac{h_1}{\sigma} \left(b + \bar{\mu} K \right) \right] \cdot \left[\left(b - \bar{\mu} h - \frac{\omega_{\Lambda} \beta_{\Lambda}^{i}}{\alpha_{g\Lambda}^{d}} \right) - b + \bar{\mu} h \right] \right\}$$
$$- \frac{1}{d_1} \left\{ \left[\omega_{\Lambda} \bar{\mu} K \beta_{\Lambda}^{d} - \frac{h_1}{\sigma} \left(b + \bar{\mu} K \right) \right] \cdot \left[\left(b + \bar{\mu} h - \frac{\omega_{\Lambda} \beta_{\Lambda}^{i}}{\alpha_{g\Lambda}^{d}} \right) \cdot e^{-h(L+S)} \right] - \frac{b + \bar{\mu} h}{e^{-h(L+S)}} \right\} \tag{8}$$

$$\alpha_{\Lambda}^{i} = \omega_{\Lambda} \beta_{\Lambda}^{i} \left\{ \left(b + \bar{\mu} h \right) - \left[\left(b - \bar{\mu} h \right) \cdot \left(\frac{b + \bar{\mu} h - \frac{\omega_{\Lambda} \beta_{\Lambda}^{i}}{\alpha_{g\Lambda}^{i}}}{b - \bar{\mu} h - \frac{\omega_{\Lambda} \beta_{\Lambda}^{i}}{\alpha_{g\Lambda}^{i}}} \right) \cdot \left[e^{-h(L+S)} \right]^2 \right] \right.$$
$$\left. - \left[\frac{\left(b + \bar{\mu} h \right)}{\left[e^{-h(L+S)} \right]^2} \cdot \left(\frac{b - \bar{\mu} h - \frac{\omega_{\Lambda} \beta_{\Lambda}^{i}}{\alpha_{g\Lambda}^{i}}}{b + \bar{\mu} h - \frac{\omega_{\Lambda} \beta_{\Lambda}^{i}}{\alpha_{g\Lambda}^{i}}} \right) - b + \bar{\mu} h \right] \right\}^{-1} \tag{9}$$

where:

$$b = 1 - \omega_{\Lambda} \left(1 - \beta_{\Lambda}^{i} \right),$$

$$\frac{h_1}{\sigma} = \frac{-\omega_{\Lambda} \bar{\mu} K \left[\beta_{\Lambda}^{d} \left(b - \bar{\mu} K \right) + \omega_{\Lambda} \beta_{\Lambda}^{i} \left(1 - \beta_{\Lambda}^{d} \right) \right]}{\left(\bar{\mu} K \right)^2 - \left[b^2 - \left(\omega_{\Lambda} \beta_{\Lambda}^{i} \right)^2 \right]},$$

$$h = \frac{\sqrt{b^2 - \left(\omega_{\Lambda} \beta_{\Lambda}^{i} \right)^2}}{\bar{\mu}} \text{ and}$$

$$d_1 = \left[\frac{\left(b + \bar{\mu} h \right)}{e^{-h(L+S)}} \cdot \left(b - \bar{\mu} h - \frac{\omega_{\Lambda} \beta_{\Lambda}^{i}}{\alpha_{g\Lambda}^{d}} \right) \right] - \left[\left(b - \bar{\mu} h \right) \cdot \left(b + \bar{\mu} h - \frac{\omega_{\Lambda} \beta_{\Lambda}^{i}}{\alpha_{g\Lambda}^{d}} \right) \cdot e^{-h(L+S)} \right]$$

The remaining issue to be described concerns the relevant expressions for $G(\mu)$, ω, β^i, β^d, and $\bar{\mu}$. In the specific case of structurally homogeneous vegetation canopy layers, the elementary scatterers are modeled as oriented plates of finite small size. Depending on the vegetation type and environmental conditions, the orientation probability of the normals to these plates may follow various distributions including planophile, erectophile, or even heliotropic. Once the leaf angle probability distribution function is given, it

becomes feasible to express the extinction coefficient of any elementary volume and thus the total extinction of the vertically homogeneous vegetation layer (e.g., Ross, 1981; Dickinson, 1983; Verstraete, 1987). This extinction coefficient, traditionally expressed with Ross (1981) G function, modulates the optical thickness of the homogeneous vegetation layer. The generic expression (Equation 10) for leaves with an orientation parameter χ is

$$G(\mu) = \frac{1}{2} + \left(\frac{4\sqrt{1-\mu^2} - \pi}{2\pi} \right) \chi^v + \left(\frac{2\mu - 1}{2} \right) \chi^h \tag{10}$$

where the leaf orientation χ, also defined as the departure of leaf angles from a random distribution, equals +1 for horizontal leaves, 0 for random leaves, and –1 for vertical leaves. χ^h and χ^v are the positive and negative parts of χ, respectively.

The $\omega\,\beta^i$ and $\omega\,\beta^d$ parameters should thus be expressed via the G function and the leaf orientation probability distribution. The $\omega\,\beta$ parameter is the integral over the appropriate leaf orientation probability distribution, performed between 0 and $\pi/2$, of the scatter parameter of an individual scattering element, leaf or stem (Norman and Jarvis, 1975). Solving the integral, the upscatter parameter for diffuse radiation is (Equation 11)

$$\omega_\Lambda \beta_\Lambda^i = \chi^v \left(\frac{\rho_\Lambda + \tau_\Lambda}{6} \right) + \chi^h \left(\frac{\rho_\Lambda - \tau_\Lambda}{3} \right) + \left(\frac{2\rho_\Lambda + \tau_\Lambda}{3} \right) \tag{11}$$

and the upscatter parameter for direct beam radiation is (Equation 12)

$$\omega_\Lambda \beta_\Lambda^d = \chi^v \frac{2c(\mu) - 1}{2} (\rho_\Lambda - \tau_\Lambda) + \chi^h c(\mu) \cdot (\rho_\Lambda - \tau_\Lambda) + \rho_\Lambda [1 - c(\mu)] + \tau_\Lambda c(\mu) \tag{12}$$

where $c(\mu)$ is a transmittance coefficient that varies between 0.5 for $\mu = 0$ and 0.1667 for $\mu = 1$.

By definition, the scattering coefficient is the sum of the reflectance and transmittance of the scattering element (Equation 13):

$$\omega_\Lambda = \rho_\Lambda + \tau_\Lambda \tag{13}$$

where ρ_Λ is a weighted combination of the leaf and stem reflectances $\left(\rho_\Lambda^{leaf}, \rho_\Lambda^{stem}\right)$ (Equation 14):

$$\rho_\Lambda = \rho_\Lambda^{leaf} w_{leaf} + \rho_\Lambda^{stem} w_{stem} \tag{14}$$

where $w_{leaf} = L/(L+S)$ and $w_{stem} = S/(L+S)$; τ_Λ is a weighted combination of the leaf and stem transmittances $\left(\tau_\Lambda^{leaf}, \tau_\Lambda^{stem}\right)$ (Equation 15)

$$\tau_\Lambda = \tau_\Lambda^{leaf} w_{leaf} + \tau_\Lambda^{stem} w_{stem} \tag{15}$$

Finally, the average inverse diffuse optical depth per unit leaf and stem area ($\overline{\mu}$) is given by Equation 16

$$\overline{\mu} = \int_0^1 \frac{\mu'}{G(\mu')} d\mu' \tag{16}$$

after Dickinson (1983). $\overline{\mu}$ varies between 0.90 and 1.04 for the planophile and erectophile cases, and 1.00 for the spherical cases.

2.2.2. Experimental site and data

Field data used in this study were measured at K34 site in the Cuieiras Biological Reserve (2º 35'S, 60º 07'W, 90 m above sea level), during the LBA project (Large-Scale Biosphere-Atmosphere Experiment in Amazonia). The Cuieiras Biological Reserve is an INPA (Instituto Nacional de Pesquisas da Amazônia) protected forest reserve, about 60 km north of Manaus, embedded in a vast area of pristine rainforest. The 50 m tall K34 tower, erected in 1999, is located on a medium sized plateau (2°36'32. 67''S, 60°12'33. 48''W, 130 m) (Araújo et al., 2002). The natural vegetation and topography of this site are representative of much of Central Amazonia.

I used incident and reflected solar radiation data, collected from June 1999 to September 2000 by a piranometer (Kipp & Zonen CM 21, Delft, Netherlands), installed at a height of 44.6 m above the forest ground surface, connected to a datalogger (CR10, Campbell Scientific, Shepshed, UK). The data were measured every 30 seconds, and the averages stored every 30 minutes.

2.2.3. Model sensitivity to canopy architectural and optical parameters

I carried out a sensitivity analysis of the albedo simulated by the model to six canopy architectural and optical parameters: the upper canopy leaf and stem orientation (χ_{up}), the lower canopy leaf orientation (χ_{lo}), upper and lower canopy leaf reflectance on visible (VIS) and near-infrared (NIR) spectral band Λ (ρ_{Λ}; $\rho_{VIS,up}$,$\rho_{VIS,lo}$, $\rho_{NIR,up}$ and $\rho_{NIR,lo}$, respectively). Other canopy architectural and optical parameters are set to the values in Table 2.1. The model was then run several times with different combinations of the parameters above, to determine in detail the sensitivity of the model to these parameters.

Table 2.1. Parameters used by the model.

Architectural parameters	Value
single-sided leaf area index (L)	6.175
single-sided stem area index (S)	0.025
fraction of overall area covered by lower canopy (f_{lo})	0.500
fraction of overall area covered by upper canopy (f_{up})	0.975
Optical parameters	
direct and diffuse beam ground albedo on visible (VIS) spectral band ($a_{g,VIS}$)	0.10
direct and diffuse beam ground albedo on near-infrared (NIR) spectral band($a_{g,NIR}$)	0.40
lower canopy leaf transmittance on visible (VIS) spectral band ($\rho_{VIS,lo}$)	0.07
upper canopy leaf transmittance on visible (VIS) spectral band ($\rho_{VIS,up}$)	0.05
lower canopy leaf transmittance on near-infrared (NIR) spectral band ($\rho_{NIR,lo}$)	0.25
upper canopy leaf transmittance on near-infrared (NIR) spectral band ($\rho_{NIR,up}$)	0.20

2.3. RESULTS AND DISCUSSION

Initial tests (not shown) demonstrated that the above canopy albedo is not sensitive to the lower canopy parameters. This is because of the high leaf and stem area indices of the upper canopy. I use $\rho_{VIS,lo} = 0.062$, $\rho_{NIR,lo} = 0.60$ and $\chi_{lo} = 0.10$ and concentrate the discussion on the sensitivity of simulated albedo to the model upper canopy architectural and optical parameters χ_{up} and,$\rho_{VIS,up}$ and $\rho_{NIR,up}$, respectively.

Several combinations of χ_{up}, $\rho_{VIS,up}$,$\rho_{NIR,up}$ were tested looking for the best mean simulated value of surface albedo for the study period. A strong sensitivity of simulated albedo to these parameters was observed, resulting in optimal values of simulated albedo for ρ_{VIS} between 0.05 and 0.07, for $\rho_{NIR,up}$ between 0.27 and 0.28, and for χ_{up} between 0.6 and 0.9 (Figure 2.2). This range of χ_{up} characterizes a predominance of upper canopy elements (leaves and stems) with low inclination angle with respect to the horizontal.

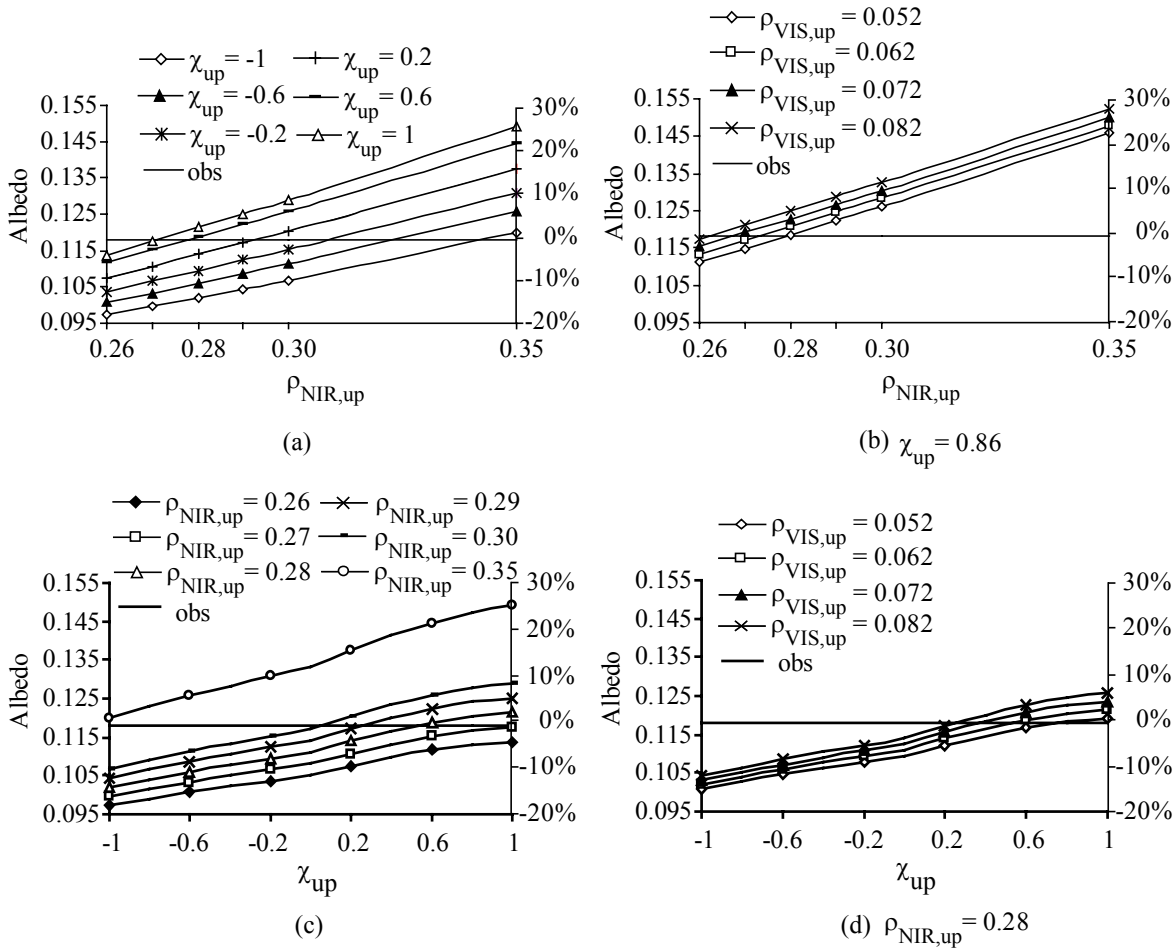

Figure 2.2. Simulated albedo as a function of $\rho_{NIR,up}$ and χ_{up}, for the Cuieiras Biological Reserve (K34).

Figure 2.3 shows the temporal variation of the observed and simulated albedos considering different values of the optical parameter χ_{up} for five selected days. In these simulations, $\rho_{NIR,up}$ = 0.275 and $\rho_{VIS,up}$ = 0.062. The model best represents the diurnal cycle with χ_{up} = 0.86.

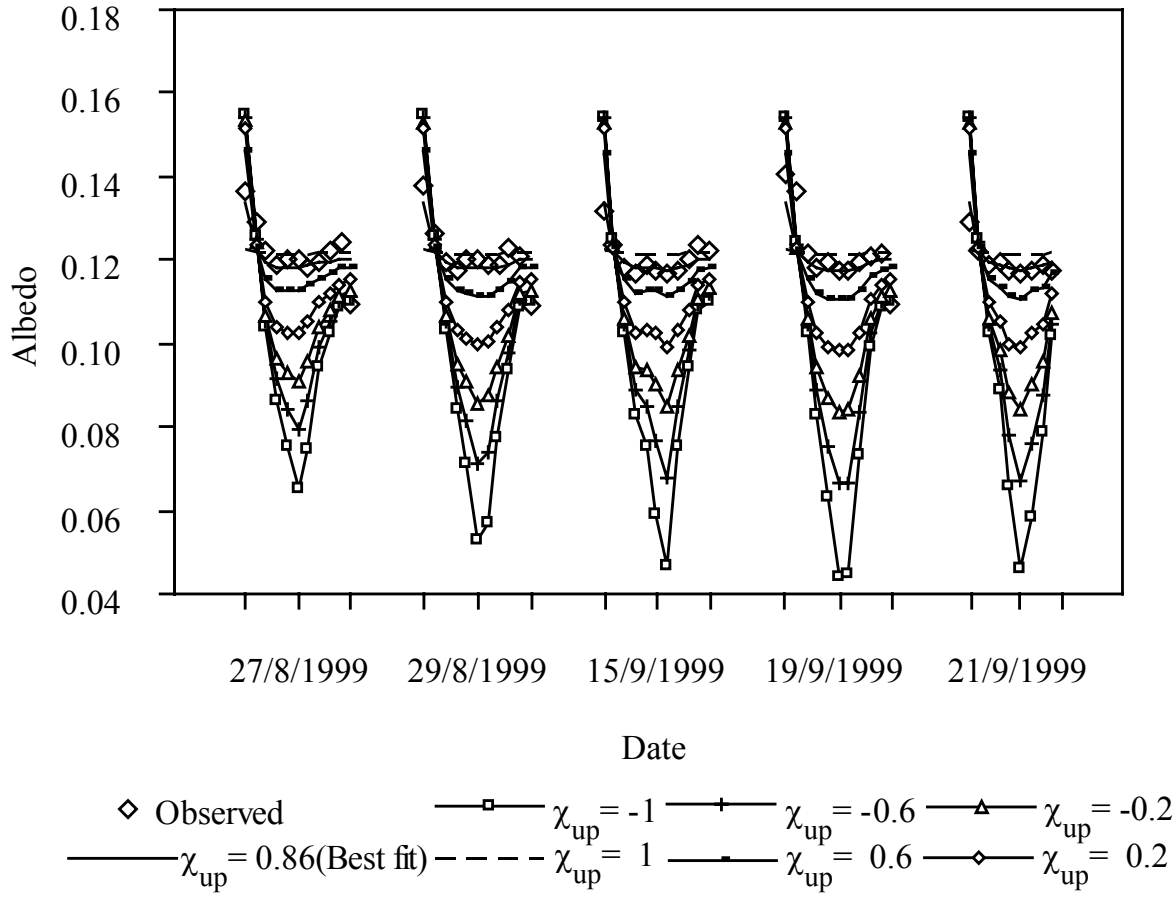

Figure 2.3. Temporal variation of the albedo observed in the Cuieiras Biological Reserve (K34) and the albedo simulated by the IBIS model, according to the upper canopy element orientation parameter.

The sensitivity of the root mean square error (RMSE) between simulated and observed albedos as a function of the variation of the canopy optical parameters is shown in Figure 2.4. This analysis indicates that the combination of the canopy optical parameters that minimize the RMSE are $\chi_{up} = 0.86$, $\rho_{VIS,up} = 0.062$, and $\rho_{NIR,up} = 0.275$, confirming the results obtained in Figures 2.2 and 2.3. Again, these parameters were obtained assuming that $\rho_{VIS,lo} = 0.062$, $\rho_{NIR,lo} = 0.60$ and $\chi_{lo} = 0.10$, L = 6.175, S = 0.025, $f_{up} = 0.975$ and $f_{lo} = 0.5$.

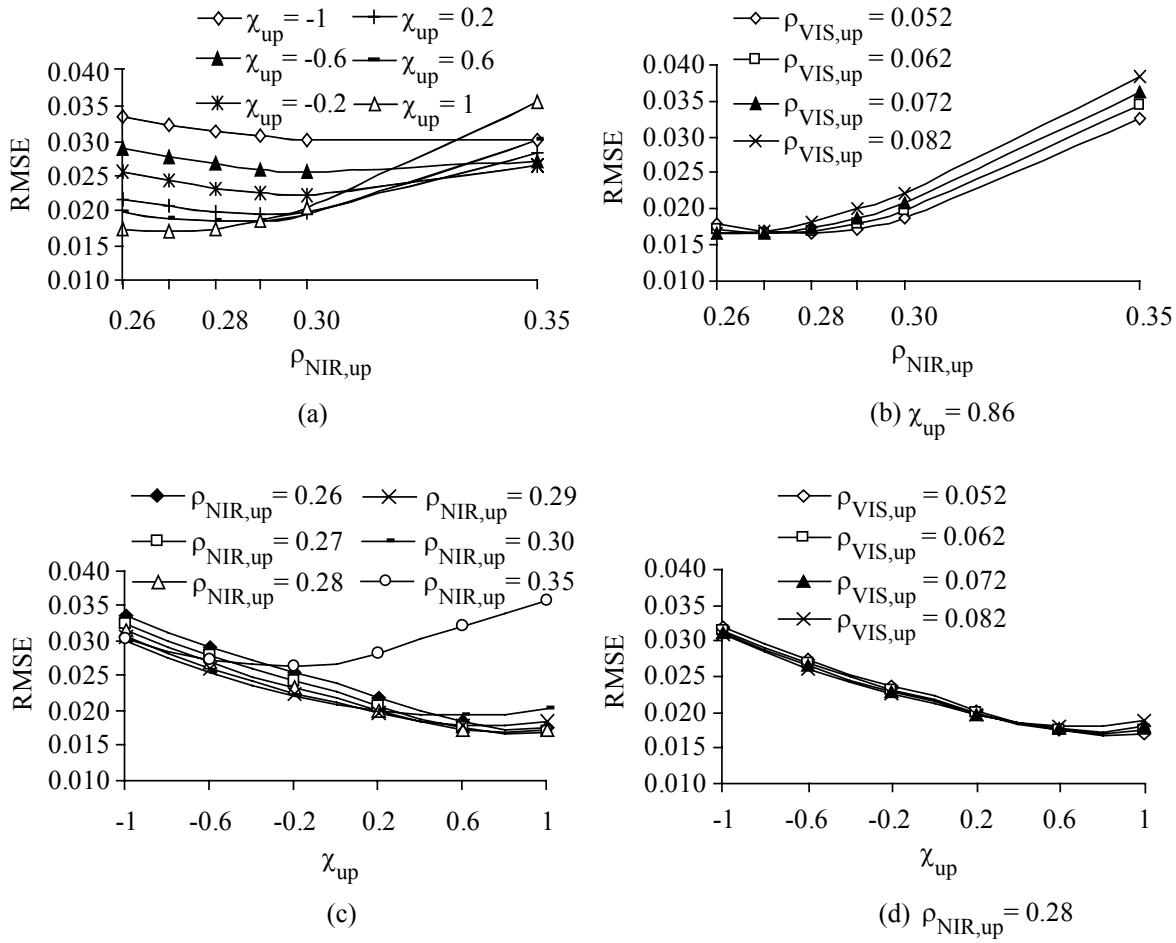

Figure 2.4. Root Mean Square Error (RMSE) between the observed and simulated albedo as a function of the canopy optical parameters $\rho_{NIR,up}$ and χ_{up}, for the Cuieiras Biological Reserve (K34).

The results indicate that the albedo simulated by IBIS is mostly sensitive to the parameters χ_{up} and $\rho_{NIR,up}$. Although Bonan (1996) and Oleson et al. (2004) reported that the good fit is obtained for χ_{up} in the range -0.4 to 0.6, in this study, the minimization of the mean relative error and the RMSE is achieved for $\chi_{up} = 0.86$. This parameter reduces significantly the effect of the zenith angle on the albedo during sunrise and sunset (Figure 2.3). Lower daily amplitudes of surface albedo are expected when the canopy architectural parameter, χ_{up}, describes the upper canopy elements as mainly horizontally distributed, as

shown in Figure 2.3. For χ_{up} = 0.6, the daily amplitude of the surface albedo is overestimated, while for χ_{up} = 1.0 it has a flat daily profile.

2.4. SUMMARY AND CONCLUSIONS

This study evaluated the sensitivity of the surface albedo simulated by IBIS to a set of tropical rainforest canopy optical parameters. The results are evaluated against albedo measurements taken above the K34 site at the Cuieiras Biological Reserve. Sensitivity analysis indicates a strong response to the parameters χ_{up} and $\rho_{NIR,up}$, a smaller sensitivity to $\rho_{VIS,up}$ and no sensitivity at all to the lower canopy parameters χ_{lo}, $\rho_{VIS,lo}$ and $\rho_{NIR,lo}$, which is consistent with the canopy structure. The combination of parameters that minimize the RMSE and mean relative error RMSE are χ_{up} = 0.86, $\rho_{VIS,up}$ = 0.062, and $\rho_{NIR,up}$ = 0.275. From the analysis of Figures 2.2, 2.3 and 2.4, however, it seems reasonable to conclude that values of χ_{up} in the range of 0.8 to 0.9, of $\rho_{VIS,up}$ in the range of 0.05 to 0.07 and $\rho_{NIR,up}$ in the range of 0.26 to 0.28 all yield results that provide the better values of RMSE, with little variation among them.

The successful simulations of tropical rainforest albedo by IBIS indicate its potential to simulate the canopy radiative transfer for narrow spectral bands, for close comparison with remote sensing products. Additional parameterizations of the canopy architectural and optical parameters according to the plant species, soil types, plant phenology, leaf water content, and soil surface wetness may improve considerably the scope of such modeling exercises, building a solid basis for stronger interactions among field observations, climate models and remote sensing products.

2.5. NOMENCLATURE

α	albedo of a vegetation canopy layer
μ	cosine of the Sun zenith angle
α^{d}	directional hemispherical reflectance
I_{in}^{d}	incident irradiance field that is purely collimated
α^{i}	indirect hemispherical reflectance
I_{in}^{i}	incident irradiance field that is purely isotropic
α_{g}	soil albedo
$\alpha_{g\text{-}lo}$	albedo of the combined lower canopy-ground system
$\alpha_{lo\text{-}up}$	albedo of the combined upper canopy-lower canopy-soil system
χ_{up}	upper canopy element orientation
χ_{lo}	lower canopy element orientation
f_{lo}	fraction of ground area covered by lower canopy
f_{up}	fraction of ground area covered by upper canopy
ρ_{Λ}	upper and lower canopy leaf reflectance by visible (VIS) and near-infrared (NIR) spectral band Λ
$\rho_{VIS,up}$	upper canopy leaf reflectance by visible (VIS) spectral band Λ
$\rho_{VIS,lo}$	lower canopy leaf reflectance by visible (VIS) spectral band Λ
$\rho_{NIR,up}$	upper canopy leaf reflectance by near-infrared (NIR) spectral band Λ
$\rho_{NIR,lo}$	lower canopy leaf reflectance by near-infrared (NIR) spectral band Λ
ρ_{Λ}^{leaf}	leaf reflectances
ρ_{Λ}^{stem}	stem reflectances
τ_{Λ}	upper and lower canopy leaf transmittance by visible (VIS) and near-infrared (NIR) spectral band Λ
$\tau_{VIS,up}$	upper canopy leaf transmittance by visible (VIS) spectral band Λ
$\tau_{VIS,lo}$	lower canopy leaf transmittance by visible (VIS) spectral band Λ
$\tau_{NIR,up}$	upper canopy leaf transmittance by near-infrared (NIR) spectral band Λ
$\tau_{NIR,lo}$	lower canopy leaf transmittance by near-infrared (NIR) spectral band Λ
τ_{Λ}^{leaf}	leaf transmittances
τ_{Λ}^{stem}	stem transmittances
$I^{\uparrow}$	upward diffuse radiative fluxes per unit incident flux
$I^{\downarrow}$	downward diffuse radiative fluxes per unit incident flux
K	optical depth of direct beam per unit leaf and stem area
$G(\mu)$	relative projected area of leaf and stem elements in the direction $\cos^{-1}\mu$
$\overline{\mu}$	average inverse diffuse optical depth per unit leaf and stem area
ω_{Λ}	scattering coefficient
β^{i}	upscatter parameters for indirect (diffuse) beam radiation
β^{d}	upscatter parameters for direct beam radiation
L	single-sided leaf area index
S	single-sided stem area index
$\alpha_{g,\Lambda}^{d}$	direct beam ground albedo for each spectral band Λ
$\alpha_{g,\Lambda}^{i}$	diffuse ground albedo for each spectral band Λ
α_{Λ}^{d}	single scattering albedo of direct fluxes
α_{Λ}^{i}	single scattering albedo of indirect fluxes

χ^h	leaf orientation for horizontal leaves
χ^v	leaf orientation for vertical leaves
b	work variable
h1	work variable
h	work variable
d1	work variable

CHAPTER 3

SIMULATIONS OF TROPICAL RAINFOREST ALBEDO: IS CANOPY WETNESS IMPORTANT?

3.1. INTRODUCTION

Surface albedo is the main factor that affects the land radiation balance, not only controlling the amount of solar energy available for heating the ground and lower atmosphere and for evaporating water (Rowe, 1991), but also affecting the atmospheric circulation and climate. Particularly in the tropics, where the solar radiation balance is stronger, changes in surface albedo have been found to influence the regional climate, as tropical deforestation studies demonstrate (Nobre et al., 1991; Dirmeyer and Shukla, 1994; Costa and Foley, 2000). An accurate simulation of the solar radiation balance is also important. For example, Berbet and Costa (2003) demonstrated that an uncertainty of 10 W $\cdot$ m^{-2} in the seasonal solar radiation balance translates into an uncertainty of 30 mm/month in the simulated rainfall, a very significant uncertainty, especially in the dry season in that

region. In this context, a good representation of albedo by climate models is essential to correctly address the tropical deforestation climate change problem.

Berbet and Costa (2003), however, also verified that even a complex, state-of-the-art; land surface scheme coupled to a climate model is unable to correctly reproduce details of seasonal variability of albedo of tropical rainforests, although it reproduces well the annual mean and some aspects of the seasonal variability. This indicates that there is still much to be learned – and incorporated into models – about the sources of variation of albedo at both hourly and monthly time scales.

At the monthly time scale, Culf et al. (1995) analyzed the surface albedo at forest sites in Amazonia. The authors reported that albedo seasonality at these sites is not related to the variation of solar elevation angle or to cloudiness, but suggested a relationship to soil moisture. Although soil moisture affects ground albedo, most likely the changes in forest albedo are related to soil moisture-correlated variables: smaller soil exposure, darker leaves (associated with the leaf water potential) and higher canopy wetness (Berbet and Costa, 2003). Canopy wetness, in particular, is a strong candidate for changing canopy albedo, because reflectance of liquid water varies, depending on the wavelength, between 0 and 5%, much lower than the 12-13% usually measured above tropical rainforest canopies. Hence the presence of liquid water on the canopy increases the absorption of solar radiation, reducing the canopy overall albedo.

Here, I investigated the role of canopy wetness in the simulated albedo of a tropical rainforest. In this study, I run simulations using three versions of the land surface/ecosystem model IBIS: the standard version using the original calibration used by Delire and Foley (1999), the same version recalibrated to fit the tropical rainforests albedo data, and a modified version that incorporates the effects of canopy wetness on calculated surface albedo. The next section describes the sites and instrumentation that measured the

albedo data used here to validate the model simulations. Sections 3 and 4 describe the IBIS model, the modifications to incorporate canopy wetness and the experiment design, while Section 5 presents and discusses the simulation results.

3.2. MATERIALS AND METHODS

3.2.1. Sites, instrumentation and data

Field data used in this study were measured at three sites in the Amazon during the ABRACOS (Anglo Brazilian Amazonian Climate Observation Study) and LBA (Large-Scale Biosphere-Atmosphere Experiment in Amazonia) projects. Ducke Reserve (02º 57'S, 59º 57' W, 80 m above sea level) is an area of protected primary forest with mean height forest canopy of 35 m, with some trees reaching up 40 m. The forest in Reserva Ducke is composed by a large variety of tree species. The tallest species in the area around the tower are *Piptadenia suaveolens Miq*., *Licania micrantha Miq*., *Bocoa viridiflora (Ducke) Cowan* and so on, with more details in Shuttleworth et al. (1984) and in Roberts et al. (1990). Cuieiras Biological Reserve (2º 35'S, 60º 07'W, 90 m above sea level) (K34) is an INPA (Instituto Nacional de Pesquisas da Amazônia) protected forest reserve, about 60 km north of Manaus, embedded in a vast area of pristine rainforest. The natural vegetation and topography of this site are representative of much of central Amazonia. These sites are surrounded by undisturbed forest for at least 5 km. Jaru Reserve (10º 05'S, 61º 55'W, at 120 m above sea level) is an IBAMA (Instituto Brasileiro do Meio Ambiente e dos Recursos Naturais Renováveis) forest reserve and is located about 80 km north of Ji-Paraná. The mean height of the forest canopy is 33 m. The tallest tree species in the area immediately surrounding the tower are *Cedrella odorata, Dioclea cf bicolor Bth., Strychnos amazonicus Krukoff* (McWilliam et al., 1996; Roberts et al., 1996) (Figure 3.1).

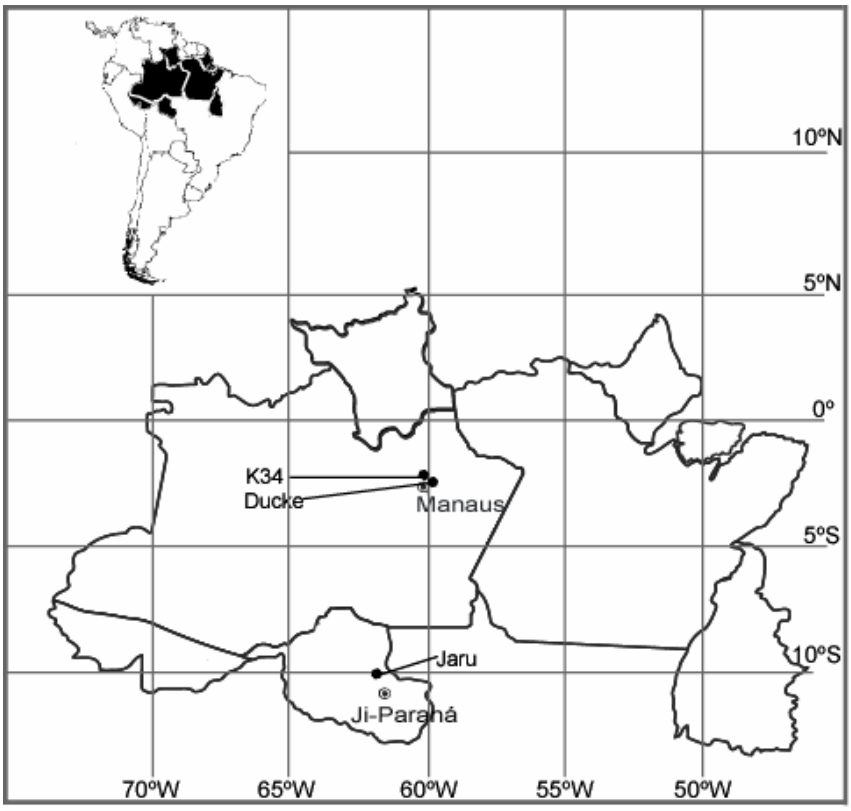

Figure 3.1. Orientation map.

At the Cuieiras Reserve, a piranometer (Kipp & Zonen, Delft, Netherlands), connected on a datalogger model (21X, Campbell Scientific) measured incident and reflected solar radiation each minute, storing the averages every 20 minutes. For the remaining sites, the incident and reflected solar radiation were measured using two solarimeters (Kipp and Zonen, Delft, the Netherlands). These instruments are part of an automatic weather station (Didcot Instruments, Abingdon, UK) connected to a datalogger (CR10, Campbell Scientific, Shepshed, UK) and hourly-averaged data were recorded.

I used incident and reflected solar radiation and precipitation data, collected from June 1999 to September 2000 at Cuieiras Reserve, from January to December of 1995 at Ducke Reserve and from January to December of 1993 at Jaru Reserve. Data used in this study are available on-line through www.cptec.inpe.br/abracos/available.html and http://lba.cptec.inpe.br/beija-flor.

3.2.2. Description of the IBIS model

To simulate the diurnal albedo of an Amazon tropical forest, I used the Integrated Biosphere Simulator–IBIS (Foley et al., 1996). It includes representations of land surface processes, like energy, water and momentum exchange between the soil-vegetation-atmosphere system, canopy physiology, vegetation phenology, vegetation dynamics, and terrestrial carbon balance. Originally, IBIS was globally calibrated (more details in Delire and Foley, 1999; Kucharik et al., 2000), and since then, it has been used in several studies of the biosphere-atmosphere interactions in Amazonia (Costa and Foley, 2000; Botta and Foley, 2002; Foley et al., 2002; Berbet and Costa, 2003).

One of the processes simulated by IBIS, of main interest here, is the exchange of solar radiation between the soil-vegetation-atmosphere system. Solar radiation transfer is calculated following the two-stream approximation, with separated calculations for direct and diffuse radiation in both visible and near-infrared bands. The canopy radiative transfer code of IBIS is standard in the literature (Norman and Jarvis, 1975; Sellers, 1985; Sellers et al., 1986; Pollard and Thompson, 1995 – Appendix A; Bonan, 1996; Oleson et al., 2004). A detailed description of the radiation transfer and albedo algorithms and model sensitivity to several parameters is presented by Yanagi and Costa (2006). In this study, I modified the IBIS canopy radiation transfer code to incorporate the effects of canopy wetness on the vegetation reflectance. Although IBIS already calculates the canopy wetness, in this work the parameters ω (scattering coefficient, eq. 3 in Sellers, 1985; eq. 11 in Sellers et al., 1986; eq. 3.5 in Oleson et al., 2004), β (upscatter parameter for diffuse radiation, eq. 3 in Sellers, 1985; eq. 11 in Sellers et al., 1986; eq. 3.6 in Oleson et al., 2004) and β_o (upscatter parameter for direct radiation, eq. 4 in Sellers, 1985; eq. 12 in Sellers et al., 1986; eq. 3.7 in Oleson et al., 2004) were modified to include the radiative effects of canopy wetness, according to Equations 1 to 4:

$$\omega = \omega^{dry} \cdot (1 - f_{wet}) + \omega^{water} \cdot f_{water} + \omega^{snow} \cdot f_{snow} \quad (1)$$

$$\beta = \omega^{dry} \cdot \beta^{dry} (1 - f_{wet}) + \omega^{water} \cdot \beta^{water} \cdot f_{water} + \omega^{snow} \cdot \beta^{snow} \cdot f_{snow} / \omega \quad (2)$$

$$\beta_o = \omega^{dry} \cdot \beta_o^{dry} (1 - f_{wet}) + \omega^{water} \cdot \beta_o^{water} \cdot f_{water} + \omega^{snow} \cdot \beta_o^{snow} \cdot f_{snow} / \omega \quad (3)$$

$$\omega^{water} = \nu \cdot \omega^{dry} \quad (4)$$

where f_{wet} is the total wet (water and snow) fraction of the canopy ($f_{wet} = f_{water} + f_{snow}$), f_{water} is the fraction of the canopy wet by liquid water and f_{snow} is the fraction of the canopy wet by snow. The superscripts *dry, water* and *snow* denote dry, wet by water and wet by snow canopies, respectively. ν is the ratio of the scattering coefficients of the canopy surfaces wet by water and dry canopy surfaces, applied individually to leaves and stems.

3.2.3. Experiment design

In this study, I conducted three simulations of the diurnal surface albedo for each of the three Amazon forest sites using the off-line IBIS version, as follows:

1) DF99: for reference to previous studies, this simulation uses the set of optical parameters used by Delire and Foley (1999);
2) DC_i, the dry-canopy (control) simulations: use the original code, without modifications to incorporate the effects of wetness on canopy reflectance. It uses a set of leaf optical parameters chosen to better fit the simulated results to the experimental data of the sites studied, minimizing the RMSE between the observed and simulated albedos. The subscript *i* may be equal to *M* for the Manaus-nearby sites (Ducke and Cuieiras Reserves), or *J* for Jaru Reserve.
3) WC_i, the wet-canopy simulations: similar to DC_i, but including the modifications described in Equations (1) through (4).

The terms dry-canopy (DC) and wet-canopy (WC), when referring to versions of the IBIS code, denote only the status of the canopy during the radiative transfer calculations. It

should be noted that both versions simulate the interception of water by the canopy, and the evaporation and dripping of the canopy-stored water.

To calibrate the DC simulations, initially I do a sensitivity analysis of the simulated albedo to several canopy optical parameters. The most sensitive parameters are the upper and lower canopy leaf orientation ($\chi_{leaf\text{-}up}$ and $\chi_{leaf\text{-}lo}$, respectively), and upper and lower canopy visible and near-infrared (NIR) leaf reflectance (α_{VIS-up}^{Leaf}, α_{VIS-lo}^{Leaf}, α_{NIR-up}^{Leaf} and α_{NIR-lo}^{Leaf}, respectively). The model is run several times with different combinations of the parameters above. Table 3.1 shows, for the DC simulations, the parameter combinations that provide the best adjustment of the diurnal albedo without considering the effect of canopy wetness. Next, this set of parameters is added to the WC version of the code, and the parameters f_{wetmax} (maximum fraction of water cover on two-sided leaf), τ_{drip} (decay time for intercepted liquid drip off) and ν (ratio of the scattering coefficients of the canopy surfaces wet by water and dry canopy surfaces, applied individually to leaves and stems) are calibrated.

Table 3.1. Optical parameters used by the DF99 calibration, and by the new calibrations using the dry-canopy (DC_i) and wet-canopy (WC_i) versions of the model, where *i* is equal to *M* for the Manaus-nearby sites (Ducke and Cuieiras Reserves) or *J* for the Jaru Reserve. $\chi_{leaf\text{-}up}$ is the upper canopy leaf orientation, $\chi_{leaf\text{-}lo}$ is the lower canopy leaf orientation, α_{VIS-lo}^{Leaf} is the lower canopy visible leaf reflectance, α_{VIS-up}^{Leaf} is the upper canopy visible leaf reflectance, α_{NIR-lo}^{Leaf} is the lower canopy NIR leaf reflectance, α_{NIR-up}^{Leaf} is the upper canopy NIR leaf reflectance, f_{wetmax} is maximum fraction of water cover on two-sided leaf, τ_{drip} is the decay time for intercepted liquid drip off and ν is the ratio of the scattering coefficients of the canopy surfaces wet by water and dry canopy surfaces, applied individually to leaves and stems. All values are dimensionless, except for τ_{drip}, which is in seconds.

		$\chi_{leaf-up}$	$\chi_{leaf-lo}$	α_{VIS-lo}^{Leaf}	α_{VIS-up}^{Leaf}	α_{NIR-lo}^{Leaf}	α_{NIR-up}^{Leaf}	f_{wetmax}	τ_{drip}	ν
All Reserves	DF99	0.00	-0.50	0.062	0.062	0.60	0.40	0.25	7200 s	–
Manaus (Ducke, Cuieiras)	DC_M	0.86	0.10	0.062	0.062	0.60	0.28	0.25	7200 s	–
	WC_M	0.86	0.10	0.062	0.062	0.60	0.28	0.80	3600 s	0.10
Jaru	DC_J	0.86	0.10	0.082	0.082	0.60	0.30	0.25	7200 s	–
	WC_J	0.86	0.10	0.082	0.082	0.60	0.30	0.80	3600 s	0.40

3.3. RESULTS AND DISCUSSION

The three IBIS versions are run for each of the three study sites. Figures from 3.2 to 3.4 show the diurnal profile of the surface albedo for Cuieiras, Ducke and Jaru Reserves, respectively, for selected days of the year. To facilitate the interpretation, the days selected represent either no-rain days – charts on the left side (a, b, c) of the figures – or days with a single daytime rainfall event – right side (d, e, f) of the figures. Figures from 3.2 and 3.3 show results for the Manaus (*M*) set of parameters, while Figure 3.4 shows results for the Jaru (*J*) set of parameters, according to Table 3.1.

The DF99 simulations overestimate the surface albedo, particularly when zenith angle is high (Figures 3.2 to 3.4). The albedo simulated by the calibrated model (DC_M and DC_J) fit better to the observed data in days without precipitation occurrence (left side of Figures 3.2 to 3.4), but the DC version of the model does not represent the observed albedo drop during precipitation events (right side of Figures 3.2 to 3.4).

WC simulations, however, show that the modified version of IBIS is able to reproduce the considerable decrease in surface albedo during precipitation hours (right side of Figures 3.2 to 3.4). This reduction in the surface albedo is consistent with an increase of the absorption of the incident solar radiation by the liquid water deposited on the leaves, increasing solar radiation absortance and reducing solar radiation reflectance.

Table 3.2 shows the statistics of observed and simulated surface albedo for the precipitation hours and for the entire time series at three Amazon rainforest sites (Cuieiras, Ducke and Jaru reserves), for the simulations based on the DF99 calibration, for the new calibration using the dry-canopy (DC) and wet-canopy (WC) versions of the model.

Table 3.2. Statistics of observed and simulated surface albedo for the entire time series and for precipitation hours at three Amazon rainforest sites (Cuieiras, Ducke and Jaru reserves), for the simulations based on the DF99 calibration, for the new calibration using the dry-canopy (DC) and wet-canopy (WC) versions of the model. $\overline{X}$ is the average albedo, ε is the mean relative error and RMSE is the root mean square error.

			Entire time series			Precipitation hours		
			$\overline{X}$	ε (%)	RMSE	$\overline{X}$	ε (%)	RMSE
Using set of optical parameters calibrated for the sites near to Manaus	Ducke Reserve	DF99	0.146	23.44	0.0398	0.139	41.58	0.0550
		DC_M	0.121	2.14	0.0219	0.120	22.13	0.0365
		WC_M	0.118	-0.03	0.0210	0.105	6.11	0.0302
		Observed	0.118	–	–	0.099	–	–
	Cuieiras Reserve	DF99	0.146	24.11	0.0384	0.142	40.79	0.0521
		DC_M	0.121	2.58	0.0169	0.120	19.16	0.0320
		WC_M	0.117	-0.73	0.0142	0.104	2.91	0.0234
		Observed	0.118	–	–	0.101	–	–
	Jaru	DF99	0.146	12.26	0.0332	0.145	19.57	0.0387
		DC_M	0.121	-7.15	0.0232	0.121	-0.35	0.0222
		WC_M	0.117	-9.68	0.0243	0.108	-10.93	0.0247
		Observed	0.130	–	–	0.121	–	–
Using set of optical parameters calibrated for Jaru site	Jaru	DF99	0.146	12.26	0.0332	0.145	19.57	0.0387
		DC_J	0.133	1.98	0.0215	0.132	9.43	0.0250
		WC_J	0.129	-0.50	0.0209	0.121	0. 40	0.0207
		Observed	0.130	–	–	0.121	–	–

Mean relative error (ε) and root mean square error (RMSE) are defined according to Equations 5 and 6:

$$\varepsilon = \frac{1}{n}\sum_{i=1}^{n}\frac{\left(X_i^s - X_i^o\right)}{X_i^o} \tag{5}$$

$$RMSE = \sqrt{\frac{\sum_{i=1}^{n}\left(X_i^s - X_i^o\right)^2}{n}} \tag{6}$$

where X^s and X^o are simulated and observed albedo and n is the number of data points. Given my interest here in the effects of canopy wetness on the simulated rainforest albedo, I analyzed the "precipitation hours" data separately from the entire data (Table 3.2). For the entire time series, for the two sites near Manaus, the new calibration (DC_M) represents a considerable improvement over the DF99 calibration, lowering the mean relative error by an order of magnitude, and the RMSE by nearly half. The inclusion of the effects of canopy wetness on the radiative transfer code further reduces ε and RMSE, consistent with the results shown in Figures 3.2 to 3.4. Looking for a single parameterization for Amazonia, I also tested the Manaus parameters at the Jaru site. However, it turns out that the average observed albedo of the Jaru site is much higher than at the Manaus sites, and the parameters used for Manaus are not suitable to Jaru. I then selected a new set of parameters for the Jaru site (DC_J). Results for Jaru site, using a site-specific calibration, show an improvement similar to the one obtained at the Manaus sites.

Although the WC simulation shows an improvement in the simulation statistics for the entire time series, the true effect of it is best seen in the analysis of data during the precipitation hours. Initially, I can verify that the DF99 and DC simulation results during precipitation hours are much worse than the equivalent result for the entire time series, which by itself indicates that a precipitation-related process is missing in the model. In addition, the WC simulations for the precipitation hours improve considerably the results when compared to the control (DC), with ε dropping by an order of magnitude and RMSE decreasing by about one-fifth.

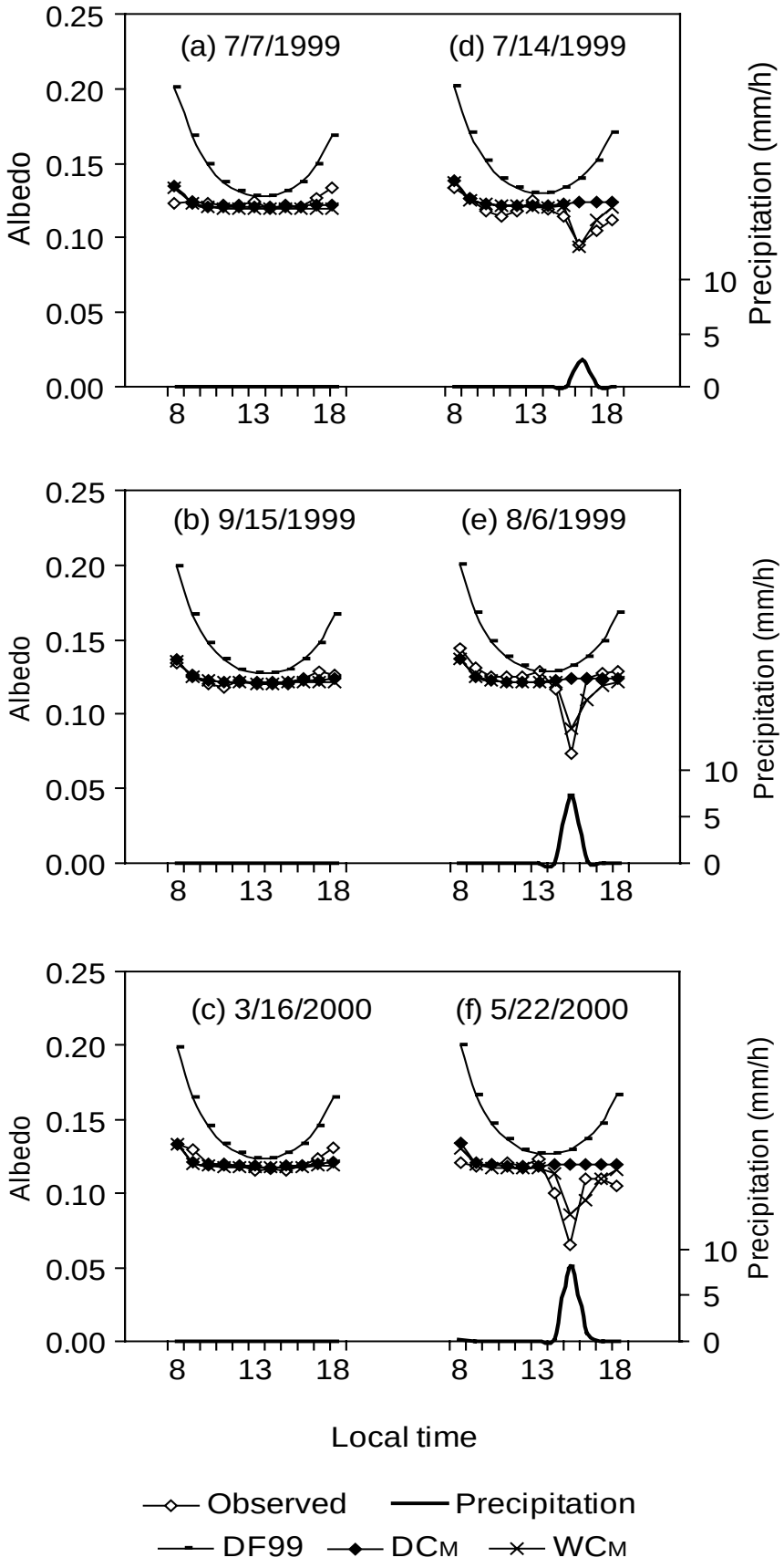

Figure 3.2. Diurnal variation of the simulated and observed surface albedo in the Cuieiras Reserve for selected days.

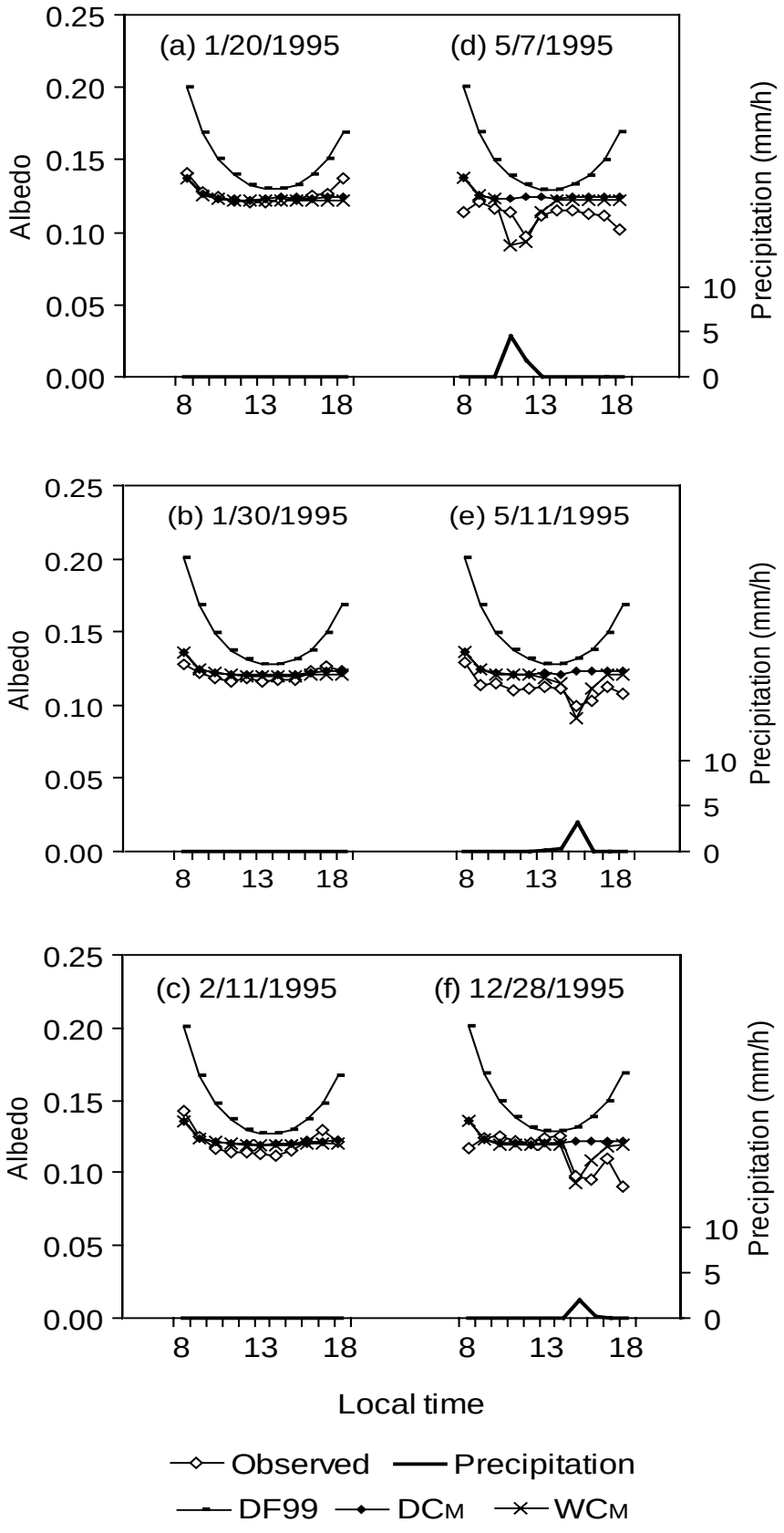

Figure 3.3. Diurnal variation of the simulated and observed surface albedo in the Ducke Reserve for selected days.

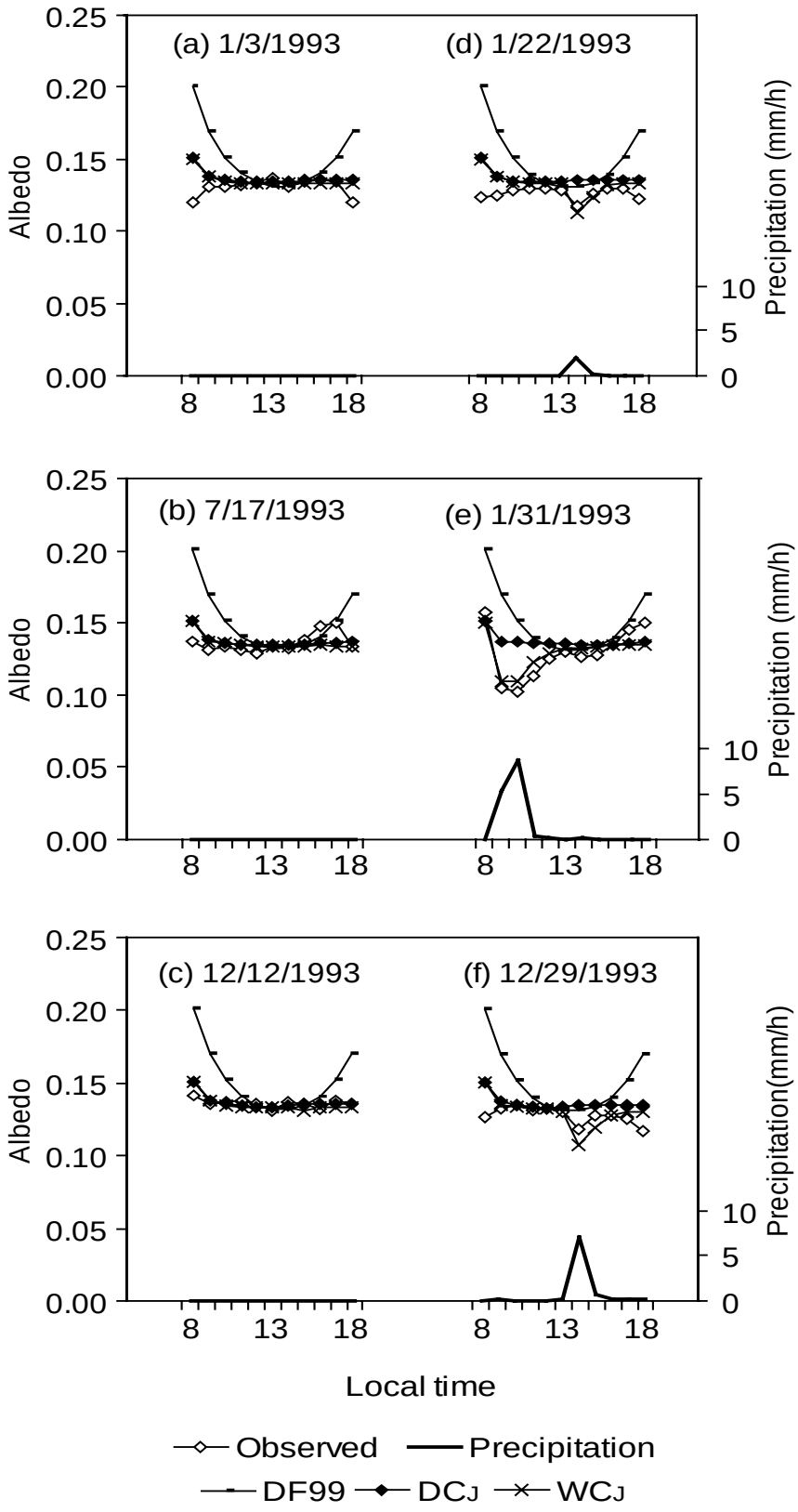

Figure 3.4. Diurnal variation of the simulated and observed surface albedo in the Jaru Reserve for selected days.

These results demonstrate that, at the hourly time scale, the incorporation of canopy wetness on the radiative transfer calculations improves substantially the simulation results, in particular for the times when the canopy is wet, but also brings an improvement to the simulation of the entire period.

I also compare the model results at the monthly time scale for the three sites studied (Figure 3.5). In all cases, the WC albedo is smaller than the DC albedo, but the changes introduced do not substantially modify the simulated albedo. As seen in Figures 3.2 to 3.4, because of evaporation and dripping, the effect of canopy wetness on the surface albedo is restricted to the duration of a rainfall event plus one or two hours. Although Amazonia is one of the rainiest climates on the Earth, the frequency of rainfall events (7.1% at Ducke, 14.2% at Cuieiras, and 17.0% at Jaru) is relatively low for a more significant effect of canopy wetness on albedo seasonality.

An exception is observed at the Ducke Reserve (Figure 3.5b), where a more pronounced drop in the WC-simulated albedo is observed in April. Even in this extreme case, the simulated decrease in monthly albedo accounts for less than half of the observed change, which let me conclude that canopy wetness alone is not sufficient to represent correctly the seasonal variability of the albedo for a tropical rainforest.

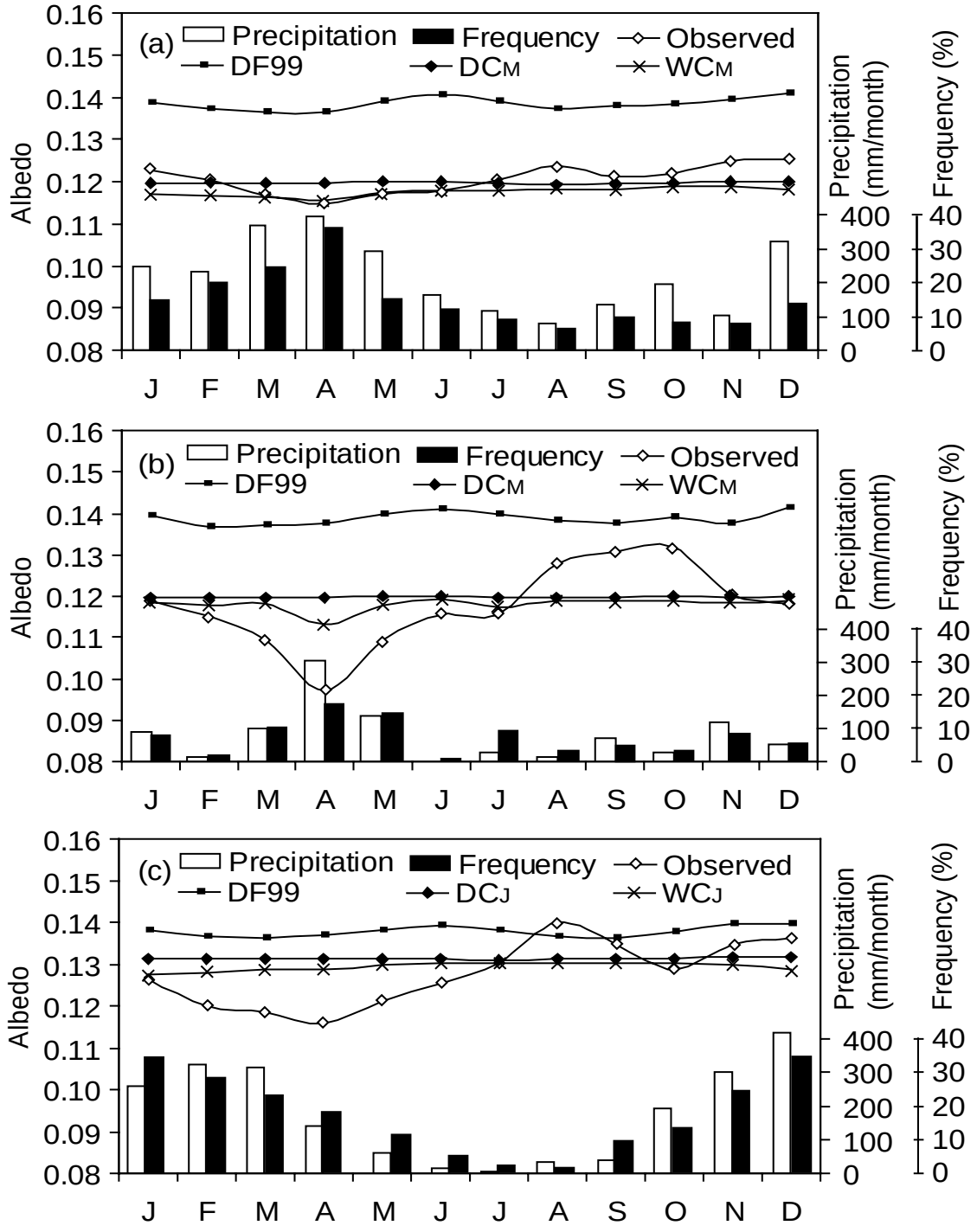

Figure 3.5. Monthly profile of the observed and simulated surface albedo, monthly precipitation and frequency of rainfall events, at three Amazon rainforest sites: (a) Cuieiras Reserve, from June 1999 to September 2000, (b) Ducke Reserve, from January to December of 1995 and (c) Jaru Reserve, from January to December of 1993.

3.4. SUMMARY AND CONCLUSIONS

The goal of this work was to study the effect of canopy wetness on the simulated albedo of a tropical rainforest. Simulations were run using three versions of the IBIS model: the standard version, the same version recalibrated to fit the tropical rainforests albedo data, and a modified version that incorporates the effects of canopy wetness on surface albedo, for three Amazon forest study sites in both hourly and monthly time scales.

The incorporation of canopy wetness on the radiative transfer calculations improves the simulation results at the hourly time scale, reproducing the observed decrease in surface albedo during precipitation hours, when the canopy is wet. Although the canopy wetness has an important effect, this effect is restricted to the times when the canopy is actually wet, a relatively short period of time at the monthly or longer time scales. Therefore, the changes introduced are not sufficient to substantially improve the representation of albedo seasonality.

While these results exclude the role of canopy wetness as a main source of seasonal variability of tropical rainforests albedo, this study narrows the choice of sources of albedo seasonal variation. Following the discussion of Culf et al. (1995) and Berbet and Costa (2003) on the subject, I recommend that future studies investigate the role of photoinhibition and leaf water potential on the seasonality of the tropical rainforest albedo. The clear definition of these roles, and their incorporation into climate models, will eventually allow us to do much more detailed studies of the climatic effects of tropical deforestation.

3.5. NOMENCLATURE

ω	scattering coefficient
β	upscatter parameter for diffuse radiation
β_o	upscatter parameter for direct radiation
f_{wet}	total wet (water and snow) fraction of the canopy
f_{water}	fraction of the canopy wet by liquid water
f_{snow}	fraction of the canopy wet by snow
ν	ratio of the scattering coefficients of the canopy surfaces wet by water and dry the canopy surfaces
$\chi_{leaf\text{-}up}$	upper canopy leaf orientation
$\chi_{leaf\text{-}lo}$	lower canopy leaf orientation
α_{VIS-up}^{Leaf}	upper canopy visible leaf reflectance
α_{VIS-lo}^{Leaf}	lower canopy visible leaf reflectance
α_{NIR-up}^{Leaf}	upper canopy near-infrared (NIR) leaf reflectance
α_{NIR-lo}^{Leaf}	lower canopy near-infrared (NIR) leaf reflectance
f_{wetmax}	maximum fraction of water cover on two-sided leaf
τ_{drip}	decay time for intercepted liquid drip off
X^s	simulated albedo
X^o	observed albedo
ε	mean relative error

CHAPTER 4

COMPARISON OF SEASONAL AND SPATIAL VARIATIONS OF ALBEDO ESTIMATED BY A CLIMATE MODEL AND ALBEDO DERIVED FROM REMOTE SENSING DATA FOR THE AMAZON TROPICAL RAINFOREST

4.1. INTRODUCTION

Albedo is the ratio of upwelling radiant energy relative to the downwelling irradiance incident upon a surface. Land surface albedo is a key land physical parameter in characterizing the surface energy budget and has frequently been considered in studies of global and regional climate. General Circulation Model (GCM) studies have demonstrated that the climate presents a strong sensitivity to surface albedo changes, originated by natural action and anthropogenic land use changes, such as desertification (Charney et al., 1977; Xue et al., 1990) and tropical deforestation (Dickinson and Henderson-Sellers, 1988; Hahmann and Dickinson, 1997; Berbet and Costa, 2003). Thus, the better representation of

surface albedo in climate models will enhance the accuracy of climate simulation and prediction.

Albedo simulated by climate models has been evaluated with field observations and satellite measurements. Field data are fundamental to validate model results, mainly because they represent more realistically a specific site studied. However, they present operational difficulties, are expensive to obtain, and only provide sparse and eventual measurements.

On the other hand, remote sensing is an important tool to obtain coherent temporal and spatial variations of surface characteristics such as albedo (Lewis et al., 1999), thus aiding the validation and improvement of model parameterization. A number of land surface albedo products have been produced based on several remote sensing devices, including the polar orbiting NOAA (National Oceanic and Atmospheric Administration) with AVHRR (Advanced Very High Resolution Radiometer) sensor, ERBE (Earth Radiation Budget Experiment), MODIS (Moderate Resolution Imaging Spectroradiometer), and the geostationary satellites GOES and METEOSAT. In many cases, data from different remote sensors were combined to generate a single product.

This chapter presents a comparison of simulated albedo computed by the NCAR Community Climate Model (CCM3) coupled to the Integrated Biosphere Simulator (IBIS) with derived albedo measurements from six remote sensing products. A comparison against field data collected at three study sites is also performed. Section 2 describes the albedo datasets analyzed. Section 3 presents and discusses the results and conclusions are summarized in Section 4.

4.2. ALBEDO DATA

4.2.1. Land surface albedo simulations

The land surface albedo simulations were produced by the National Center for Atmospheric Research (NCAR) Community Climate Model version 3 (CCM3, Kiehl et al., 1998) coupled with an updated version of the Integrated Biosphere Simulator (IBIS) of Foley et al. (1996) and Kucharik et al. (2000). I refer to this coupled model as CCM3–IBIS (Delire et al., 2002). CCM3 is a spectral atmosphere model with spatial resolution of T42 (the spectral representation of the horizontal fields is truncated at the 42nd wavenumber using a triangular truncation; horizontal fields are converted to a 2.81° x 2.81° grid) and has 18 vertical levels and operates with a 20-min time step (Kiehl et al., 1998). IBIS is an integrated model of land surface processes, vegetation dynamics and carbon cycle. IBIS has two vegetation layers (i.e., trees and short vegetation) and a variable number of soil layers. In IBIS, the exchange of solar radiation between the soil-vegetation-atmosphere system is calculated following the standard two-stream approximation, with separate calculations for direct and diffuse radiation in both visible (VIS) and near-infrared (NIR) bands. A detailed description of the albedo algorithm and model sensitivity to several parameters is presented by Yanagi and Costa (2006). In these simulations, IBIS operates on the same T42 spatial grid as the CCM3 atmospheric model.

4.2.2. Remote sensing albedo

In this work, I used land surface albedo from six remote sensing products: Csiszar and Gutman (1999) – CG99, ERBE, SRB-ISLSCP2, UMD (GOES/METEOSAT/AVHRR), MODIS white-sky, and MODIS black-sky (Table 4.1).

Table 4.1. Main characteristics of the remote sensing albedo products.

Remote sensing product and sensors involved	**Spectral resolution**	**Spatial resolution**	**Temporal resolution**	**Used period**	**Sky condition**	**Average albedo**	**Source**
CG99 (AVHRR – Advanced Very High-Resolution Radiometer)	Channel 1 (0.58-0.68 μm, VIS) and Channel 2 (0.72-1.1μm, NIR)	0.5ºx0.5º 1.1 km	monthly	1985-1991	Clear-sky	11.0 %	Csiszar and Gutman,1999
ERBE (Earth Radiation Budget Experiment)	Shortwave channel 1 (0.2-5.0 μm)	1ºx1º 35-50km	monthly	1986-1990	Clear-sky	15.5 %	Barkstrom, 1984
SRB-ISLSCP2	Shortwave channel (0.3-5.0 μm)	1ºx1º	monthly	1986-1995	All-sky	15.0 %	Stackhouse et al., 2000; Stackhouse et al., 2003
UMD (GOES-METEOSAT-AVHRR)	Shortwave channel (0.3-5.0 μm)	0.5ºx0.5º 30 km	monthly	1990-1992	All-sky	15.0 %	Pinker, 2002
MODIS (Moderate Resolution Imaging Spectroradiometer). Albedo product (MOD43B)	bb3 brodband (0.3-5.0 μm)	0.5ºx0.5º (1 km)	16-day	2000-2001	White-sky	15.3 %	Lucht et al.,2000a; Schaaf et al., 2002
					Black-sky	13.5 %	

AVHRR visible (0.58-0.68 μm, channel 1) and near-infrared (0.72-1.1 μm, channel 2) reflectances at 0.5ºx0.5º of spatial resolution were used to calculate the Amazon surface albedo. AVHRR is flown onboard the polar orbiter "NOAA" operational environmental satellites series. AVHRR has no on-board calibration capability for the VIS and near-IR channels used for generating the albedo product. Pre-launch calibration coefficients should not be used because of the degradation of the instrument sensitivity. The channel 1 and 2 digital counts were converted to reflectance values using post-launch calibration coefficients, using the formulae derived by Rao and Chen (1995, 1996). AVHRR uses top-of-the atmosphere (TOA) narrow-to-broadband conversion equation developed by Hucek and Jacobowitz (1995), and ERBE (Suttles et al., 1988) model to account for the bi-directional effects. The atmospheric correction was done using the model by Li and Garand (1994) and the normalization to overhead Sun illumination angle was done by the formula proposed by Briegleb et al. (1986).

I uses the ERBE shortwave (0.2-5.0 μm) channel reflectance at 1ºx1º spatial resolution obtained from re-gridded of original 2.5º x 2.5º resolution. ERBE sensor was launched on the ERBS (Earth Radiation Budget Satellite). Ground calibration sources consist of a reference black-body and an integrating sphere in a vacuum chamber. In flight, an internal black-body, evacuated tungsten lamps, and observation of the Sun are used to check the stability and precision of instruments. Hourly clear-sky radiative fluxes in a grid box are calculated as the averaged fluxes of the clear pixels, which are then converted from radiance through the ERBE angular-directional models (Suttles et al., 1988). Cloud-free scenes are identified through an algorithm that adopts a maximum likelihood estimation technique (Wielicki and Green, 1989).

Surface Radiative Budget (SRB) data for all-sky condition albedo, based on ISLSCP2 (The International Satellite Land Surface Climatology Project) observations, were

calculated from shortwave (0.3-5.0 μm) reflectances at 1ºx1º spatial resolution. No instruments were directly used in the generation of this NASA/GEWEX SRB dataset. All inputs used were higher level products provided by other institutions, as example, all satellite derived radiance and cloud data are from the ISCCP DX data set. Calibration information for ISCCP is available in Brest et al. (1997). Conversion of both narrowband visible cloud and clear radiances into broadband radiances is computed by the Pinker/Laszlo algorithm (Pinker and Laszlo, 1992) and then an angular distribution model (ADM) is applied to convert this radiance to a top-of-atmosphere (TOA) albedo. The TOA albedos for the all-sky conditions are then matched using a radiative transfer model with the meteorological inputs. The advantage of this technique is that the resulting surface fluxes are consistent with the TOA albedos.

Albedos derived from the product GOES/METEOSAT/AVHRR (UMD) and ancillary data, as available from the Global Energy and Water Cycle Experiment (GEWEX) ISCCP DX, were calculated through the shortwave reflectance (0.3-5.0 μm) at 0.5ºx0.5º spatial resolution. These data are also available from the NASA/GEWEX/ISCCP DX observations, as produced in the Department of Meteorology, University of Maryland (UMD) (Pinker, 2002) as part of the LBA (Large-Scale Biosphere-Atmosphere Experiment in Amazonia) Project. Since the ISCCP cloud analysis uses only radiances from the spectral channels common to all radiometers, namely ‘‘visible’’ (wavelength approximately 0.6 μm, called VIS) and ‘‘window’’ infrared (wavelength approximately 1.1 μm, called IR), only these radiances have been calibrated and normalized by ISCCP (Brest and Rossow 1992; Rossow et al. 1992; Desormeaux et al. 1993; Rossow et al. 1996). Data are corrected for Rayleigh scattering and daily variations of solar irradiance and ozone absorption as a function of illumination and viewing geometry (Brest et al., 1997). Indeed, the ISCCP calibration

procedure differs from most in that instead of using one small selected site (e.g., a desert target), it is used a wide variety of targets and the entire globe itself as a target.

MODIS MOD43B albedo product, white-sky (diffuse) and black-sky (direct at solar noon), were determined from shortwave reflectance (0.3-5.0 μm, bb3 broadband) at 0.5ºx0.5º spatial resolution. The MODIS instrument was launched on board NASA's Terra platform. MODIS have four main On-Board Calibrators (Blackbody - BB, Solar Diffuser - SD, Solar Diffuser Stability Monitor - SDSM, and the Spectroradiometric Calibration Assembly - SRCA) that generate various stimuli to provide radiometric, spectral and spatial calibration of the MODIS instrument. The BB is the prime calibration source for the thermal bands located from 3.5 μm to 14.4 μm, while the SD provides a diffuse, solar-illuminated calibration source or the visible, near infrared, and shortwave infrared bands (0.4 μm $\leq \lambda <$ 2.2 μm). The SDSM tracks changes in the reflectance of the SD via reference to the Sun so that potential instrument changes are not incorrectly attributed to changes in this calibration source. The SRCA is a multifunction calibration instrument that provides in-flight spectral, radiometric and spatial calibration. Two additional calibration techniques that MODIS uses are views of the moon and deep space. The MODIS albedo algorithm adopts a semi-empirical, kernel-driven linear Bidirectional Reflectance Distribution Function (BRDF) to characterize the anisotropy of the global surface (Lucht et al., 2000a; Schaaf et al., 2002). The BRDF model relies on the weighted sum of three parameters that are retrieved from the multi-spectral, multi-date, cloud-free atmospherically-connected surface reflectances associated.

To plot the anomaly maps, I aggregated the half-degree and one-degree products to a 2.8º x 2.8º grid, compatible with the CCM3 output. When necessary, a linear interpolation was used to fill the missing values for the ERBE, MODIS white-sky and MODIS black-sky products.

4.2.3. Field albedo measurements

Field data used in this study were measured at three sites in the Amazon region during the ABRACOS (Anglo Brazilian Amazonian Climate Observation Study) and LBA (Large-Scale Biosphere-Atmosphere Experiment in Amazonia) projects. Ducke and Cuieiras (K34) Reserves (02º 57'S, 59º 57' W and 02º 35'S, 60º 06' W) are INPA (Instituto Nacional de Pesquisas da Amazônia) protected forest reserves, about 25 km north-east and 60 km north of Manaus, respectively. Jaru Reserve (10º 05'S, 61º 55"W) is an IBAMA (Instituto Brasileiro do Meio Ambiente e dos Recursos Naturais Renováveis) Forest Reserve and is located about 80 km north of Ji-Paraná in Rondônia State. At the Cuieiras Reserve a piranometer (Kipp & Zonen, Delft, Netherlands), connected to a datalogger model (CR10, Campbell Scientific) measured incident and reflected solar radiation each 30 minutes. For the remaining sites, the incident and reflected solar radiation were measured using two solarimeters (Kipp and Zonen, Delft, the Netherlands). These instruments are part of an automatic weather station (Didcot Instruments, Abingdon, UK) connected to a datalogger (CR10, Campbell Scientific, Shepshed, UK) and hourly-averaged data were recorded. I used incident and reflected solar radiation data, collected from June 1999 to September 2000 at Cuieiras Reserve, from January to December of 1995 at Ducke Reserve and from January to December of 1993 at Jaru Reserve. Data used in this study are available on-line through www.cptec.inpe.br/abracos/available.html and http://lba.cptec.inpe.br/beija-flor.

4.3. RESULTS AND DISCUSSION

Initially, IBIS was calibrated against data measured at Jaru Biological Reserve, with an absolute error of - 0.002 and a root mean square error of 0.007.

Figure 4.1 shows, for the Amazon region, the spatial variability of the average annual albedo (a) simulated by IBIS, and derived remotely sensed products: (b) CG99, (c) ERBE, (d)

SRB/ISLSCP2, (e) UMD, (f) MODIS Black-sky and (g) MODIS white-sky and the respective differences: (h) IBIS–CG99, (i) IBIS–ERBE, (j) IBIS–SRB/ISLSCP2, (k) IBIS–UMD, (l) IBIS–MODIS Black-sky and (m) IBIS–MODIS white-sky.

It can be seen through the anomaly maps (Figures 4.1h to 4.1n) that the remote sensing albedo products that present best agreements related to CCM3 were MODIS-bsa (difference -1) and the CG99 (difference +1.5), as showed in the Figures 1b and 1e, respectively. The other products SRB/ISLSCP2, UMD, MODIS-wsa and ERBE present average anomalies of -2.5, -2.5, -2.8 and -3.0, respectively. The smallest differences between CCM3 model and MODIS-bsa that calculate wholly direct radiation probably occur because CCM3 may be giving higher weighting to direct radiation rather than to diffuse radiation in the algorithm used to calculate the albedo. In addition, the worst simulation of MODIS white- compared to black-sky albedos may be explained by the overestimation the increase of albedo with solar zenith angle (Oleson et al., 2003). The authors found 1% to 5% to VIS and 1% to 15% in the NIR, while in this work MODIS white-sky albedo overestimated the black-sky albedo in 13% approximately.

Differences among the remotely sensed albedos from several products studied may be attributed by the different spectral distribution of incoming radiation and the capacity of the algorithms of each product to filter the confounding effects such as atmospheric scattering and absorption anisotropy, inadequate spatial sampling and narrowband to broadband conversions (Oleson et al., 2003). In addition, although all of these instruments have been carefully calibrated, some differences among them are expected (Smith et al., 2006), including the continuous degradation while they are in orbit (eg. degradation of spectral response of each channel).

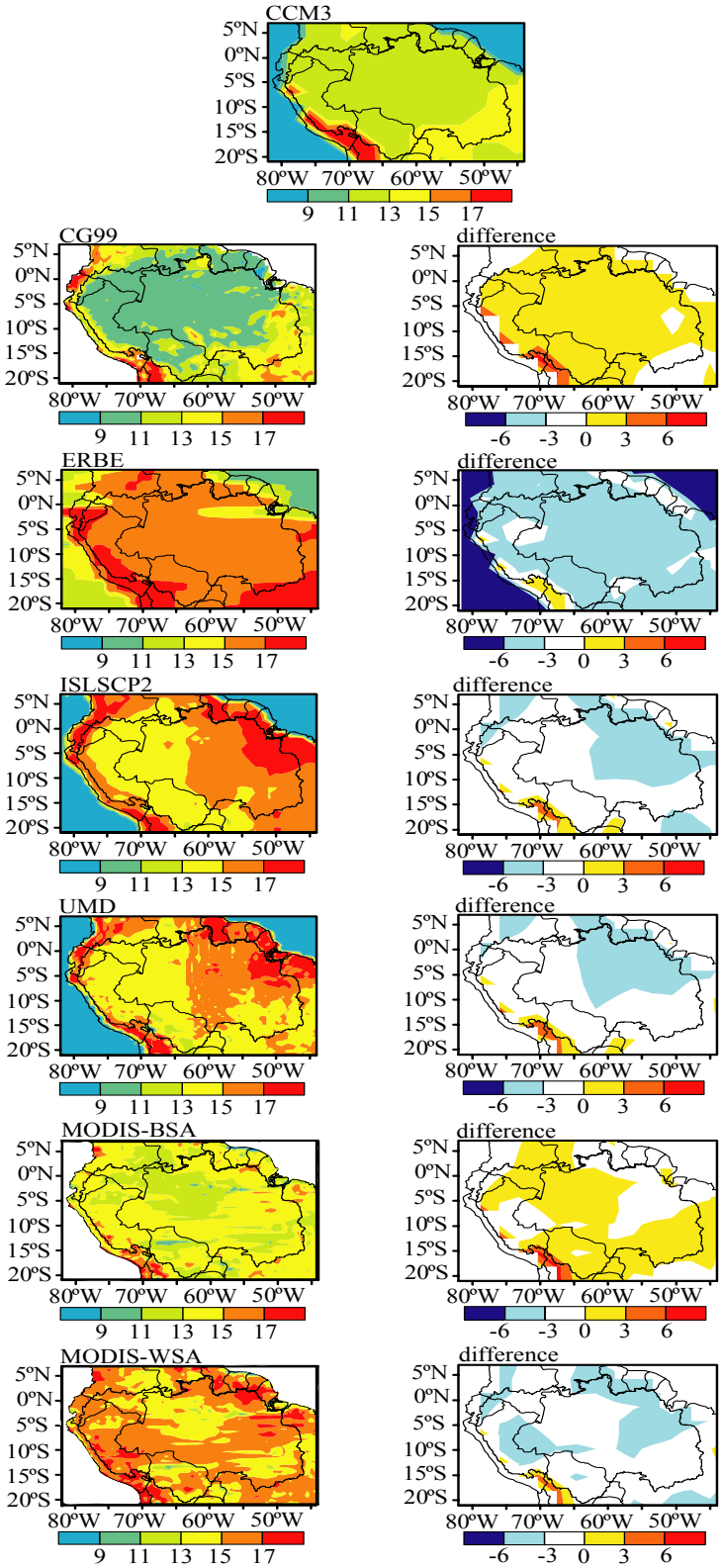

Figure 4.1. Spatial variability of the surface albedo simulated by the (a) CCM3 model and albedo products derived from six remote sensing for Amazon basin: (b) CG99, (c) ERBE, (d) SRB/ISLSCP2, (e) UMD, (f) MODIS Black-sky and (g) MODIS white-sky and it respective anomalies: (h) CCM3-CG99, (i) CCM3-ERBE, (j) CCM3-SRB/ISLSCP2, (k) CCM3-UMD, (l) CCM3-MODIS Black-sky and (m) CCM3-MODIS white-sky.

Figure 4.2 shows the seasonal profile of the CCM3 simulated albedo and albedo products derived from six remote sensing (CG99, ERBE, SRB-ISLSCP2, UMD, MODIS White-sky and black-sky) for the Amazon basin and also representation of field albedo data at the Biological Reserves of Cuieiras (K34), Ducke and Jaru. Overall, an overestimation of the albedo derived from the satellites products in relation to the CCM3 model was observed, except for CG99 product that underestimated it. Brest et al. (1997) examining a complete 8-year record of cloud and surface properties obtained with the first calibration reveals a systematic "step-down" in monthly global mean VIS reflectance at each transition of polar orbit from NOAA-7 to NOAA-9 between January and February 1985, and from NOAA-9 to NOAA-11 between October and November 1988 (Klein and Hartman, 1993; Rossow and Cairns, 1995). On the other hand, Csiszar and Gutman (1999) affirm that heavy aerosol loading introduces errors for extremely low or high albedos. It can be observed during the end of the dry-season, because the biomass burning aerosols. In addition, the initial monthly product showed obvious aerosol signal in tropical evergreen regions; hence monthly values were replaced by yearly minima in those areas. The amplitudes among the simulated albedo (CCM3) and those generated by the satellite products as well those measured punctually at the field by meteorological tower were smaller under the less rainy period (from June to August), except for ERBE product. The better agreement for this period is probably due to best chance for obtaining cloud- and smoke-free background values.

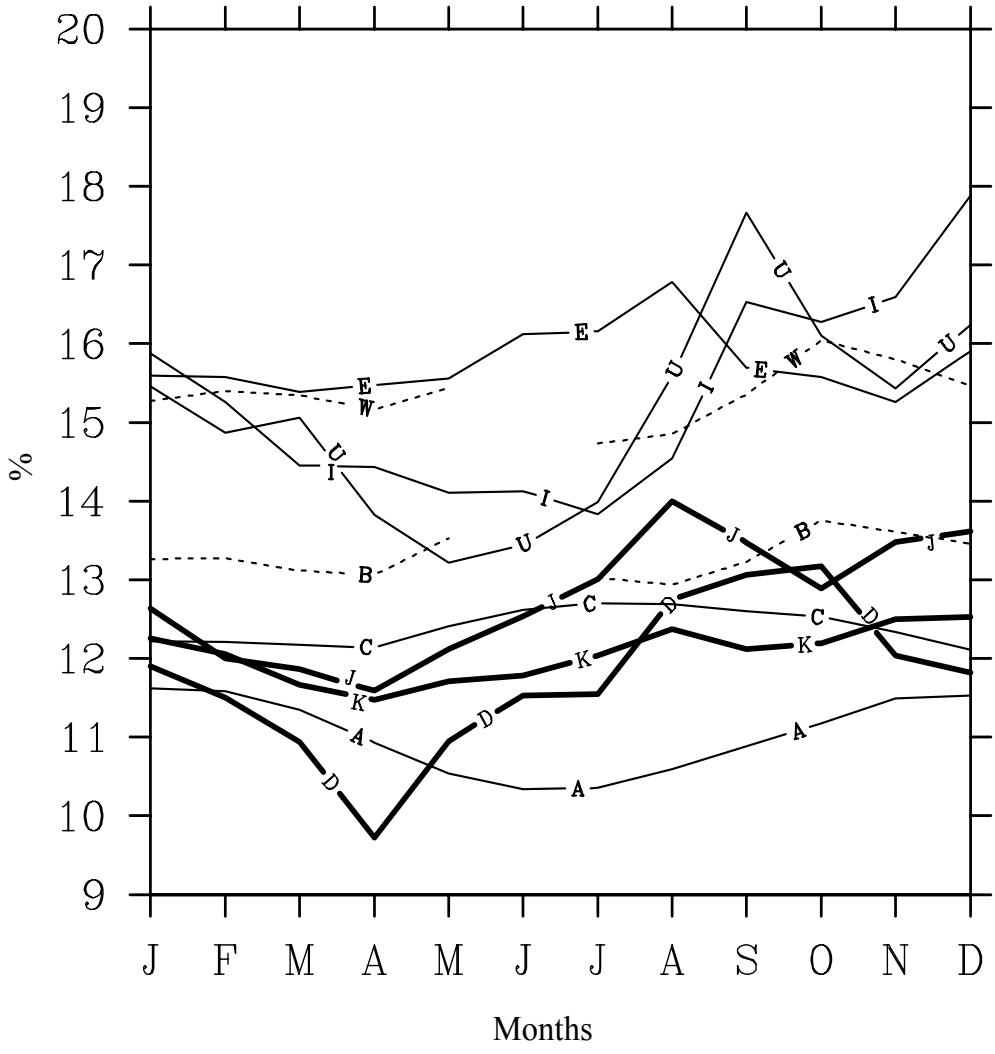

Figure 4.2. Seasonal variability of the surface albedo simulated by the CCM3 model and albedo products derived from six remote sensing for Amazon basin, and measured at three study sites.

Figure 4.3 shows the seasonal profile of the albedo simulated by the CCM3 model and the albedo derived by the six remote sensing products for the representative pixels which include the micrometeorological towers of the Biological Reserves of (a) Cuieiras (K34) and Ducke and (b) Jaru. Observing the isolated pixel, a good adjustment of the field measured data at the three sites: Cuieiras and Ducke, located at Amazonas State (Figura 4.4a); and at Jaru (Figura 4.4b), located at Rondônia State. Overall, MODIS-bsa presented the smallest amplitude when compared to field measurements and CCM3 simulation data, again. The smallest albedo differences among the satellite products and simulated by the CCM3 model were observed from June to August (less rainy period), probably because there are less cloudiness as confirmed by amount of pixels contaminated by cloud (Durieux et al., 2003), reducing the number of pixels contaminated by clouds, except for ERBE product (Figure 4.3b). Highest albedo differences were found for the Biological Reserves of Cuieiras and Ducke, probably due to both are located nearby urban-areas, causing higher vegetation cover variability (Figure 4.3a).

As can be seen in Figures 4.2 and 4.3, the greatest differences between the albedos computed by CCM3 and ERBE, from June to August, probably are due to aerosol effects not included in the calculation and some due to the fact that ERBE may designate scenes as clear when they have a small amount of sub-pixel cloudiness in their view. For the other months, higher amplitude values may be attributed by the cloud contamination of the scenes (especially during the rainy season, from December to May), the instruments errors, the sampling errors, and the uncertainties in models used in the data processing. Indeed, the increase of biomass burning aerosols in the atmosphere, with peak in September, contributes to the increase of the amplitude among the satellite albedo products and CCM3 albedo model, especially for the pixel comprising the Jaru Reserve (Ji-Paraná, RO), which is located in the Amazon arc of

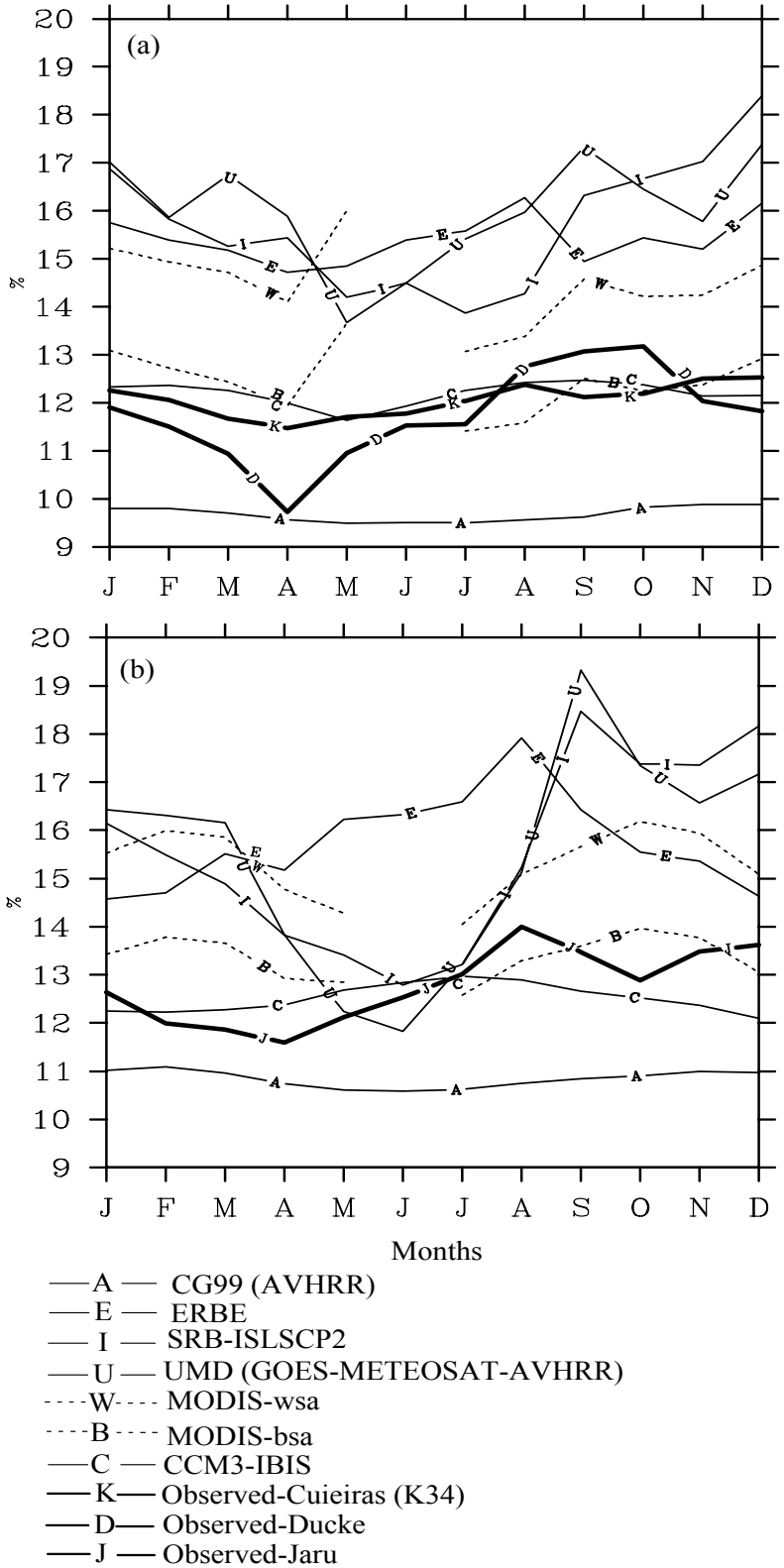

Figure 4.3. Seasonal variability of the surface albedo simulated by the CCM3 model and albedo products derived from six remote sensing for the pixels comprising the three study sites, and albedo measured at the (a) Manaus (Cuieiras and Ducke) and (b) Jaru sites.

deforestation. In this specific site, UMD and SRB/ISLSCP2 products presented greatest variation in relation to the CCM3 model and the field-observed albedos.

In spite of field measurement albedo data is adequate to characterize a specific site; some differences are foreseen when compared to remotely sensed data, because some spatial variability is expected in the vicinity of any tower even in relatively homogenous locations (Lucht et al., 2000b).

Although validation of a satellite derived albedo is almost impossible, once aircraft measurements cover large areas, ground truth albedo can be used as a procedure to assess the uncertainty of the estimated product (Lucht et al., 2000b; Justice et al., 2000; Jin et al. 2003).

In spite of some improvements of the remote sensing albedo products have been observed during the last years, it is important to point out that incorporation of more accurate models and atmospheric information at different steps of the retrieval procedure may improve the quality of albedo products.

4.4. SUMMARY AND CONCLUSIONS

In this work, simulated albedo is computed by CCM3 coupled with IBIS and compared against six different albedo products derived from remote sensing: CG99, ERBE, SRB-ISLSCP2, UMD, MODIS white-sky and MODIS black-sky), including also representation of field albedo data at three study sites (Cuieiras, Ducke, and Jaru Reserves). A considerable variation among the albedo estimated by the different remote sensing products was observed, including great seasonal differences. MODIS black-sky albedo product presents the smallest amplitude in relation to the CCM3 simulated and field observed albedos. Biomass burning aerosols released to atmosphere, especially during the end of dry season, introduces increased errors to the surface albedo retrieved from UMD, SRB-ISLSCP2 and ERBE. These results suggest that some caution be exercised when using satellite albedo products over the Amazon basin and

more accurate sensors and algorithms need to be developed for reducing the uncertainties involved in the data processing.

CHAPTER 5

RADIATIVE PROCESSES OF PRECIPITATION CHANGE AFTER TROPICAL DEFORESTATION

5.1. INTRODUCTION

Amazon is one of the regions where the regional climate response to the underneath vegetation is most intense. According to several studies, that studied slightly different scenarios using different climate models, a large-scale conversion of tropical rainforest to pastureland leads to a decrease in local precipitation, which is linearly related to surface albedo changes (Figure 5.1).

Despite this general agreement, there are still many unanswered questions regarding the effects of tropical deforestation on the regional climate. For example, it has not been explained why some experiments, like Nobre et al. (1991), show a consistent decrease in precipitation over all the deforested area, while others (eg. Lean and Rowntree, 1997; Costa and Foley, 2000) show different spatial patterns of decrease/increase of

precipitation, with a predominance of decrease. In addition, there is a contradiction between large-scale numerical deforestation studies, which predict a decrease in cloudiness and precipitation, and the observations of the current climate above deforested areas, which show increased cloudiness (Cutrim et al., 1995; Negri et al., 2004). The answer to these questions may lie on the competing effects that non-radiative and radiative processes have on the determination of precipitation change after a tropical deforestation, as well as on the linear response of precipitation to surface albedo (Dirmeyer and Shukla, 1994; Berbet and Costa, 2003, among others).

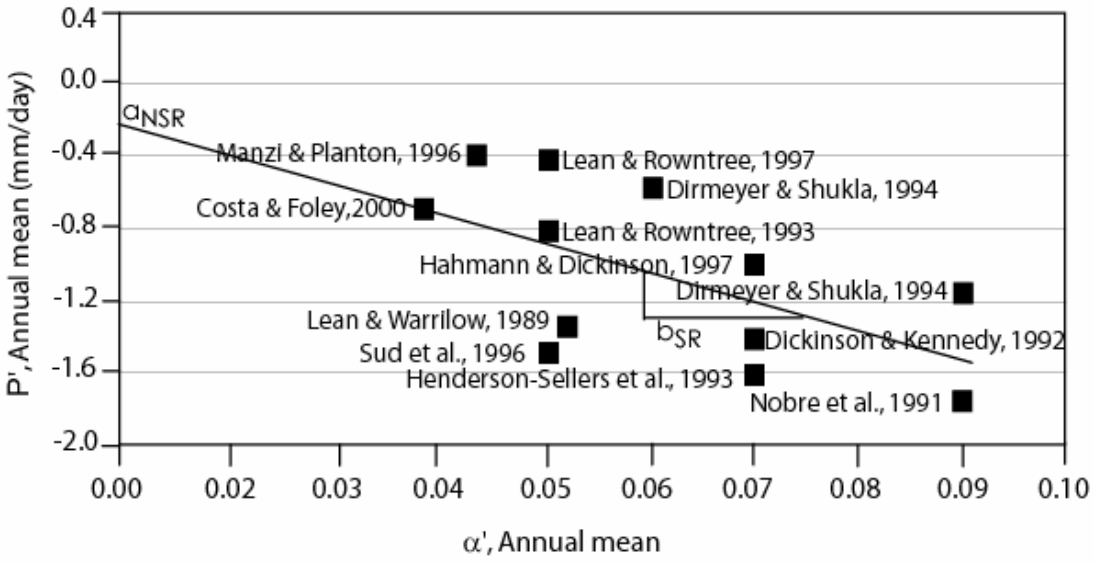

Figure 5.1. Annual mean precipitation profile as a function of albedo changes for different climatic experiments.

In this context, I run eleven simulations using the NCAR Community Climate Model (CCM3) coupled to the Integrated Biosphere Simulator (IBIS) to carefully investigate these processes. This chapter concentrates on the radiative processes of the precipitation change after tropical deforestation, while a companion paper will investigate the effects of non-radiative processes on the Amazon precipitation changes. The numerical

experiment is designed to cover a wide range of changes in land surface albedo and in surface net radiation, so that reliable relationships between precipitation change and radiative budget could be obtained.

This chapter is organized in 8 sections: Sections 2 and 3 describe the models used and the experiment design, Sections 4 to 6 present the results of the numerical climate experiment and Sections 7 and 8 present a discussion and conclusions.

5.2. MATERIALS AND METHODS

5.2.1. Description of the CCM3-IBIS model

The NCAR Community Climate Model – CCM3 (Kiehl et al., 1998) is a spectral atmosphere model of the horizontal fields. The model operates at a resolution of T42, at about 2.81° x 2.81° and has 18 vertical levels and operates with a 20-min step. The diagnosis of cloud fraction represents a generalization of the scheme introduced by Slingo (1987) and depends on relative humidity, vertical pressure velocity, ω; atmospheric stability; and the convective mass flux associated with parameterized moist convection. Three types of cloud are diagnosed by the scheme: convective cloud, layered cloud, and low-level marine stratus (Kiehl et al., 1998). Precipitation occurs in two forms: stable and convective. When the column is stable to moist convection, only stable precipitation occurs whenever saturated conditions exist. The phase of precipitation for surface accumulation depends on low-level temperature. Convective precipitation occurs when the column is unstable to moist convection and this precipitation process is monthly independent of the cloud prediction scheme and of the radiative properties of clouds (Kiehl et al., 1998).

The land surface radiation budget is computed by the Integrated Biosphere Simulator – IBIS (Foley et al., 1996). IBIS has two vegetation layers (i.e., trees and short vegetation), a variable number of soil layers, and includes representations of land surface

processes, like energy, water and momentum exchange between the soil-vegetation-atmosphere system, and also includes vegetation dynamics component that, in this study is disabled (use only static vegetation). In IBIS, the exchange of solar radiation between the soil-vegetation-atmosphere system is calculated following the standard two-stream approximation, with separate calculations for direct and diffuse radiation in both visible (VIS) and near-infrared (NIR) bands. In these simulations, IBIS operated on the same T42 spatial resolution as the CCM3 atmospheric model. I also modified the IBIS model to introduce a new land cover type, a soybean cropland. This new land cover type is based on the physiology of a C3 grass, but has specific phenology parameterizations that emulate a soybean crop that grow in Amazonia.

5.2.2. Experiment design

A climate experiment is designed to elucidate the radiative effects of precipitation change after tropical deforestation on regional climate in Amazon. All of the simulations are run for 12 years, using the same initial conditions, but only the last 10 years are averaged to analyze the results. The first two years of simulation are discarded, and are used to let the model reaches an equilibrium state, specifically with respect to soil moisture. In all simulations, sea surface temperature and atmospheric composition are set to the average of 1990 decade.

In this study, I conducted eleven simulations, described below:

(a) Control runs (Rainforest land cover): We run two repetitions (F^a, F^b), where the only difference between them is the albedo of the rainforest, which is set to 0.125 (F^a) and 0.129 (F^b), respectively (Culf et al., 1995). LAI and biomass of the rainforest are set to 5.94 m^2 m^{-2} and 10.36 kg C m^{-2} (Roberts et al., 1996; Medina and Cuevas, 1996);

(b) Pasture land expansion. It is divided in three different simulations, where pastureland partially replaces the original rainforest in each Amazonia grid cell, increasing gradually from 0% (control run) to 25%, 50% and 75%. For each level of deforestation, I run two repetitions ($P^{a}_{25\%}$, $P^{b}_{25\%}$, $P^{a}_{50\%}$, $P^{b}_{50\%}$, $P^{a}_{75\%}$, $P^{b}_{75\%}$) where the unique difference between them is the albedo of the pasture, which is set to 0.177 and 0.182, respectively (Culf et al., 1995). Average LAI of the pastureland is set to 3.18 $m^2\ m^{-2}$ (Roberts et al., 1996; Medina and Cuevas, 1996);

(c) Soybean land expansion. It is divided in three simulations, where each Amazonia grid cell partially replaces the original rainforest by pastureland, increasing gradually from 0% (control run) to 25% ($S_{25\%}$), 50% ($S_{50\%)}$ and 75% ($S_{75\%}$).

In this climate experiment, I assumed a planting date of January 5th as most representative for the region, representing an increasing of albedo and LAI during harvest with maximum peak of 0.26 and 5.98 $m^2\ m^{-2}$, respectively, in March 19th, decreasing after the harvest in May when the leaves fall and dry, completing, this way, the seasonal cycle of soybean crop. In our model representation of soybean albedo, I chose to represent the values of albedo according to the literature that suggest a peak of 0.26 (Blad and Baker, 1972; André and Viswanadhan, 1983; Fontana et al., 1991).

5.3. RESULTS

5.3.1. Precipitation dependence on surface radiation balance

In this study, I evaluated the radiative processes of precipitation change after tropical deforestation through the analysis of the anomaly fields of precipitation (P'), surface reflected radiation (Sr'), surface net radiation (Rn'), total cloud cover (C') and vertical wind velocity (ω') between deforested (pasture and soybean) and forested conditions, considering the deforestation levels of 25%, 50% and 75% for both pasture and

soybean cropland. The use of pasture and soybean land covers for the deforested cases, as well as the use of different deforestation levels, allows the study of a wider range of surface radiation anomalies, helping to establish the relationships between the variables.

Figure 5.2 shows the linear relationship between the precipitation anomalies, P' (difference between $P^{ab}_{25\%}$, $P^{ab}_{50\%}$, $P^{ab}_{75\%}$ and F^{ab}) against the annual mean albedo anomalies, α' (Figure 5.2a) and against the annual mean net radiation, Rn' (Figure 5.2b) for the

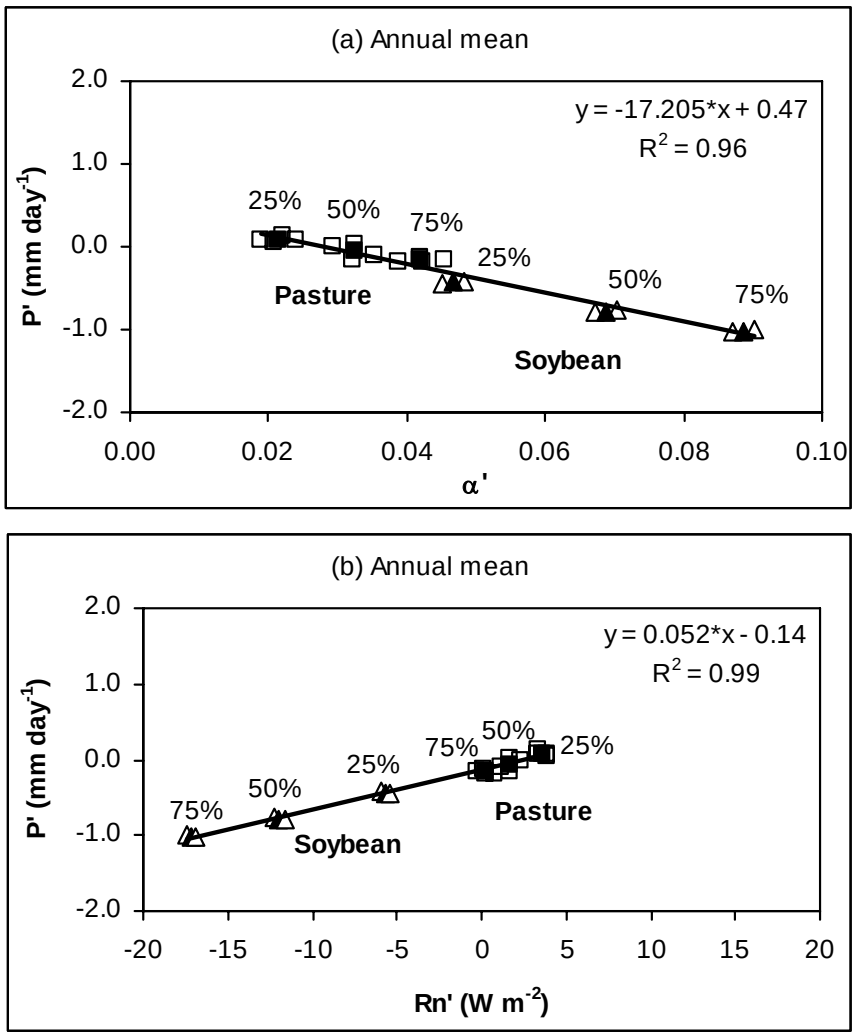

Figure 5.2. Annual mean precipitation anomaly as a function of albedo anomaly (a) and net radiation anomaly (b), for different levels of pastureland and soybean cropland expansions.

different types of land cover (pasture and soybeans) and different levels of deforestation (25%, 50% and 75%). Changes in land surface albedo and in surface net radiation explain about 96% ($P<10^{-15}$) and 99% ($P<10^{-21}$) of the precipitation anomaly variance. These results are similar to those presented in Figure 5.1, although they have less dispersion, due to the use of a single climate model.

To represent the seasonal variability in both incoming radiation (S_{in}) and surface albedo, I studied the changes in the precipitation after deforestation against changes in the reflected radiation after deforestation (Sr', $Sr = S_{in}\ \alpha$.) and surface net radiation (Rn') at the semester and trimester time scales. In these analyses, each point represents an average of each band of latitude, totaling eight bands throughout the studied area.

In a semester basis (Figure 5.3), it is observed a linear decrease of precipitation anomaly with the increase of Sr' variance (R^2 varies from 42 to 47%) and with the decrease of Rn' (R^2 varies from 56 to 73%). The same profile is observed at a trimester basis (Figure 5.4). Overall, 26% ($P<10^{-13}$) of variance in P' is explained by the variance in Sr' when all trimesters are analyzed (Figure 5.4e), agreeing with the 28% found by Berbet and Costa (2003). For each 10 W m^{-2} increase in Sr', the precipitation is reduced by approximately 0.63 mm day^{-1}, while a reduction of 10 W·m^{-2} in Rn' induces a decrease in the range of 0.31- 0.38 mm day^{-1}.

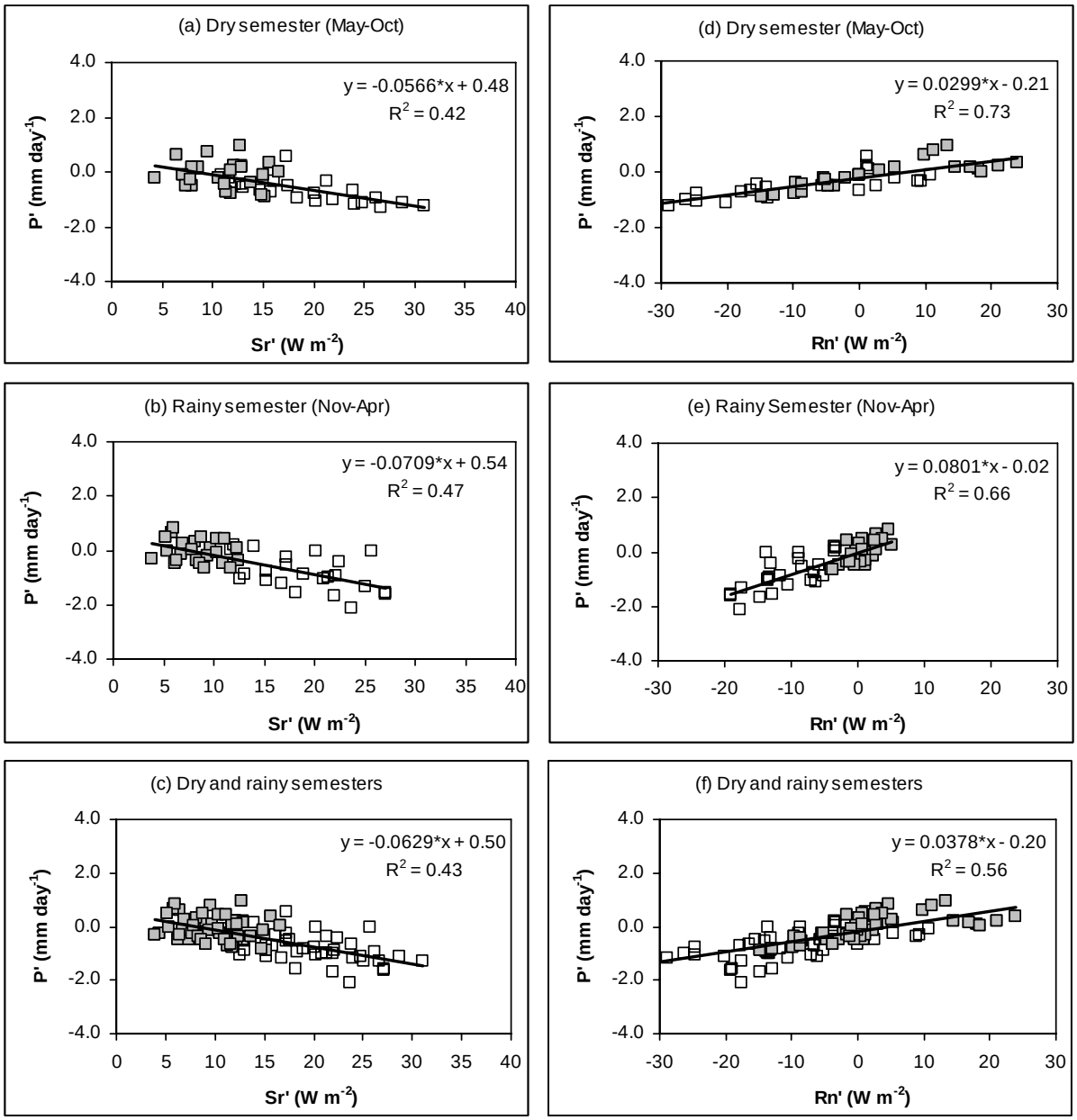

Figure 5.3. Semester mean precipitation anomaly as a function of albedo anomaly for the dry semester (a), rainy semester (b), and both (c), and as a function of net radiation anomaly for the dry semester (d), rainy semester and both (f). White squares represent pastureland and gray squares represent soybean cropland.

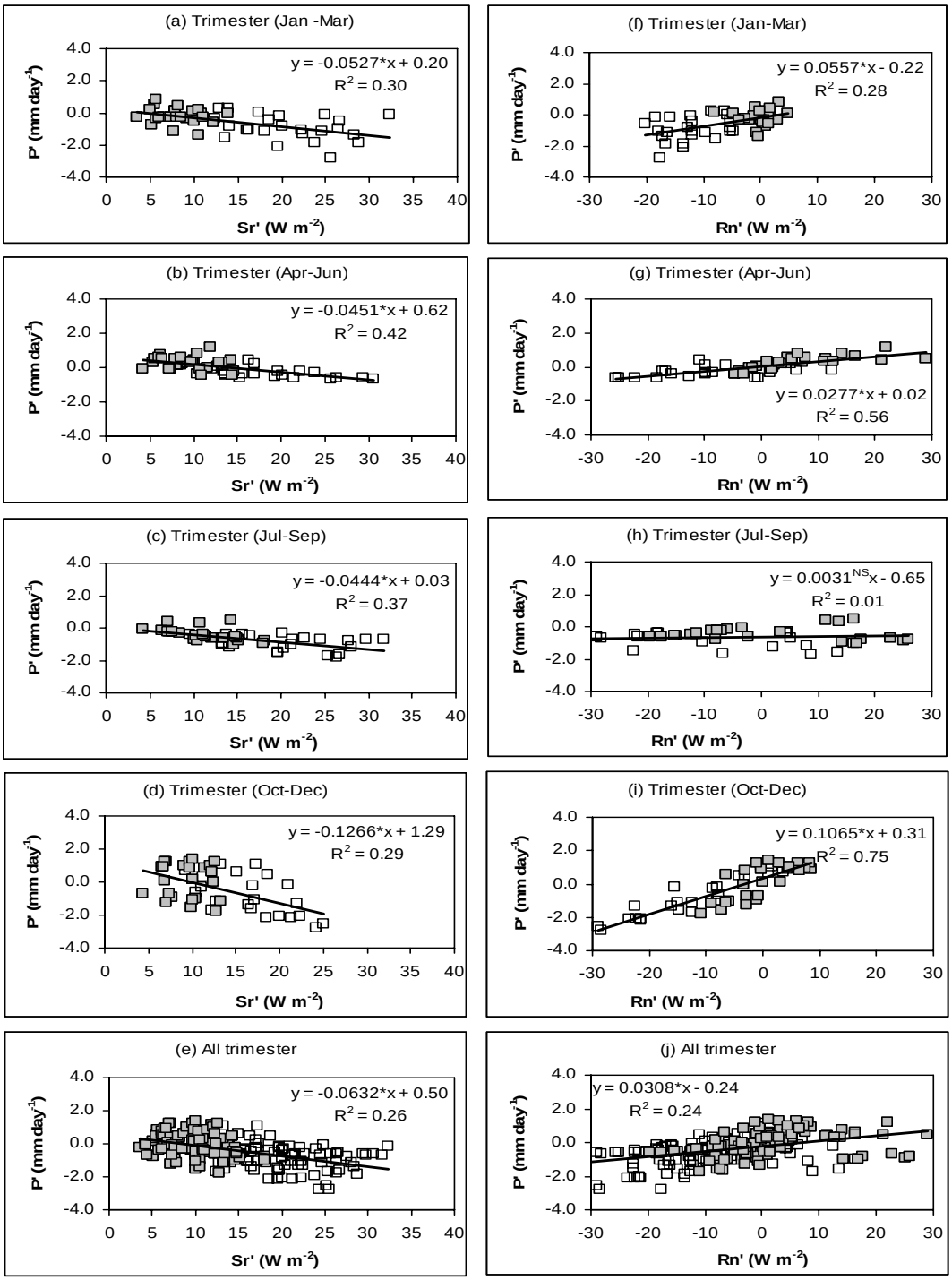

Figure 5.4. Trimester mean precipitation anomaly as a function of albedo anomaly for the January to March trimester (a), April to June trimester (b), July to September trimester (c), October to December trimester (d) and all trimesters (e), and as a function of net radiation anomaly for the January to March trimester (f), April to June trimester (g), July to September trimester (h), October to December trimester (i) and all trimesters (j). White squares represent pastureland and gray squares represent soybean cropland.

5.3.2. Clouds dependence on surface radiation balance and feedbacks on the incoming solar radiance

Figure 5.5 shows the annual mean cloudiness anomalies (C') as a function of albedo and net radiation anomalies. Changes in land surface albedo and in annual mean net radiation explain about 97% ($P<10^{-16}$) and 88% ($P<10^{-10}$) of the cloudiness variance, respectively, when different types of land cover and levels of deforestation were considered. An increase in α' or a decrease in Rn' induces a decrease in C'.

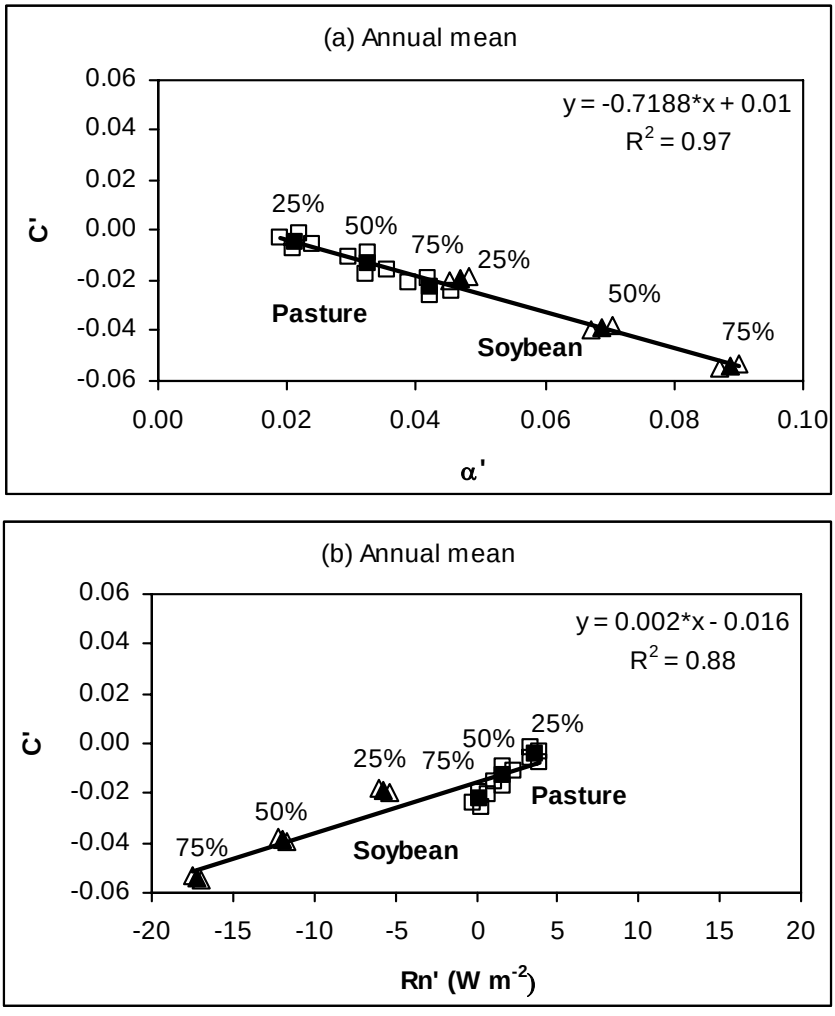

Figure 5.5. Annual mean total cloud anomaly as a function of albedo anomaly (a) and net radiation anomaly (b), for different levels of pastureland and soybean cropland expansions.

Similar results are found at the semester (Figure 5.6) and trimester (Figure 5.7) basis. Variations in C' are better explained by Sr' and Rn' during the rainy season than during the dry season (Figures 5.6b, 5.6c, 5.7a, 5.7f and 5.7i). Note that positive values of C' are common for low levels of pastureland expansion (low Sr'). This is consistent with the results found by several authors. Initially, Chu et al. (1994) analyzed outgoing longwave radiation (OLR) from 1974 to 1990 and monthly rainfall totals at Belém and Manaus. Both analyses showed increasing trends in cloudiness and precipitation (related to an increase in convection) associated with deforestation over almost the entire Amazon basin. The most significant increase in convection was found in the western equatorial part of Amazonia, along the eastern slope of the Andes, where rainfall is most abundant. In addition, Cutrim et al. (1995) using the GOES (Geostationary Operational Environmental Satellite) visible imagery, demonstrated that an enhanced frequency of shallow cumulus cloudiness is formed primarily over deforested regions and over topographic elevations during the dry season in the Amazon.

Furthermore, Negri et al. (2004) observed that in the dry season, when the effects of the surface are not overwhelmed by large-scale weather disturbances, cumulus cloudiness, deep convective cloudiness, and rainfall occurrence are larger over the deforested and savanna regions than over areas of dense forest. This can be in response to a local circulation initiated by the differential heating of the region's varying forestation. Finally, Durieux et al. (2003) verified during the wet season that convective cloudiness is stronger over deforested areas, while a significant decrease in convective cloudiness is seen during the dry season, together with an increase in low-level clouds, mainly made up of shallow cumulus clouds, that with subsequent expansion of deforestation these clouds tend to stabilize.

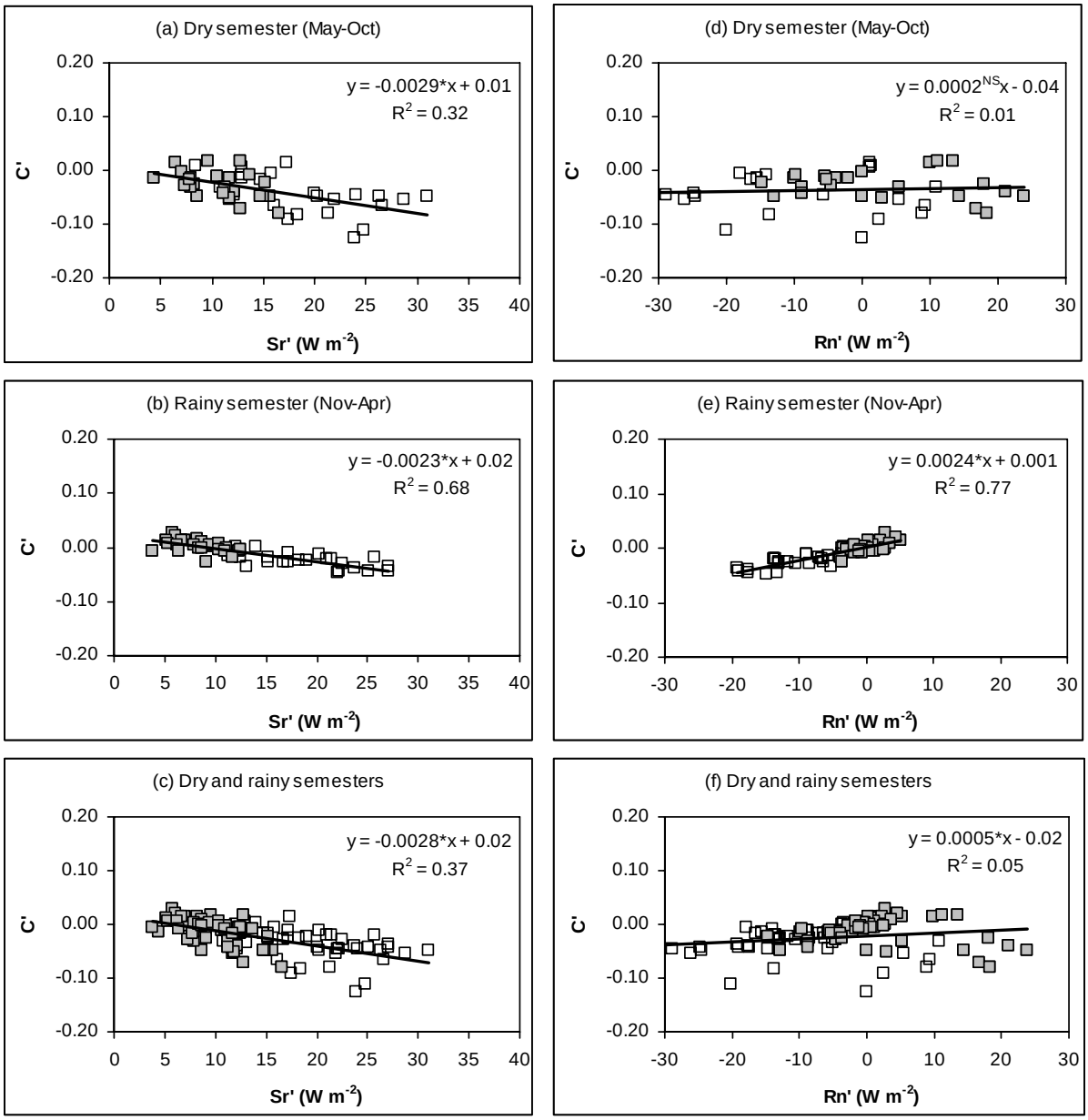

Figure 5.6. Semester mean total cloud anomaly as a function of albedo anomaly for the dry semester (a), rainy semester (b), and both (c), and as a function of net radiation anomaly for the dry semester (d), rainy semester and both (f). White squares represent pastureland and gray squares represent soybean cropland.

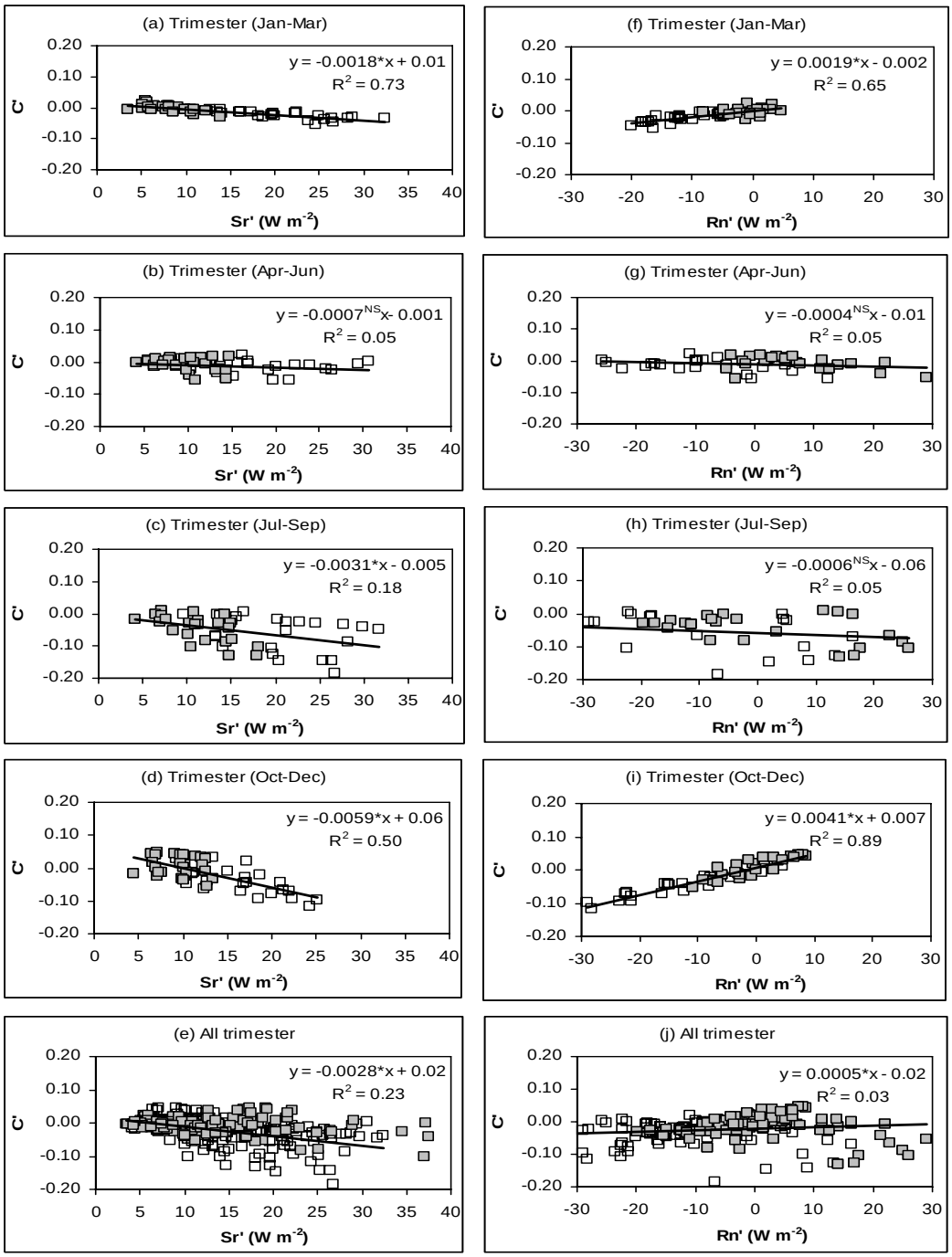

Figure 5.7. Trimester mean total cloud anomaly as a function of albedo anomaly for the January to March trimester (a), April to June trimester (b), July to September trimester (c), October to December trimester (d) and all trimesters (e), and as a function of net radiation anomaly for the January to March trimester (f), April to June trimester (g), July to September trimester (h), October to December trimester (i) and all trimesters (j). White squares represent pastureland and gray squares represent soybean cropland.

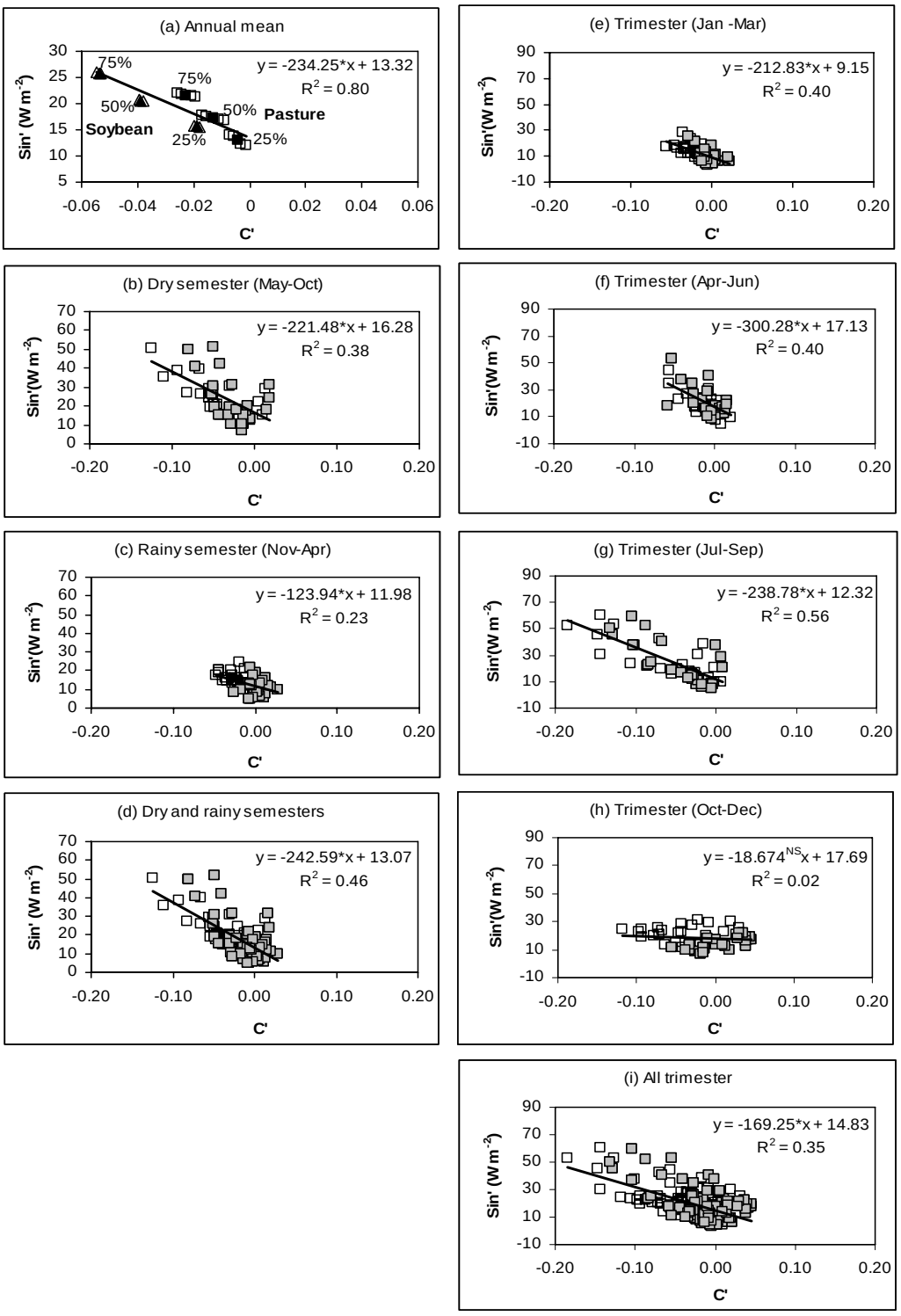

Figure 5.8. Annual mean incoming solar radiation anomaly as a function of total cloud anomaly (a) for different levels of pastureland and soybean cropland expansions. Semester mean incoming solar radiation anomaly as a function of total cloud anomaly for the dry semester (a), rainy semester (b), and both (c). Trimester mean incoming solar radiation anomaly as a function of total cloud anomaly for the January to March trimester (a), April to June trimester (b), July to September trimester (c), October to December trimester (d) and all trimesters (e). White squares represent pastureland and gray squares represent soybean cropland.

The incoming radiation cloud feedbacks are shown in Figure 5.8. Changes in annual mean cloudiness explain about 80% ($P<10^{-7}$) of the annual mean incoming solar radiation variance. A linear relationship is observed for all studied cases, presenting a positive anomaly that decreases with the increase of cloudiness anomaly. The higher dispersion of the data, compared to the previous analyses, is probably due to the several types of clouds and optical properties present in the region

5.3.3. Convection dependence on surface radiation balance

Figure 5.9 shows the relationship between vertical wind velocity anomaly at 500 hPa (ω') and albedo and net radiation anomalies for different types of land cover and different levels of deforestation. A positive anomaly indicates a stronger subsidence over the studied area. Changes in land surface albedo and in net radiation explain about 89% ($P<10^{-11}$) and 97% ($P<10^{-17}$) of the vertical wind variance, respectively.

Similar results are found at the semester (Figure 5.10) and trimester basis (Figure 5.11). Following the results for the cloudiness, ω' is more dependent on Sr' and Rn' during the rainy season than during the dry season (Figure 5.10), in particular during Oct-Dec (Figure 5.11d and 5.11i).

Figure 5.12 shows the linear relationship of the precipitation anomalies as a function of ω' in an annual, semester and trimester basis. At the annual basis, 98% ($P<10^{-17}$) of variation of the precipitation anomaly is explained by the changes in ω'. The precipitation anomaly reduces with the increase of the ω' anomaly. Changes in Rn' and α', due to the replacement of forest in different types of land cover (pasture and soybean crop), cause changes on precipitation and vertical wind velocity. Similar profile is verified at the semester and trimester analysis (Figures 5.12b to 5.12i).

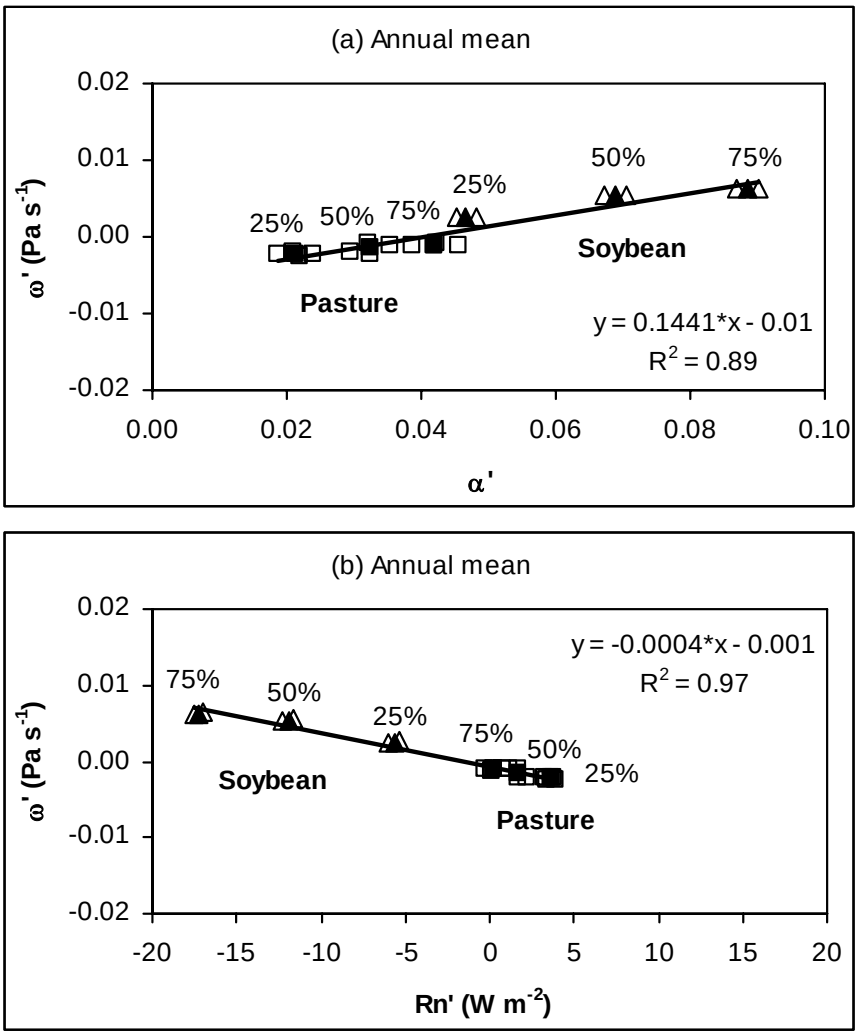

Figure 5.9. Annual mean vertical velocity anomaly as a function of albedo anomaly (a) and net radiation anomaly (b), for different levels of pastureland and soybean cropland expansions.

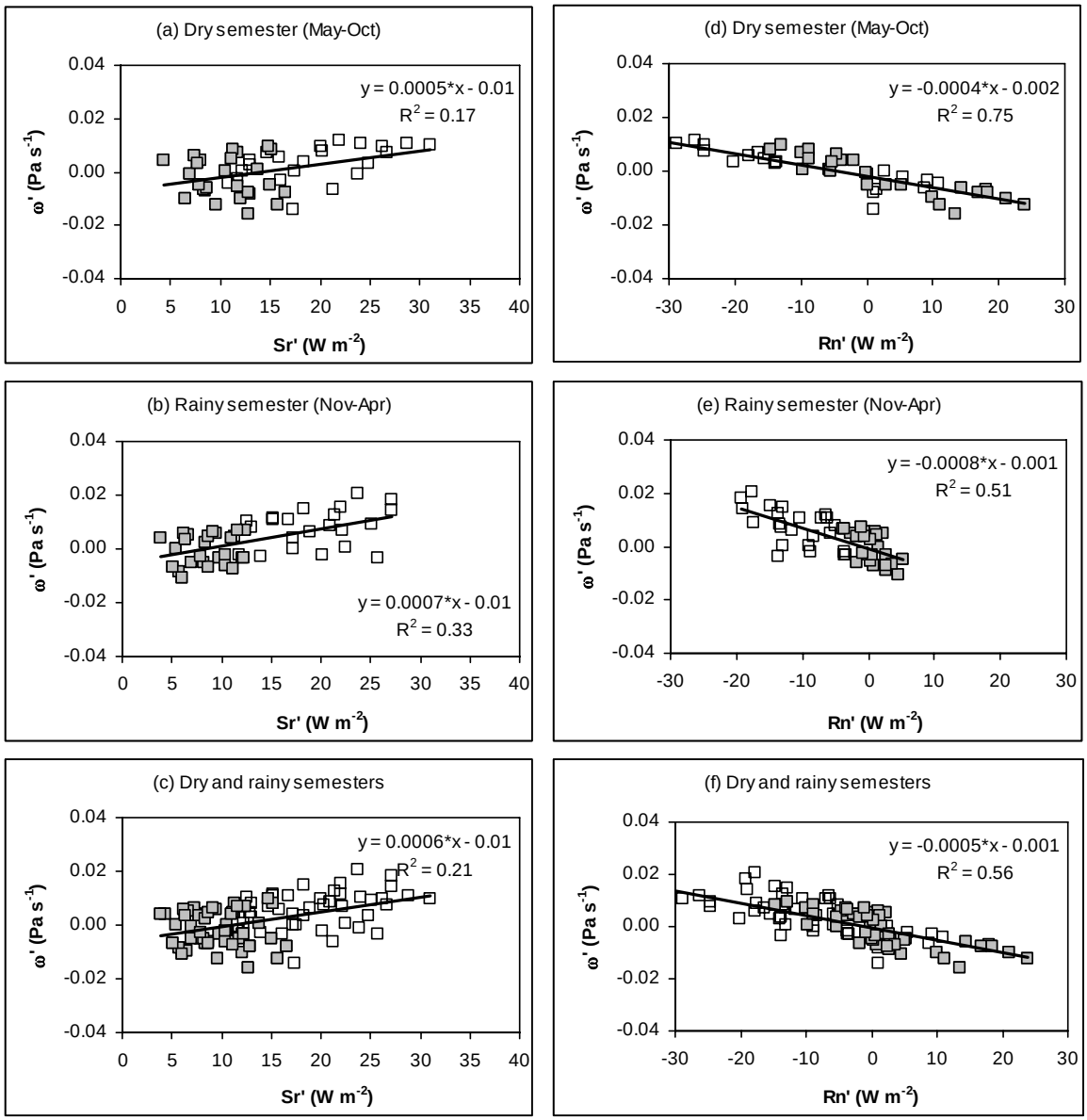

Figure 5.10. Semester mean vertical velocity anomaly as a function of albedo anomaly for the dry semester (a), rainy semester (b), and both (c), and as a function of net radiation anomaly for the dry semester (d), rainy semester and both (f). White squares represent pastureland and gray squares represent soybean cropland.

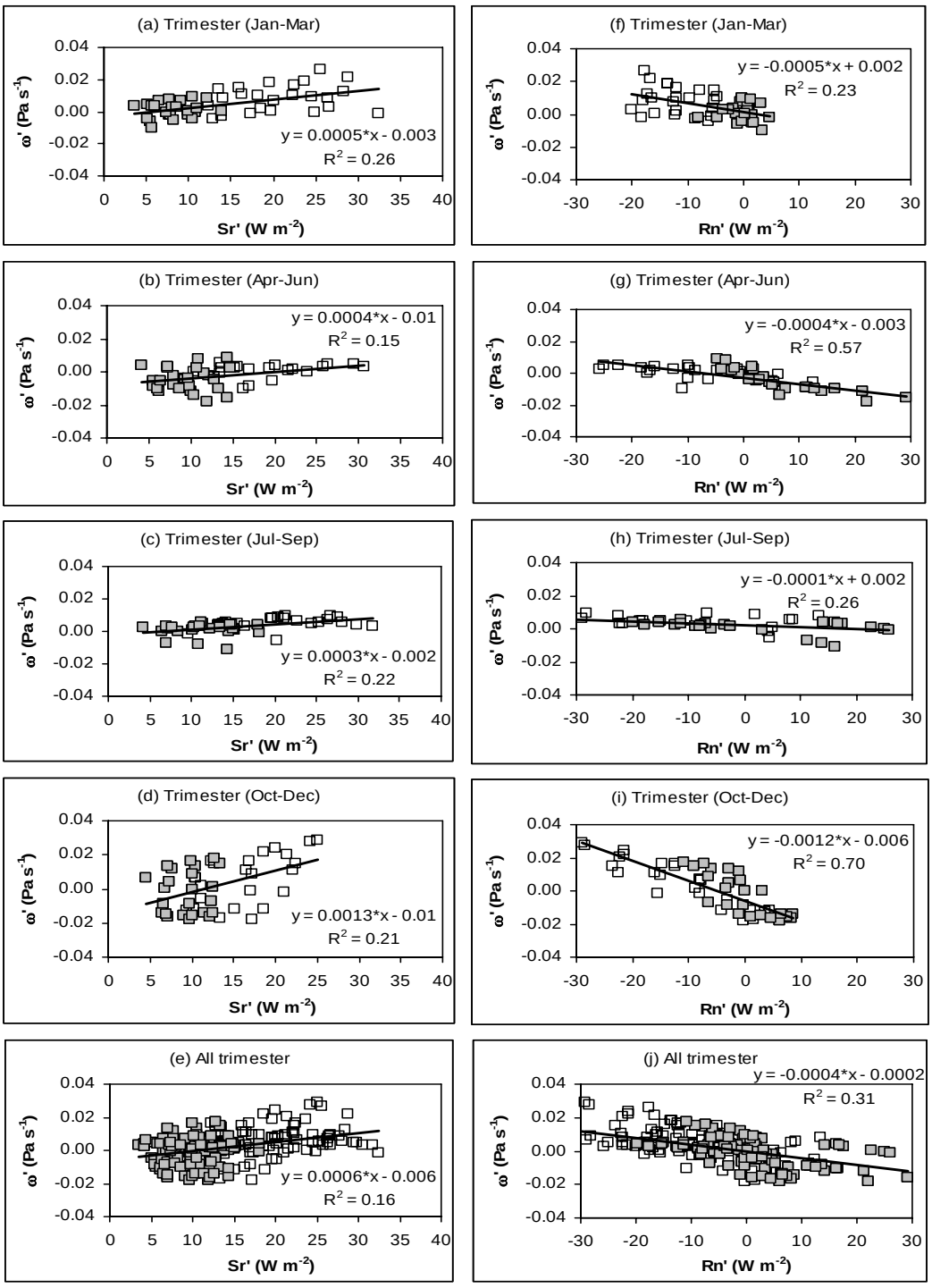

Figure 5.11. Trimester mean vertical velocity anomaly as a function of albedo anomaly for the January to March trimester (a), April to June trimester (b), July to September trimester (c), October to December trimester (d) and all trimesters (e), and as a function of net radiation anomaly for the January to March trimester (f), April to June trimester (g), July to September trimester (h), October to December trimester (i) and all trimesters (j). White squares represent pastureland and gray squares represent soybean cropland.

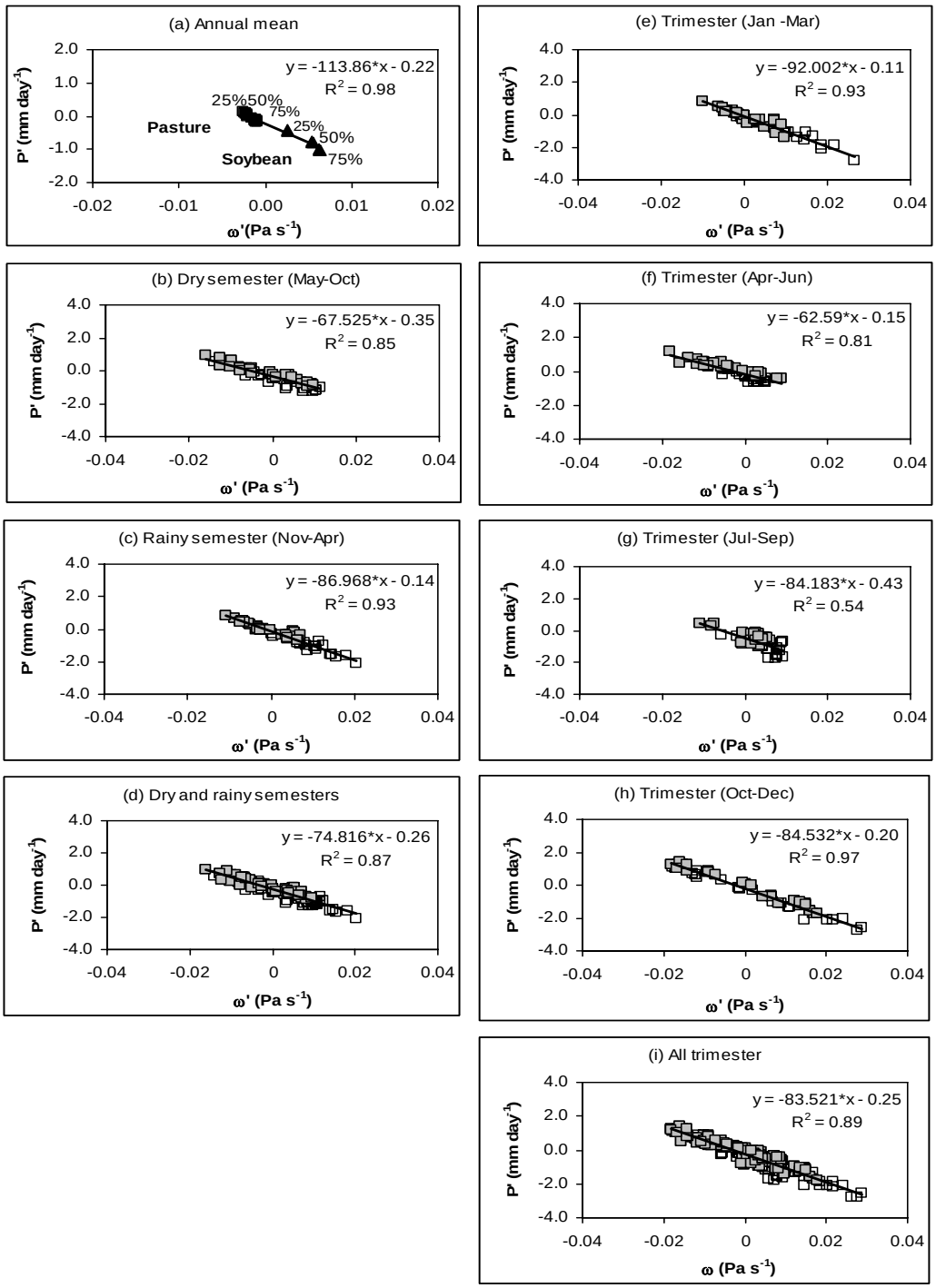

Figure 5.12. Annual mean precipitation anomaly as a function of vertical velocity anomaly (a) for different levels of pastureland and soybean cropland expansions. Semester mean precipitation anomaly as a function of vertical velocity anomaly for the dry semester (a), rainy semester (b), and both (c). Trimester mean precipitation anomaly as a function of vertical velocity anomaly for the January to March trimester (a), April to June trimester (b), July to September trimester (c), October to December trimester (d) and all trimesters (e). White squares represent pastureland and gray squares represent soybean cropland.

Figures 5.13 and 5.14 show the seasonal profile of vertical wind velocity at 500 hPa, ω, for forest (F^{ab}) (Figures 5.13a, 5.13b, 5.14a and 5.14b) and for their anomalies (ω') over different types of land cover and different levels of deforestation ($P^{ab}_{25\%}$ - F^{ab}: Figures 5.13c and 5.13d, $P^{ab}_{50\%}$ - F^{ab}: Figures 5.13e and 5.13f, $P^{ab}_{75\%}$ - F^{ab}: Figures 5.13g and 5.13h, $S_{25\%}$ - F^{ab}: Figures 5.14c and 5.14d, $S_{50\%}$ - F^{ab}: Figures 5.14e and 5.14f, $S_{75\%}$ - F^{ab}: Figures 5.14g and 5.14h). The left column represents the rainy season (February to April), and for the right column represents the dry season (July to August). A strong convection is observed in the tropical forest throughout of the rainy season, decreasing in dry season. On the other hand, Amazon land surface deforestation result in a reduction in convection and precipitation, generating stronger subsidence motions over the region (ω'>0), once the albedo values increase and cause reduction in Rn' as a response to the reduction of land cover, as verified for the soybean cropland analyzed in this study (Figures 5.13c to 5.13h and 5.14c to 5.14h).

Seasonal precipitation profile is also observed in the Forest (F^{ab}) and in the anomalies for different types of land cover ($P^{ab}_{25\%}$ $P^{ab}_{50\%}$ $P^{ab}_{75\%}$, $S_{25\%}$, $S_{50\%}$, $S_{75\%}$) and in different levels of deforestation at 500 hPa, considering the three rainiest months (February to April) and driest months (June to August) (Figures 5.15 and 5.16). In the Amazon region the rainfall is mainly of convective origin. In the forest the evapotranspiration is continuous throughout the year, presenting deep roots and also more available radiation, associated mainly to the smaller value of albedo. This profile can be evidenced in the rainy season (Figures 5.15a and 5.16a) and a little less in the dry season, where a subsidence motions begins to be evidenced. That motion expands with the increase of deforestation from 25% to 75%, modifying the rainfall pattern. The combined effects of changes in α', ω' and C' results changes in the rainfall. Figures 5.15c to 5.15h and 5.16c to 5.16h show a

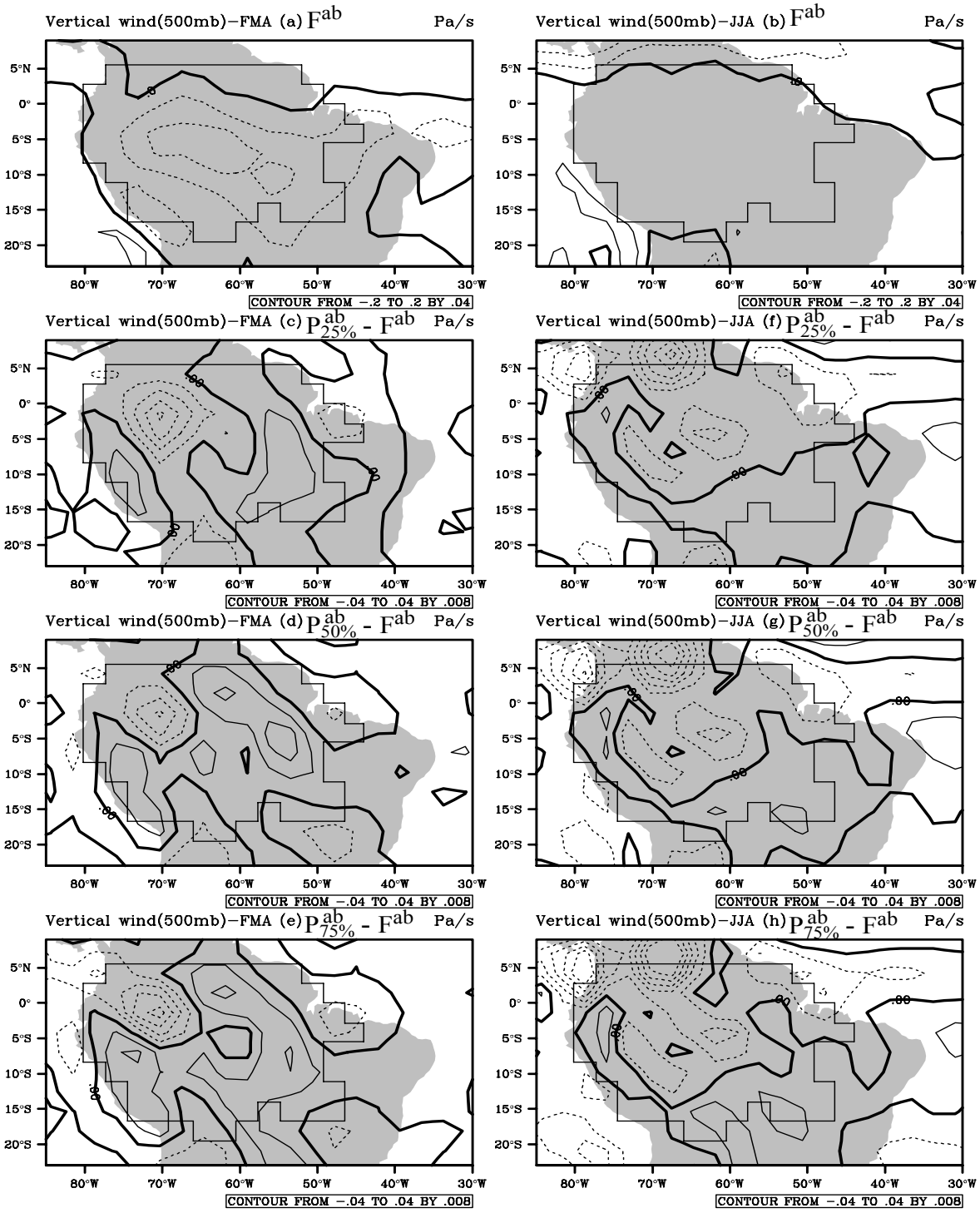

Figure 5.13. Seasonal profile of vertical velocity at 500 hPa, in forest (F^{ab}) for the February to April trimester (rainy season) (a) for the June to August trimester (dry season) (b) for the vertical velocity anomalies in different levels of pastureland expansions: $P^{ab}_{25\%} - F^{ab}$ (c), $P^{ab}_{50\%} - F^{ab}$ (d) and $P^{ab}_{75\%} - F^{ab}$ (e) for the February to April trimester, respectively, and for the anomalies $P^{ab}_{25\%} - F^{ab}$ (c), $P^{ab}_{50\%} - F^{ab}$ (g) and $P^{ab}_{75\%} - F^{ab}$ (h) for the June to August trimester, respectively. Positive values are represented by solid line and indicate decrease in vertical motion and negative values are represented by dashed line and indicate increase in vertical motion.

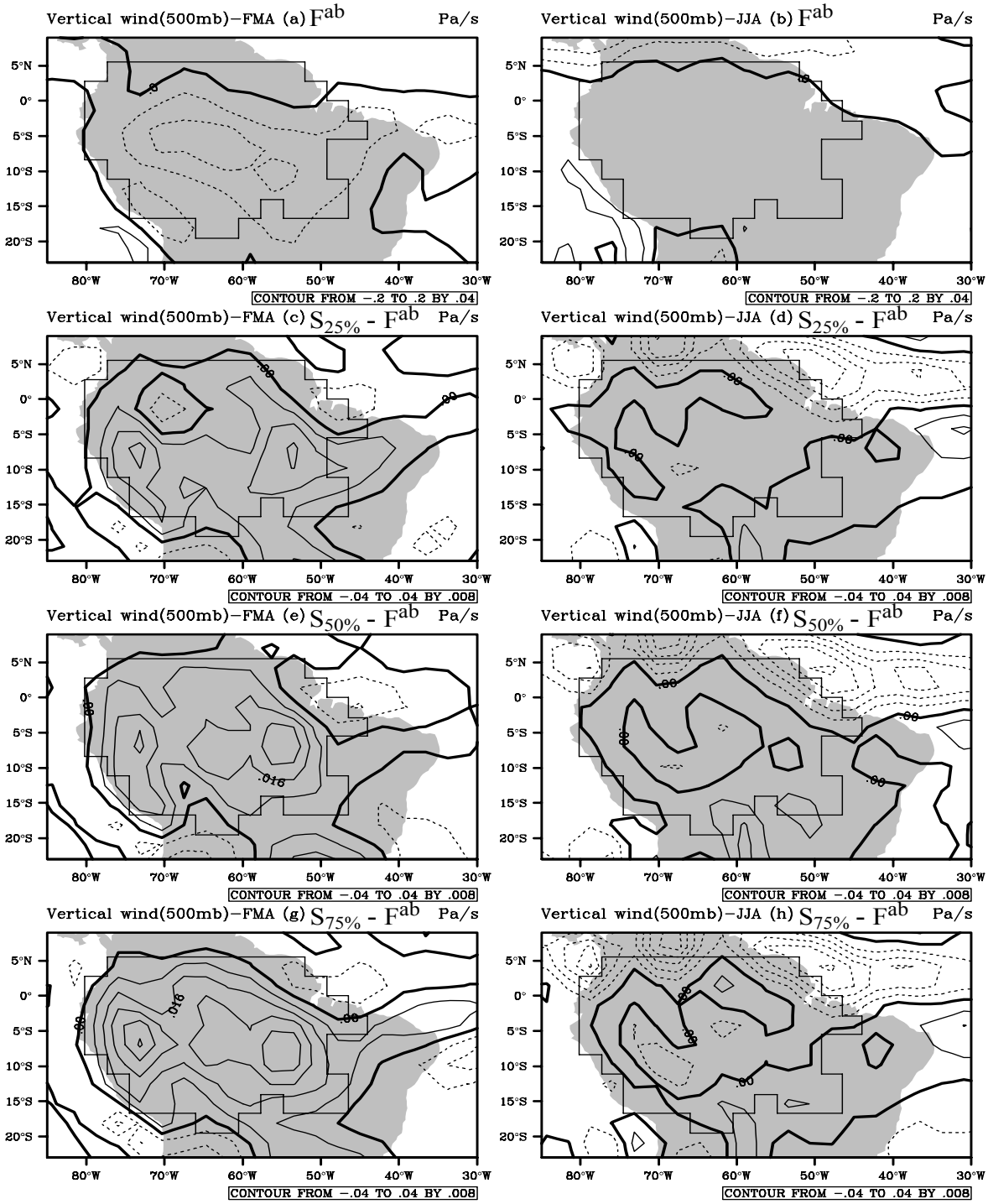

Figure 5.14. Seasonal profile of vertical velocity at 500 hPa, in forest (F^{ab}) for the February to April trimester (rainy season) (a) for the June to August trimester (dry season) (b) for the vertical velocity anomalies in different levels of soybean cropland expansions: $S_{25\%} - F^{ab}$ (c), $S_{50\%} - F^{ab}$ (d) and $S_{75\%} - F^{ab}$ (e) for the February to April trimester, respectively, and for the anomalies $S_{25\%} - F^{ab}$ (c), $S_{50\%} - F^{ab}$ (g) and $S_{75\%} - F^{ab}$ (h) for the June to August trimester, respectively. Positive values are represented by solid line and indicate decrease in vertical motion and negative values are represented by dashed line and indicate increase in vertical motion.

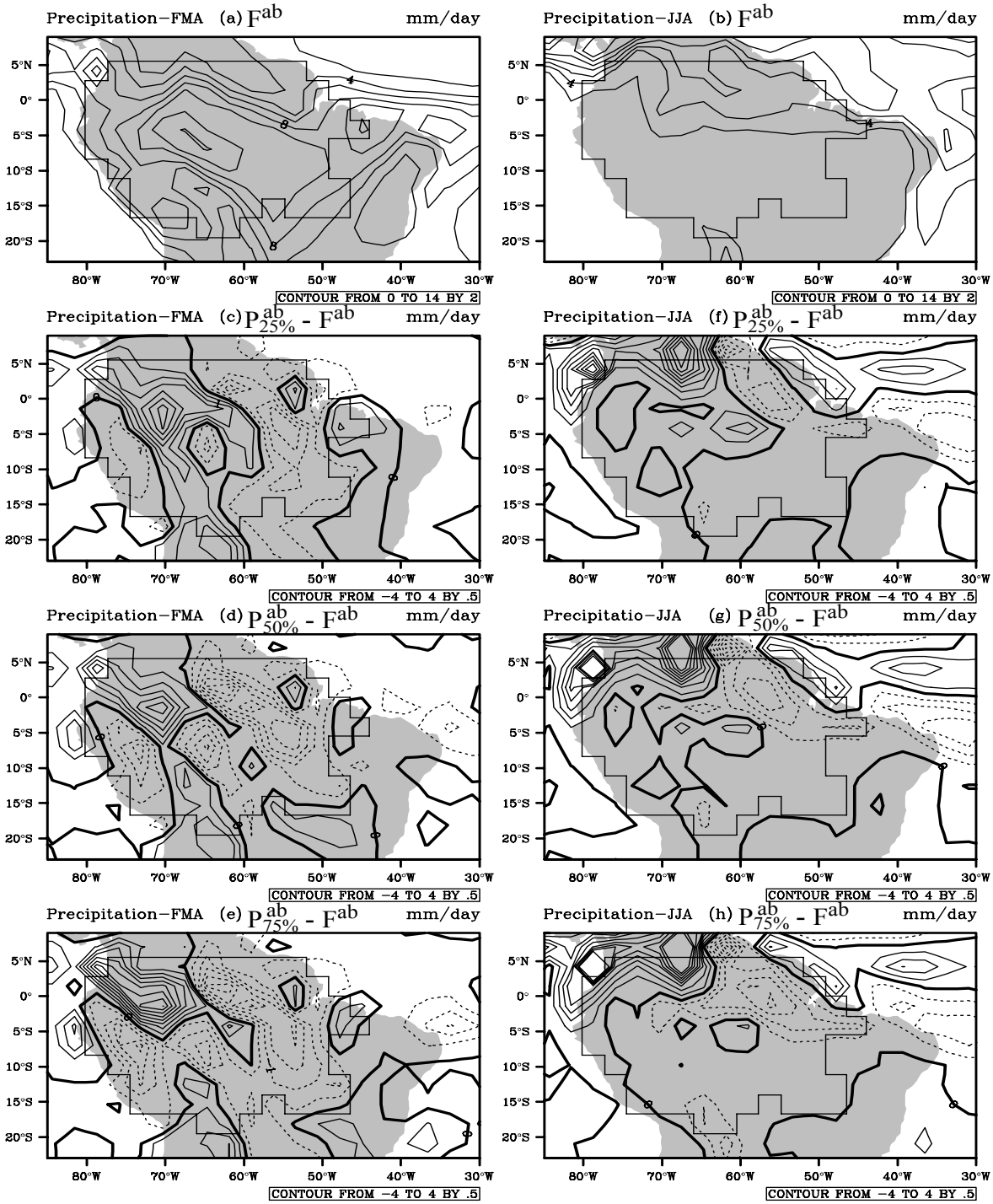

Figure 5.15. Seasonal profile of precipitation at 500 hPa, in forest (F^{ab}) for the February to April trimester (rainy season) (a) for the June to August trimester (dry season) (b) for the precipitation anomalies in different levels of pastureland expansions: $P^{ab}_{25\%} - F^{ab}$ (c), $P^{ab}_{50\%} - F^{ab}$ (d) and $P^{ab}_{75\%} - F^{ab}$ (e) for the February to April trimester, respectively, and for the anomalies $P^{ab}_{25\%} - F^{ab}$ (c), $P^{ab}_{50\%} - F^{ab}$ (g) and $P^{ab}_{75\%} - F^{ab}$ (h) for the June to August trimester, respectively. Negative values are represented by dashed line and indicate decrease in pasture precipitation and positive values are represented by solid line and indicate increase in pasture precipitation.

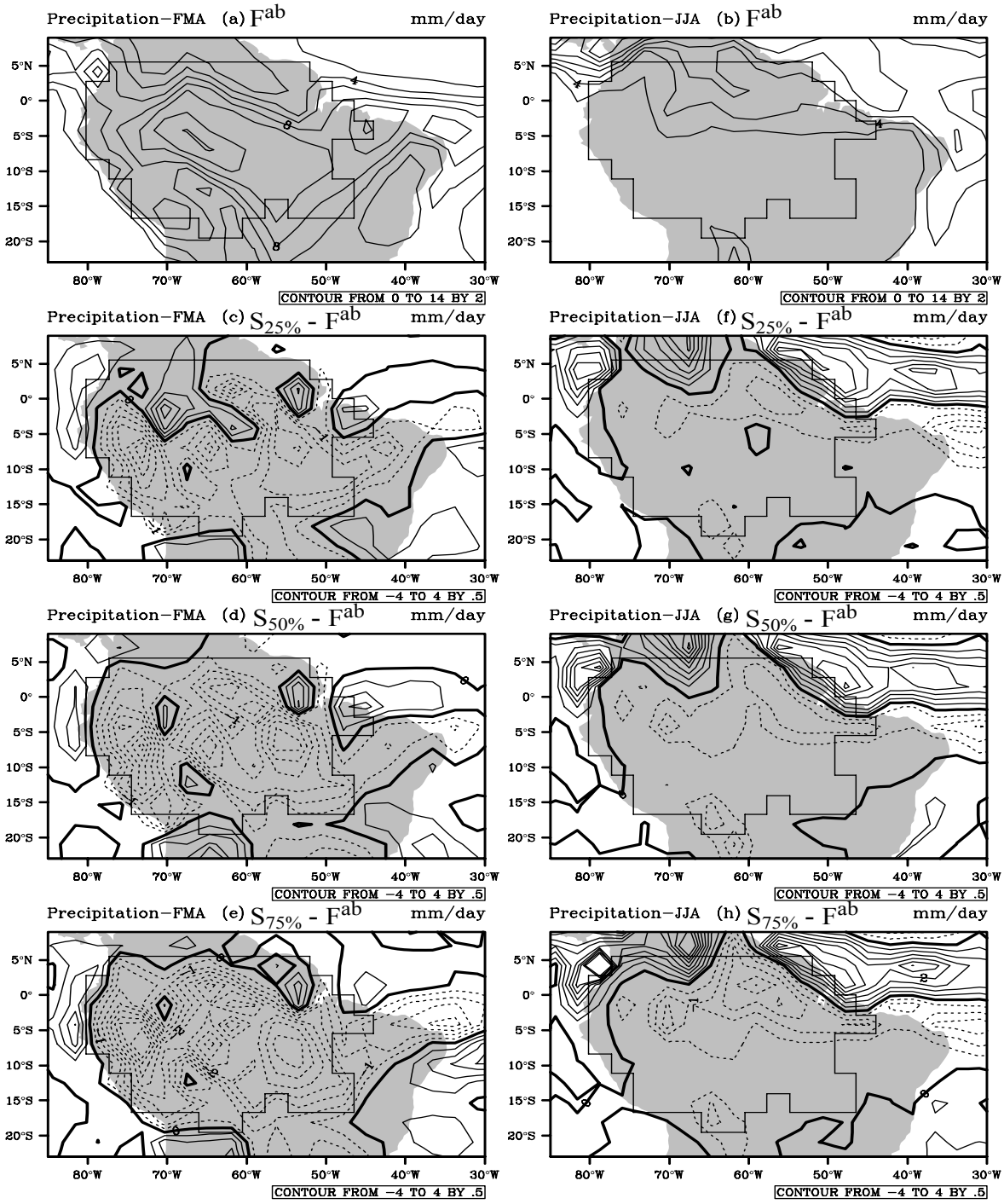

Figure 5.16. Seasonal profile of precipitation at 500 hPa, in forest (F^{ab}) for the February to April trimester (rainy season) (a) for the June to August trimester (dry season) (b) for the precipitation anomalies in different levels of soybean cropland expansions: $S_{25\%}$ - F^{ab} (c), $S_{50\%}$ - F^{ab} (d) and $S_{75\%}$ - F^{ab} (e) for the February to April trimester, respectively, and for the anomalies $S_{25\%}$ - F^{ab} (c), $S_{50\%}$ - F^{ab} (g) and $S_{75\%}$ - F^{ab} (h) for the June to August trimester, respectively. Negative values are represented by dashed line and indicate decrease in pasture precipitation and positive values are represented by solid line and indicate increase in pasture precipitation.

fairly significant decrease in rainfall over the deforested region, implicating in reduced ascent at 500 hPa. This decrease is statistically significant at 95% level of confidence (Table 5.2).

Table 5.2. Coefficient of determination (R^2) of the linear regression analysis between Rn' (surface net radiation), ω' (wind vertical velocity), C' (total cloud) and P' (precipitation) versus the variables in the left bar.

	Rn'	**ω'**	**C'**	**P'**
Sr'	0.93	0.85	0.98	0.93
Rn'	–	0.97	0.88	0.97
ω'	–	–	0.82	0.98
C'	–	–	–	0.91

5.4. DISCUSSION

This climate experiment was designed to cover a wide range of variation in land surface albedo and in the surface net radiation, by replacing a low-albedo rainforest by two land cover types, a mid-albedo pastureland and a high-albedo soybean cropland, considering different levels of deforestation (25%, 50% and 75%). The choice of low deforestation levels also allows a closer comparison to the (current) observed variations.

A summary of all experiments is presented in Table 5.1. Simulated mean values of precipitation and evaporation for tropical rainforest are 5.44 and 3.85 mm day^{-1}. Several authors, reviewed by Costa and Foley (1998), found mean precipitation values from 5.19 to 6.36 mm day^{-1}, with an average of 5.84 mm day^{-1}. Annual mean evapotranspiration from LBA towers values range from 3.30 to 3.68 mm day^{-1} (Biajoli, 2006). Deforestation had a

Table 5.1. Annual mean of the variables and of some parameters: Rn (net radiation), Sin (downward solar radiation), Sout (upward solar radiation), Lin-Lout (longwave balance), P (precipitation), E (evaporation), LE (latent heat flux) and H (sensible heat flux) for the simulations F^{ab} (Forest, control run), $P^{ab}_{25\%}$ (75% forest and 25% pasture), $P^{ab}_{50\%}$ (50% forest and 50% pasture), $P^{ab}_{75\%}$ (25% forest and 75% pasture), S25% (75% forest and 25% soybean), S50% (50% forest and 50% soybean), S75% (25% forest and 75% soybean), P_{total} (extrapolating to 100% of forest replaced by pasture), S_{total} (extrapolating to 100% of forest replaced by soybean), P_{total} - F^{ab} (difference between pasture and forest) and S_{total} - F^{ab} (difference between soybean and forest).

	Experiment										
	F^{ab}	$P^{ab}_{25\%}$	$P^{ab}_{50\%}$	$P^{ab}_{75\%}$	$S_{25\%}$	$S_{50\%}$	$S_{75\%}$	P_{total}	S_{total}	P_{total} - F^{ab}	S_{total} - F^{ab}
Rn (W m^{-2})	139.0	143.0	141.0	139.2	133.3	127.0	122.0	137.5	116.0	-1.4	-23.0
LE (W m^{-2})	112.8	107.7	101.7	95.7	100.8	91.6	82.8	89.7	73.8	-23.1	-39.0
H (W m^{-2})	27.9	36.3	40.2	44.6	33.7	36.4	39.7	48.7	42.7	-20.8	-14.8
Sin (W m^{-2})	216.2	229.2	233.4	237.8	231.9	236.8	242.0	242.0	247.1	+25.8	+30.9
Sout (W m^{-2})	27.5	34.0	37.2	40.2	40.2	46.3	52.1	43.3	58.1	+15.8	+30.6
Lin-Lout (W m^{-2})	49.8	52.7	55.6	57.1	58.4	63.4	68.2	59.3	73.1	+9.5	+23.5
P (mm day^{-1})	5.44	5.52	5.38	5.28	5.01	4.66	4.42	5.16	4.13	-0.28	-1.31
E (mm day^{-1})	3.85	3.67	3.48	3.28	3.43	3.13	2.83	3.09	2.53	-0.76	-1.31
α	0.127	0.148	0.159	0.169	0.174	0.196	0.216	0.179	0.237	+0.052	+0.110
C	0.729	0.725	0.716	0.707	0.710	0.691	0.676	0.698	0.658	-0.032	-0.071

substantial effect on the climate of the tropical forest region examined as a reduction in precipitation of -0.3 mm day^{-1} and in evaporation of -0.8 mm day^{-1}.

The radiative mechanism for precipitation reduction after tropical deforestation goes as follows: The increased albedo reduces the surface net radiation. In a region where convection is strong, this weakens the convective activity, reducing cloudiness and precipitation. The cloud reduction, however, increases the incoming radiation, introducing a negative feedback on the process. The final precipitation decrease is smaller in the presence of the cloud feedback than it would be in their absence (Figures 5.17 and 5.18).

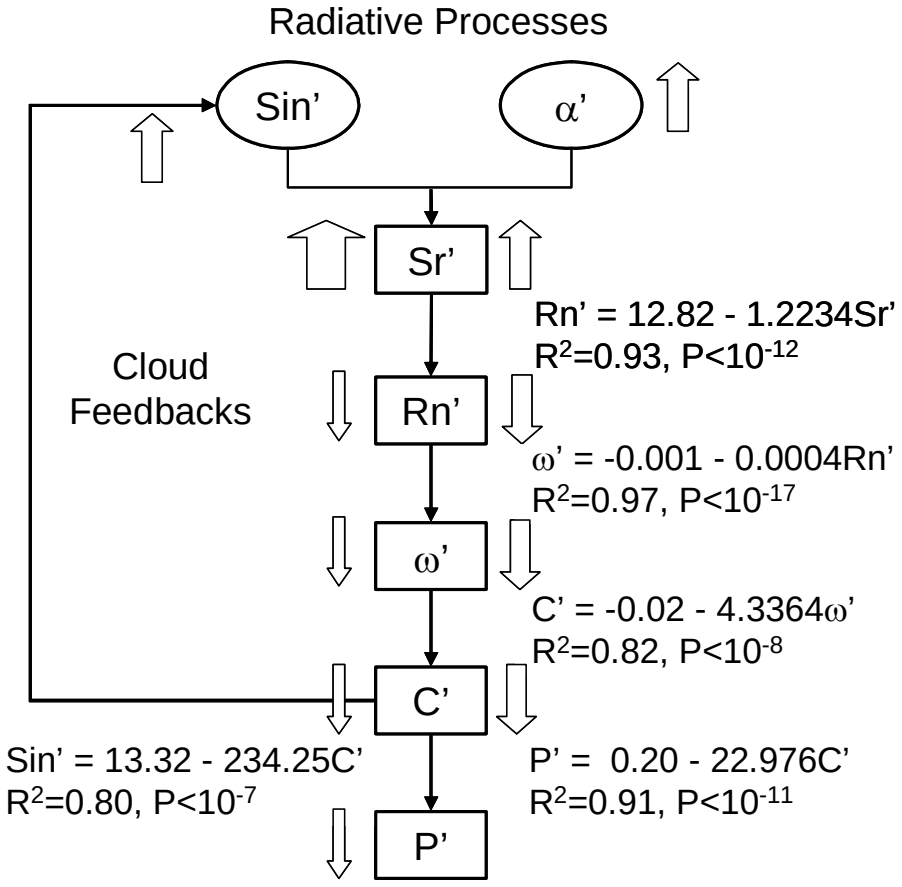

Figure 5.17. Diagram of anomalies of radiative processes.

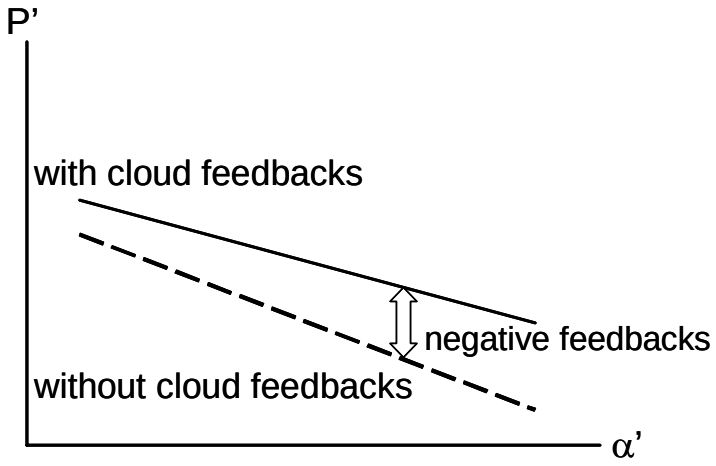

Figure 5.18. Schematic representation of the precipitation changes with and without cloud feedbacks.

The results of this study not only agree with previous observational, modeling and theoretical studies on the subject, but also help explain the dichotomy between the decreasing precipitation results from full large-scale deforestation climate experiments, and the observed increase in cloudiness and precipitation over mesoscale deforested regions. The next paragraphs discuss each of these points.

Results of incoming solar radiation and surface net radiation from this experiment diverge of the results observed from the ABRACOS experiment, which was especially designed to contrast the microclimatology of forested and deforested conditions. In this study incoming solar radiation assumed the values of 216.2 and 242.0 W m^{-2} for forest and pasture, respectively and, surface net radiation assumed the values of 139.0 and 137.5 W m^{-2} (Table 5.1). On the other hand, Culf et al. (1996) analyzing results from ABRACOS experiment found 193.63 and 192.59 W m^{-2} for incoming solar radiation and 131.25 and 116.67 W m^{-2} for surface net radiation for forest and pasture in the Jí-Paraná region, respectively; while Nobre et al. (1996) encountered 228.01 and 218.75 W m^{-2} for incoming solar radiation and, 138.89 and 122.69 W m^{-2} for surface net radiation, respectively. These

divergences probably occur due to the scale which the observations were made. Incoming solar radiation and surface net radiation increase over deforested area in the model in study because the cloudy feedbacks. On the other hand, contiguous area of pasture in the ABRACOS experiment probably was very little so that these feedbacks occurred.

The results also help explain several inconsistencies among previous published modeling results. I will separate the discussion in two: climate sensitivity to increased albedo, and the role of albedo in determining spatial patterns of increase/decrease in precipitation.

Most Amazon deforestation climate experiments show an average decrease in precipitation over the deforested area. Some experiments, however, like Nobre et al. (1991), show a consistent decrease in precipitation over all the deforested area, while others (eg. Lean and Rowntree, 1997; Costa and Foley, 2000; Voldoire and Royer, 2004) show different spatial patterns of decrease/increase of precipitation, but with a predominance of decrease. This different behavior is easily explained by Figures 5.3 and 5.4. In these figures, the mid-albedo pastureland is represented by gray boxes, while the high-albedo soybean cropland is represented by the white boxes. Each box represents the average state for a group of deforested Amazon grid cells over a band of latitude. From these figures, it is clear that, the higher the increase in Sr (α), the lower the likelihood of a group of grid cells to show a positive anomaly of precipitation. Thus, the low values of land surface albedo anomaly in Costa and Foley (2000) – 0.035 – and in Lean and Rowntree (1997) – 0.05 – are consistent with a spatial patterns of mixed decrease and increase of precipitation, while the high land surface albedo anomaly in Nobre et al. (1991) – 0.09 – is consistent with a regular pattern of precipitation decrease. Thus, the discrepancies in the regional precipitation patterns in the literature are mainly radiatively controlled, and are, in fact, a consequence of the land surface albedo choice of the modeler.

Our results are also consistent with the theoretical studies published. The theoretical background about the precipitation changes after a tropical deforestation can be traced to three main articles. Charney (1975) hypothesized that the subsidence over the Sahara desert, at that time explained only by the descendent branch of the Hadley cell, might be strengthened by its high albedo. Charney theory considered a dry atmosphere, and could not be applied to humid tropical regions like the Amazon rainforest. Later, Eltahir (1996) proposed a similar theory that considered a moist atmosphere. According to the author, the increase of surface albedo after deforestation cause a reduction in the net surface radiation, which cools the upper atmosphere over the deforested area, inducing a direct thermal circulation causing a descendent motion over the deforested region, which results in subsidence. Zeng and Neelin (1999) completed Eltahir's theory, using linear assumptions to describe the radiative processes, and the energy, water balance and cloud-radiative feedback mechanisms in the atmospheric column. His final formulation proposes a linear relationship between P' and $(S_{in} \cdot \alpha)$', or Sr', similar to the statistically significant regression equations in Figures 5.3 and 5.4.

The anomaly in precipitation is explained by radiative and non-radiative processes. The precipitation change after a tropical deforestation may be explained by the simplified equation 1

$$P' = a_{NR} + b_R \, Rn' \qquad (1)$$

where P' is the anomaly in precipitation, Rn' is the increase in surface net radiation, a_{NR} is a linear coefficient, related to non-radiative processes, and b_R is an angular coefficient, related to radiative processes (Figure 5.1). From our analysis, usually the non-radiative term (a_{NR}) is small (< 0.3 mm.day^{-1}), while the radiative term dominates ($b_R \cdot Rn'$ may be as high as -2 mm·day^{-1}). To facilitate comparisons among the experiments, I may choose to write P' as a function of the land surface albedo (α') using the simplified equation 2

$$P' = a_{NSR} + b_{SR}\,\alpha' \qquad (2)$$

where a_{NSR} is a linear coefficient related to non-solar radiation processes (includes non-radiative processes and long wave radiation feedbacks), and b_{SR} is an angular coefficient related to the solar radiation processes only, which may also be defined as the Amazon climate sensitivity to increased land surface albedo. From Figure 5.2, the precipitation sensitivity from this experiment is -0.17 $mm.day^{-1}$ per 0.01 increase in land surface albedo. This is consistent with the sensitivity calculated using the results found by Dirmeyer and Shukla (1994) – about -0.19 $mm.day^{-1}$ per 0.01 increase in land surface albedo (using the COLA/SSiB GCM), and with the slope of Figure 5.1 regression line (-0.16 $mm.day^{-1}$ per 0.01 increase in land surface albedo). Note that Equation (2) may only be used at the annual mean scale. The linear coefficient a_{NSR} may also be estimated using the results above. From my analysis, $a_{NSR} \sim 0.47$ mm day^{-1}; from Dirmeyer and Shukla (1994) data, I calculate that it is 0.27 mm day^{-1}.

Considering only the non-radiative effects of deforestation (equivalent to assume Rn'=0), the decrease in roughness length, leaf area index, and rooting depth, cause a decrease in the latent heat flux, and an increase in surface temperature, sensible heat flux, atmospheric instability, cloudiness, and precipitation. On the other hand, the radiative effects, caused primarily by increases in surface albedo, but also by long-wave and cloud-radiative feedbacks, cause a decrease in both surface heat fluxes (due to reduced radiation absorbed by the surface), resulting in a loss of radiative energy from the Amazon land surface, cooling off the atmospheric column over the deforestation which induces a thermally driven circulation that results in subsidence, with subsequent reduction in convection, cloudiness, and precipitation.

This competitive effect explains why, although most Amazon deforestation climate experiments show an average decrease in precipitation over the deforested area, it is

possible to find experiments that actually show an average increase. Depending on the parameterizations used, precipitation may increase or decrease. For the coefficients obtained not only by this study, but also by Dirmeyer and Shukla (1994), an increase in land surface albedo of about 0.03 is necessary in order to offset the non-radiative processes that tend to increase precipitation. For most of the cases in the literature, consistent with a full deforestation, the choices of parameters were so that it resulted in a decrease in average precipitation. In partial deforestation scenarios, the average increase in land surface albedo over a large grid cell is small, leading to a very small precipitation change.

5.5. CONCLUSIONS

This study evaluated the radiative processes of the precipitation change after tropical deforestation and its effects on regional climate in Amazon, considering different levels of deforestation (25%, 50% and 75%), and different types of land cover replacements for the original rainforest land cover. The results showed that the changes in precipitation are linearly related to the anomaly in net surface radiation, and the change in precipitation due to radiative mechanisms may be an order of magnitude higher than those due to non-radiative mechanisms. The basic mechanism proposed for precipitation reduction after tropical deforestation starts with the decrease in surface net radiation due to the increased albedo after deforestation. In a region where convection is strong, this weakens the convective activity, reducing cloudiness and precipitation. The cloud reduction, however, increases the incoming radiation, introducing a negative feedback on the process. The final precipitation decrease is smaller in the presence of the cloud feedback than it would be in their absence. Competitive non-radiative mechanisms tend to increase precipitation. The non-radiative processes of the precipitation change after tropical deforestation will be analyzed in a companion paper.

This study explains, for the first time, why it is consistent to observe increased cloudiness and precipitation under partial deforestation scenarios, and to still believe that large-scale deforestation might lead to a decrease in precipitation. Furthermore, if the large-scale deforestation is related to the expansion of croplands, the precipitation change may be much higher than if caused by the expansion of pasturelands. This contrast will also be explored by a further study.

5.6. NOMENCLATURE

F^a	control run (Rainforest land cover)-1st repetition
F^b	control run (Rainforest land cover)-2ns repetition
$P^a_{25\%}$	rainforest partially replaces pastureland (level of deforestation 25%) -1st repetition
$P^b_{25\%}$	rainforest partially replaces pastureland (level of deforestation 25%)-2nd repetition
$P^a_{50\%}$	rainforest partially replaces pastureland (level of deforestation 50%)-1st repetition
$P^b_{50\%}$	rainforest partially replaces pastureland (level of deforestation 50%)-2nd repetition
$P^a_{75\%}$	rainforest partially replaces pastureland (level of deforestation 75%)-1st repetition
$P^b_{75\%}$	rainforest partially replaces pastureland (level of deforestation 75%)-2nd repetition
P’	anomaly fields of precipitation between deforested (pasture and soybean) and forested conditions
$S_{25\%}$	rainforest partially replaces soybean (level of deforestation 25%)
$S_{50\%}$	rainforest partially replaces soybean (level of deforestation 50%)
$S_{75\%}$	rainforest partially replaces soybean (level of deforestation 75%)
Sr’	anomaly surface reflected radiation between deforested (pasture and soybean) and forested conditions
Rn’	anomaly surface net radiation between deforested (pasture and soybean) and forested conditions
C’	anomaly total cloud cover between deforested (pasture and soybean) and forested conditions
ω’	anomaly vertical wind velocity between deforested (pasture and soybean) and forested conditions
S_{in}’	anomaly incoming radiation between deforested (pasture and soybean) and forested conditions
S_{in}	incoming radiation
a_{NR}	linear coefficient, related to non-radiative processes
b_R	an angular coefficient, related to radiative processes
a_{NSR}	linear coefficient related to non-solar radiation processes (includes non-radiative processes and long wave radiation feedbacks)
b_{SR}	an angular coefficient related to the solar radiation processes only

CHAPTER 6

GENERAL CONCLUSIONS

6.1. OVERVIEW

It is known that a more realistic representation of the land surface is important to improve the climate simulated by General Circulation Models (GCMs). In particular, the surface albedo is an important source of uncertainties related to the surface radiative budgets. In the tropics, such as in Amazon tropical rainforest, where the solar radiation balance is stronger, changes in surface albedo caused by deforestation have been demonstrated to influence the regional climate (Nobre et al., 1991; Dirmeyer and Shukla, 1994; Hahmann and Dickinson, 1997; Costa and Foley, 2000; Berbet and Costa, 2003). Hence, a more realistic representation of albedo in GCMs will significantly improve the accuracy of climate simulation and prediction.

In this Dissertation, It is used measured field data, state-of-art numerical models and remote sensing products to investigate the sources of spatial and temporal variation of

surface albedo of an Amazon tropical rainforest and the role of changes in surface albedo, after deforestation, on the regional climate. To study this challenging subject, this dissertation was divided in five chapters, where the conclusion of each chapter is summarized below.

In chapter 1, it was studied the main sources of variation of surface albedo of Amazonian tropical vegetation, at both the hourly and monthly time scales. In addition to the traditional sources of variation (land cover and zenith angle) it was examined the role of canopy wetness and atmospheric transmissivity on the surface albedo and the respective interactions. Field data used in this analysis were collected at six micrometeorological sites (four forests and two pasturelands) during ABRACOS (Anglo Brazilian Amazonian Climate Observation Study) and LBA projects (Large-Scale Biosphere-Atmosphere Experiment in Amazonia). At the hourly-scale, land cover variation (L) (forest, pasture), atmospheric transmissivity (τ) and canopy wetness (ω) are the most important sources of variation, while at monthly scale, only land cover and atmospheric transmissivity are important. Reduction of 0.004 in the surface albedo due to canopy wetness is observed for both ecosystems, forest and pastureland. The results presented here let me to conclude that, although the difference in surface albedo (α') is partially dependent on τ (a consequence of the interaction $L \cdot \tau$), it is independent of the canopy wetness. It is also noted that, when simulating the land surface albedo, neither the role of atmospheric transmissivity nor the role of canopy wetness is well represented in land surface models today.

In chapter 2, it was evaluated the sensitivity of the surface albedo simulated by the Integrated Biosphere Simulator (IBIS) to a set of tropical rainforest canopy architectural and optical parameters. The parameters tested in this study are the orientation and reflectance of the leaves of upper and lower canopies in the visible (VIS) and near-infrared

(NIR) spectral bands. The results were evaluated against albedo measurements taken above the K34 site at the INPA (Instituto Nacional de Pesquisas da Amazonia) Cuieiras Biological Reserve. The sensitivity analysis indicates a strong response to the upper canopy leaves orientation (χ_{up}) and to the reflectivity in the near-infrared spectral band ($\rho_{NIR,up}$), a smaller sensitivity to the reflectivity in the visible spectral band ($\rho_{VIS,up}$) and no sensitivity at all to the lower canopy parameters, which is consistent with the canopy structure. The combination of parameters that minimized the RMSE and mean relative error are $\chi_{up} = 0.86$, $\rho_{VIS,up} = 0.062$, and $\rho_{NIR,up} = 0.275$. These parameterizations allow the improvement of the accuracy of the land surface albedo simulations obtained by IBIS model, indicating its potential to simulate the canopy radiative transfer for narrow spectral bands, allowing in the future, a close comparison with remote sensing products.

In chapter 3, the role of canopy wetness on the simulated albedo of Amazon tropical rainforest was investigated, once it is the third most important source of variation at hourly scale. Simulations were run using three versions (0-D) of the land surface/ecosystem IBIS model. The results demonstrated that, while the incorporation of canopy wetness on the radiative transfer calculation improves the simulated surface albedos at hourly time scale, no substantial improvement was verified at monthly or longer time scales, because radiative effect of the canopy wetness is restricted to very short times, when the canopy is actually wet. However, these results exclude the role canopy wetness as a main source of seasonal variability of tropical rainforest albedo

In chapter 4, six different products of land surface albedo derived from different remote sensors are compared with the albedo simulated by the Community Climate Model (CCM3) coupled to the Integrated Biosphere Simulator (IBIS). Field measurements collected at three sites in Amazon are also included as reference data. The results presented in this chapter let me to conclude that the albedos estimated from different remote sensing

systems data vary considerably in the range between 0.10 and 0.20, and there are substantial differences in seasonality. Field measurements and modeled albedo vary seasonally from 0.11 to 0.14, and only the black-sky product albedo from MODIS matched to the field-observed albedo seasonality.

In chapter 5, eleven simulations using the CCM3-IBIS were run to investigate the radiative processes of the precipitation change after deforestation and its effects on the regional climate in Amazon, considering different levels of deforestation (25%, 50% and 75%), and different types of land cover replacements (pasture and soybean) for the original rainforest land cover. Results show that the changes in precipitation are linearly related to the anomaly in net surface radiation, and the change in precipitation due to radiative mechanisms may be an order of magnitude higher than those due to non-radiative mechanisms. Radiative processes dominate because precipitation in the region is largely convective. A reduction in net radiation weakens the convective activity, reducing cloudiness and precipitation. While cloud-radiative negative feedbacks inhibit a larger climate change* (precipitation decrease), competitive non-radiative mechanisms tend to increase precipitation.

6.2. CONCLUSIONS

An overview on the results and individual conclusions of each chapter lead me to argue that the regional climate of Amazon is strongly controlled by the radiative processes changes in surface albedo and net radiation – caused by changes in land cover due to the replacement of forest in pasturelands and croplands – are fundamental, explaining over 90% of the variance in the precipitation change.

* The term climate change refers only to the precipitation change.

The degree of importance of each source of variation of surface albedo found in Chapter 1 and the parameterization of the model obtained from the sensitivity analyses in Chapter 2 are important to define priority improvements in the representation of albedo in GCMs, once the state-of-the-art land surface models are still unable to reproduce realistically the seasonal variability of surface albedo of forested and deforested areas (Bebert and Costa, 2003). The results found in this dissertation, show that land cover and atmospheric transmissivity are the two most important sources of surface albedo variance and are in agreement with the significantly differences between surface albedos of forest and pasture found by several authors (Oguntoyinbo, 1970; Shuttleworth et al., 1984; Bastable et al., 1983 and Culf et al., 1996) and with the influence of zenith angle and interaction between atmospheric transmissivity and zenith angle on surface albedo found by Pinker et al. (1980), Shuttleworth et al. (1984), McCaughey (1987) and Giambelluca et al. (1999).

A third source of variation of surface albedo found in this dissertation is the canopy wetness. Although Culf et al. (1995) suggested that surface albedo seasonality is related to soil moisture, Berbet and Costa (2003) suggested that most likely the changes in forest albedo are related to soil moisture-correlated variables: smaller soil exposure, darker leaves (associated with the leaf water potential) and higher canopy wetness. Simulations using the IBIS model with changes in the radiative transfer code to incorporate the radiative effects of the canopy wetness show that canopy wetness is not evidenced as a possible source of variation of surface albedo at seasonal-scale time, excluding the role canopy wetness as a main source of seasonal variability of tropical rainforest albedo as evidenced in the Chapter 3. However, these modifications in the IBIS code reproduced well the significant decrease in surface albedo during the precipitation hours, confirming the results found in Chapter 1.

Land surface parameterizations have been poorly represented because of limited observations (Zhou et al., 2003), and the only practical and economical approach to large-scale characterization of land surface parameters is remote sensing (Hu et al., 2000). Although the unquestionable importance of remote sensing as key tool to study the global environment and its evolution throughout the last decades, in Chapter 4 of this dissertation it is found that satellite products for the Amazon tropical rainforests present severe limitations, due to the significant difference among the six different remote sensing systems studied. For the Amazon region, the albedos estimated vary considerable in the range between 0.10 and 0.20, and there are substantial differences in seasonality.

Numerous studies with GCMs suggest that tropical deforestation can result in regional-scale climate change, increasing particularly reducing precipitation. Simulation results from the CCM3 GCM (Chapter 5) show that an increase in the surface albedo (caused by the replacement of forest by pastureland and soybean cropland) reduces energy balance, convection and cloud formation generating an anomalous subsidence motion resulting in the reduction of rainfall over the Amazon. These results agree with most of investigations about the effect of deforestation over Amazon basin (Nobre et al., 1991; Eltahir, 1996; Werth and Avissar, 2002; Hoffmann et al., 2003). The cloud reduction, however, increases the incoming radiation, introducing a negative feedback on the radiative process. The final precipitation decrease is smaller in the presence of the cloud feedback than it would be in their absence.

6.3. RECOMMENDATIONS FOR FUTURE RESEARCH

The results presented in this dissertation elucidated some points related to the sources of spatial and temporal variation of an Amazon tropical rainforest surface albedo, and to the role of surface albedo changes, after Amazon tropical deforestation, in the regional climate. It, however, provoked several new lines of research:

- Following the discussion in Chapter 1 and by Culf et al. (1995) and by Berbet and Costa (2003), I recommend that future work should investigate the role of senescence, leaf age and leaf water potential on the seasonality of the tropical rainforest albedo. It is expected with the inclusion of these factors and other additional sources of variation in the land surface models, further improvements in accuracy providing more detailed studies of the climatic effects of tropical deforestation. A specific field experiment setup is needed, though.
- Future additional parameterizations of the canopy architectural (e.g., single-sided leaf and stem area indexes, fraction of overall area covered by lower and upper canopies) and optical (e.g., direct and diffuse beams ground albedo on visible and near-infrared spectral bands, lower and upper canopies leaf transmittances on visible and near-infrared spectral bands) parameters according to the plant species, soil types, plant phenology, leaf water content, and soil surface wetness may improve considerably the scope of such modeling exercises, building a solid basis for stronger interactions between field observations, climate models and remote sensing products.
- More robust algorithms to retrieve the surface albedos from remote sensing products should be developed and tested to reduce the uncertainties related to the effects of atmospheric scattering and absorption, anisotropy, inadequate temporal, spatial and spectral sampling, and narrowband to broadband conversion.

- Further simulations involving more realistic climate change should be performed considering realistic scenarios of agriculture expansion in Amazonia.
- It is also important to investigate the non-radiative climate processes due to deforestation. It is also important to built new datasets for soybean cropland parameterizations, which nowadays have been the crop with more expansion in Amazon region.

GENERAL REFERENCES

André, R.G.B. and Y. Viswanadhan, 1983: Radiation balance of soybeans grown in Brazil. *Agricultural Meteorology*, 30, 150-173.

Araújo, A. C., A. D. Nobre, B. Kruijt, J. A. Elbers, R. Dallarosa, P. Stefani, C. von Randow, A. O. Manzi, A. D. Culf, J. H. C. Gash, R. Valentini, P. Kabat, 2002: Comparative measurements of carbon dioxide fluxes from two nearby towers in a central Amazonian rainforest: The Manaus LBA site, *J. Geophys. Res.*, 107: D8090, doi:10.1029/2001JD000676.

Asner, G. P., 1998: Biophysical and biogeochemical sources of reflectance in canopy reflectance. *Remote sens. Environ.*, 64, 234-253.

Asner, G. P., C. A. Wessman, C. A. Bateson, and J. L. Privette, 2000: Impact of tissue, canopy, and landscape factors on the hyperspectral reflectance variability of arid ecosystems. *Remote sens. Environ.,* 74, 69–84.

Barkstrom, B. R., 1984: The Earth Radiation Budget Experiment (ERBE), *Bull. Amer. Meteorol. Soc.*, 65, 1170-1185.

Bastable, H.G., W. J. Shuttleworth, R. L. G. Dallarosa, G. Fisher, and C. A. Nobre, 1993: Observations of climate, albedo and surface radiation over cleared and undisturbed Amazonia forest. *Int. J. Climatol.*, 13, 783-796.

Bégué, A., J. L. Roujean, N. P. Hanan, S. D. Prince, M. Thawley, A. Huete, D. Tanré, 1996: Shortwave radiation budget of Sahelian vegetation: 1. Techniques of measurement and results during HAPEX – Sahel. *Agr. Forest Meteorol.*, 79, 79-96.

Berbet, M. L. C. and M. H. Costa, 2003: Climate change after tropical deforestation: seasonal variability of surface albedo and its effects on precipitation change, *J. Climate*, 16, 2099-2104.

Biajoli, M. C., 2006: Relatório final de atividades referentes à Bolsa FUNCATE, Categoria Formação em C&T – Tipo II. *UFV*, p.12.

Blad, B. L. and D. G. Baker, 1972: Reflected radiation from a soybean crop. *Agron. J.*, 64, 277-280.

Bonan, G. B., 1996: *A Land surface model (LSM version 1.0) for ecological, hydrological, and atmospheric studies: technical description and user's guide*. NCAR Technical note TN-417+STR, 150p.

Botta, A. and J. A. Foley, 2002: Effect of climatic variability and disturbances on the Amazonian terrestrial ecosystems dynamics. *Global Biogeochem. Cy.*, 16 (4), doi: 10.1029/2000GB001338.

Brest, C. L. and W. B. Rossow, 1992: Radiometric calibration and monitoring of NOAA AVHRR data for ISCCP. *Int. J. Remote Sens.,* 13, 235–273.

Brest, C., W. B. Rossow, and M. D. Roiter, 1997: Update of Radiance Calibrations for ISCCP, *J. Atmos. Ocean. Tech.,* 14, 1091-1109.

Briegleb, B. P., P Minnis, V. Ramanathan, and E. Harrison, 1986: Comparison of regional clear-sky albedos inferred from satellite observations and model computations. *J. Climate Appl. Meteor*., 25, 214-226.

Charney, J. G., 1975: Dynamics of deserts and drought in the Sahel. *Q. J. Roy. Meteor. Soc.*, 101, 193-202.

Charney, J. G., W. J. Quirk, S. H. Chow, and J. Kornifield, 1977: A comparative study of the effects of albedo change on drought in semi-arid regions*, J. Atmos. Sci.*, 34, 1366-1385.

Chu, P. S., Z. R. Yu, and S. Hastenrath, 1994: Detecting climate change concurrent with deforestation in the Amazon Basin: Which way has it gone? *Bull. Amer. Meteor. Soc*., 75, 579-582.

Coakley, J. A. and P. Chylek, 1975: The two-stream approximation in radiative transfer: Including the angle of incident radiation. *J. Atmos. Sci.,* 32: 249-261.

Cochran, W. G. and G. M. Cox, 1992: *Experimental designs*. John Wiley and Sons, 2st ed., 611p.

Costa, M. H. and J. A. Foley, 1998: A comparison of precipitation datasets for the Amazon basin. *Geophys. Res. Lett.,* 25, 155–158.

Costa, M. H. and J. A. Foley, 2000: Combined effects of deforestation and doubled atmospheric CO2 concentrations on the climate of Amazonia. *J. Climate,* 13, 18–34.

Csiszar, I. and G. Gutman, 1999: Mapping global land surface albedo from NOAA/AVHRR. *J. Geophys. Res*., 104, 6215-6228.

Culf, A. D., G. Fisch, and M. G. Hodnett, 1995: The albedo of Amazonian forest and ranch land. *J. Climate*, 8, 1544-1554.

Culf, A. D., J. L. Esteves, A. O.Marques Filho, H. R. Rocha, 1996: Radiation, temperature and humidity over forest and pasture in Amazonia. In: Gash, J. H. C., Nobre, C. A., Roberts, J. M., Victoria, R. L. *Amazonian deforestation and climate*. New York: John Wiley & Sons, 175-191.

Cutrim, E., D. W. Martin, and R. Rabin, 1995: Enhancement of cumulus clouds over deforested lands in Amazonia. *Bull. Amer.Meteor. Soc.,* 76, 1801-1805.

Delire, C. and J. A Foley, 1999: Evaluating the performance of a land surface/ ecosystem model with biophysical measurements from contrasting environments. *J. Geophys. Res.,* 104, 16895-16909.

Delire, C., J. A. Foley, S. Thompson, 2002: Evaluating the carbon cycle of a coupled atmosphere-biosphere model. *Global Biogeochemical Cycles*, 17, article n° 1012.

Desormeaux, Y., W. B. Rossow, C. L. Brest, and G. G. Campbell, 1993: Normalization and calibration of geostationary satellite radiances for ISCCP. *J. Atmos. Ocean. Tech.,* 10, 304–325.

Dickinson, R. E. and A. Henderson-Sellers, 1988: Modelling tropical deforestation: A study of GCM land-surface parametrizations. *Q. J. Roy. Meteor. Soc.*, 144, 439-462.

Dickinson, R. E. and P. Kennedy, 1992: Impacts on regional climate of Amazon deforestation. *Geophys. Res. Lett.,* 19, 1947–1950.

Dickinson, R. E., 1983: Land surface processes and climate-surface albedos and energy balance. *Adv. Geophys*., 25:305-353.

Dirmeyer, P. A. and J. Shukla, 1994: Albedo as a modulator of climate response to tropical deforestation. *J. Geophys. Res.*, 99, 20863-20877.

Dorman, J. L. and P. J. Sellers, 1989: A global climatology of albedo, roughness length and stomatal resistance for atmospheric general circulation models as represented by the Simple Biosphere Model (SiB). *Journal of Applied Meteorology*, 28, 833-855.

Durieux, L., L. A. T. Machado, and H. Laurent, 2003: The impact of deforestation on cloud cover over the Amazon arc of deforestation. *Remote Sens. Environ.*, 86, 132-140.

Eck, T. F. and D. W. Deering, 1992: Canopy albedo and transmittance in a spruce-hemlock forest in mid-September. *Agr. For. Meteorol.*, .59, 237-248.

Eltahir, E. A. B., 1996: Role of vegetation in sustaining large-scale atmospheric circulations in the tropics. *J. Geophys. Res.*, 101, 4255-4268.

Fisch, G., I. R. Wright, and H. G. Bastable, 1994: Albedo of tropical grass: A case study of pre- and post-burning. *Int. J. Climatol.,* 14, 102–107.

Foley, J. A., A. Botta, M. T. Coe, and M. H. Costa, 2002: El Niño-Southern Oscillation and the climate, ecosystems and rivers of Amazonia. *Global Biogeochem. Cy*, 16, 1132. doi: 10.1029/2002GB001872.

Foley, J. A., I. C. Prentice, N. Ramankutty, S. Levis, D. Pollard, S. Sitch, and A. Haxeltine, 1996: An integrated biosphere model of land surface processes, terrestrial carbon balance and vegetation dynamics. *Global Biogeochem. Cy.*, 10, 603-628.

Fontana, D. C., M. A. Berlato, and H. Bergamaschi, 1991: Soybean radiation balance in subtropical region, *Pesquisa Agropecuaria Brasileira*, 26, 411-418 (in portuguese with abstract in English).

Giambelluca, T.W., J. Fox, S. Yarnasarn, P. Onibutr, and M. A. Nullet, 1999: Dry-season radiation balance of land covers replacing forest in northern Thailand. *Agr. Forest. Meteorol.*, 95, 53-65.

Hahmann, A. N. and R. E. Dickinson, 1997: RCCM2/BATS Model over Tropical South America: Applications to Tropical Deforestation, *J. Climate*, 10, 1944-1964.

Henderson-Sellers, A., R. E. Dickinson, T. B. Durbidge, P. J. Kennedy, K. McGuffie, and A. J. Pitman, 1993: Tropical deforestation: Modeling local to regional scale climate change. *J. Geophys. Res.,* 98, 7289–7315.

Hoffmann, W. A., W. Schroeder, and R. Jackson, 2003: Regional feedbacks among fire, climate, and tropical deforestation. *J. Geophys. Res.*, 108, 4721, doi:10.1029/2003JD003494.

Hu, B., W. Lucht, A. Strahler, C. Schaaf, and M. Smith, 2000: Surface albedos and angle-corrected NDVI from AVHRR observations of South America, *Remote Sens. Environ.*, 71,119-132.

Hucek, R. and H. Jacobowitz, 1995: Impact of scene dependence on AVHRR albedo models. *J. Atmos. Ocean. Tech. 12*, 697-711.

Jin, Y., C. B. Schaaf, C. E. Woodcock, F. Gao, X. Li, A. H. Strahler, W. Lucht, and S. Liang, 2003: Consistency of Moderate-Resolution Imaging Spectroradiometer surface bidirectional reflectance distribution function and albedo retrievals, 2, Validation, *J. Geophys. Res.*, 108(D5), 4159, doi:10.1029/2002JD002804.

Justice, C. O., R. E. Wolfe, N. El Saleous, J. Descloitres, E. Vermote, D. Roy, J. Owens, and E. Masuoka, 2000: The availability and status of MODIS land products. The Earth Observer, 12 (6), 10– 18.

Kiehl, J. T., J. J. Hack, G. B. Bonan, B. A. Boville, D. L. Williamson, and P. J. Rasch, 1998: The National Center for Atmospheric Research Community Climate Model: CCM3, *J. Climate*, 11, 1131-1149.

Klein, S. A. and D. L. Hartmann, 1993: Spurious trend in the ISCCP C2 dataset. *Geophys. Res. Lett.,* 20, 455–458.

Kondratyev, K. Y., 1972: *Radiation processes in the atmosphere*, No. 309. Geneva, WMO.

Kucharik, C. J., J. A. Foley, C. Delire, V. A. Fisher, M. T. Coe, S. T. Gower, J. D. Lenters, C. Young-Molling, J. M. Norman, and N. Ramankutty, 2000: Testing the performance of a dynamic global ecosystem model: Water balance, carbon balance end vegetation structure. *Global Biogeochem. Cy.,* 14, 795-825.

Lean, J. and D. A. Warrilow, 1989: Simulation of the regional climatic impact of Amazon deforestation. *Nature*, 342, 411-413.

Lean, J. and P. R. Rowntree, 1997: Understanding the sensitivity of a GCM simulation of Amazonia deforestation to the specification of vegetation and soil characteristics. *J. Climate*, 10, 1216-1235.

Lean, J., Rowntree, P. R., 1993: A GCM simulation of the impact of Amazonian deforestation on climate using an improved canopy representation. *Q. J. Roy. Meteor. Soc.,* 119, 509–530.

Lewis, P., M. I. Disney, M. J. Barnsley, and J. -P. Muller, 1999: Deriving albedo for HAPEX-Sahel from ASAS data using kernel-driven BRDF models, *Hydrol. Earth Syst. Sc.*, 3, 1-13.

Li, Z. and L. Garand, 1994: Estimation of surface albedo from space: A parametrization for global application. *J. Geophys. Res., 99*, 8335-8350.

Lucht, W., A. H. Hyman, A. H. Strahler, M. J. Barnsley, P. Hobson, and J.-P. Muller, 2000a: A comparison of satellite-derived spectral albedos to ground-based broadband albedo measurements modeled to satellite spatial scale for a semi-desert landscape, *Remote Sens. Environ.*, 74, 85-9.

Lucht, W., C. B. Schaaf, and A. H. Strahler, 2000b: An algorithm for the retrieval of albedo from space using semiempirical BRDF models. *IEEE T. Geosci. Remote Sens.*, 38,977– 38,998.

Manzi, O., and S. Planton, 1996: Calibration of a GCM using ABRACOS and ARME data and simulation of Amazonian deforestation. In: Gash, J.H.C., Nobre, C.A., Roberts, J.M., Victoria, R.L. (Eds.), *Amazonian Deforestation and Climate*, 1st ed. John Wiley and Sons, Chichester, 505–530.

McCaughey, J. H., 1987: The albedo of a mature mixed forest and a clear-cut site at Petawawa, Ontario. *Agr. Forest. Meteorol.*, 40, 251-263.

McWilliam, A-L.C., O. M. R. Cabral, B. M. Gomes, J. L. Esteves, and J. M. Roberts, 1996: Forest and pasture leaf-gas exchange in south-west Amazonia. In: Gash, J.H.C., Nobre, C.A., Roberts, J.M., Victoria, R.L. (Eds.), Amazonian Deforestation and Climate, 1st ed. John Wiley and Sons, Chichester, 265-286.

Meador, W. E. and W. R. Weaver, 1980: Two-stream approximations to radiative transfer in planetary atmospheres: a unified description of existing methods and a new improvement. *J. Atmos. Sci.*, 37: 630-643.

Medina, E. and E. Cuevas, 1996: Biomass production in nutrient limited rainforest: implications for responses to global change. In: Gash, J.H.C., Nobre, C.A., Roberts, J.M., Victoria, R.L. (Eds.), *Amazonian Deforestation and Climate*, 1st ed. John Wiley and Sons, Chichester, pp. 221–239.

Negri, A. J., R. F. Adler, L. Xu, and J. Surratt, 2004: The Impact of Amazonian Deforestation on Dry Season Rainfall. *J. Climate*, 17, 1306-1319.

Nobre, C. A., G. Fisch, H. R. Rocha, R. F. Lyra, E. P. Rocha, A. C. L. Costa, and V. N. Ubarana, 1996: Observations of the atmospheric boundary layer in Rondônia, In: Gash, J.H.C., Nobre, C.A., Roberts, J.M., Victoria, R.L. (Eds.), *Amazonian Deforestation and Climate*, 1st ed. John Wiley and Sons, Chichester, pp. 413-424.

Nobre, C., P. Sellers, and J. Shukla, 1991: Amazonian deforestation and regional climate change, *J. Climate*, 4, 957-988.

Norman, J. M. and P.G. Jarvis, 1975: Photosynthesis in Sitka Spruce. V. Radiation penetration theory and a test case. *J. Appl. Ecol.*, 12:839-878.

Nouvellon, Y., A. Bégué, M. S. Moran, D. L. Seen, S. Rambal, D. Luquet, G. Chehbouni, and Y. Inoue, 2000: PAR extinction in shortgrass ecosystems: effects of clumping, sky conditions and soil albedo. *Agr. Forest Meteorol.*, 105, 21-41.

Oguntoyinbo, J. L., 1970: Reflection coefficient of natural crops and urban surfaces in Nigeria. *Q. J. Roy. Meteor. Soc.*, 96, 430-441

Oleson, K.W., G. B. Bonan, C. Schaaf, F. Gao, Y. Jin, and A. Strahler, 2003: Assessment of global climate model land surface using MODIS data, *Geophys. Res. Lett.,* 30, doi:10.1029/2002GL016749.

Oleson, K.W.; Y. Dai, G. B. Bonan, M. Bosilovich, R. Dickinson, P. Dirmeyer, F. Hoffman, P. Houser, S. Levis, G-Y. Niu, P. Thornton, M. Vertenstein, Z.-L. Yang, and

X. Zeng, 2004: T*echnical description of the Community Land Model (CLM)*. NCAR Technical note TN-461+STR, 174p.

Pinker, R. T. and I. Laszlo, 1992: Modeling surface solar irradiance for satellite applications on a global scale, *J. Appl. Meteor.,* 31, 194-211.

Pinker, R. T., O. E. Thompson, and T. F. Eck, 1980: The albedo of a tropical evergreen forest. *Q. J. Roy. Meteor. Soc.*, 106, 551-558.

Pinker, R., 2002: Satellite Estimates of Radiative Fluxes in the Western Hemisphere. College Park, Maryland: The Global Land Cover Facility.

Pinty, B., T., R. E. Lavergne, J.-L Dickinson, N. Widlowski, Gobron, and M. M. Verstraete, 2006: Simplifying the interaction of land surfaces with radiation for relating remote sensing products to climate models, *J. Geophys. Res.*, 111, D02116, doi:10.1029/2005JD005952.

Pollard, D. and S. Thompson, 1995: The effect of doubling stomatal resistance in a global climate model. *Global Planat. Change*, 10: 129-161.

Rao, C.R.N. and J. Chen, 1995: Inter-satellite calibration linkages for the visible and near-infrared channels of the Advanced Very High Resolution Radiometer on the NOAA-7, -9 and –11 spacecraft. *Int. J. Remote Sens., 16*, 1931-1942.

Rao, C. R. N. and J. Chen, 1996: Post-launch calibration of the visible and near-infrared channels of the Advanced Very High Resolution Radiometer on the NOAA-14 spacecraft. *Int. J. Remote Sens.*, 17, 2743-2747.

Roberts, J. M., O. M. R. Cabral, J. P. Costa, A-L.C. McWilliam, and T. D. A. Sá, 1996: An overview of the leaf area index and physiological measurements during ABRACOS. In: Gash, J.H.C., Nobre, C.A., Roberts, J.M., Victoria, R.L. (Eds.), *Amazonian Deforestation and Climate*, 1st ed. John Wiley and Sons, Chichester, UK. pp 287-306.

Roberts, J. M., O. M. R.Cabral, and L. F. Aguiar, 1990: Stomatal and boundary layer conductances measured in a terra firme rain forest. *J. Appl. Ecol.* 27, 336-353.

Ross, J. 1981: *The Radiation Regime and Architecture of Plant Stands*, 391 pp., Springer, New York.

Rossow, W. B. and B. Cairns, 1995: Monitoring changes of clouds. *Climatic Change,* 31, 175–217.

Rossow, W. B., A. Walker, D. Beuschel, and M. Roiter, 1996: International Satellite Cloud Climatology Project (ISCCP) documentation of new cloud datasets. World Climate Research Programme (ICSU and WMO), WMO/TD-737 Geneva, Switzerland, 115 pp. [Available from ISSCP Global Processing Center, NASA GSFC Institute for Space Studies, 2880 Broadway, New York, NY 10025.]

Rossow, W. B., Y. Desormeaux, C. L. Brest, and A. Walker, 1992: International Satellite Cloud Climatology Project (ISCCP) radiance calibration report. World Climate Research Programme (ICSU and WMO), WMO/TD-520 Geneva, Switzerland, 104 pp. [Available from ISSCP Global Processing Center, NASA GSFC Institute for Space Studies, 2880 Broadway, New York, NY 10025.].

Rowe, C. M., 1991: Modeling land-surface albedos from vegetation canopy architecture. *Phys. Geogr.*, 12(2), 93– 114.

SAS, 2001: User's guide (Release 8.2) Statistical Analysis System Institute, Inc., Cary, NC.

Schaaf, C. B., F. Gao, A. H. Strahler, W. Lucht, X. Li, T. Tsang, N. C. Strugnell, X. Zhang, Y. Jin, J. P. Muller, P. Lewis, M. Barnsley, P. Hobson, M. Disney, G. Roberts, M. Dunderdale, C. Doll, R. P. D'entremont, B. Hu, S. Liang, J. L. Privette, and D. Roy, 2002: First operational BRDF, albedo nadir reflectance products from MODIS. *Remote Sens. Environ.*, 83, 135–148.

Sellers, P. J., 1985: Canopy reflectance, photosynthesis and transpiration. *Int. J. Remote Sens.,* 6:1335-1372.

Sellers, P. J., Y. Mintz, Y. Sud, and A. Dalcher, 1986: A simple biosphere model (SiB) for use within general circulation models. *J. Atm. Sci*. 43, 505–531.

Shuttleworth, W.J., J. H. C. Gash, C. R. Lloyd, J. M. Roberts, A. O. Marques, G. Fisch, P. Silva, M. N. G. Ribeiro, L. C. B. Molion, L. D. A. Sá, C. A. Nobre, O. M. R. Cabral, S. R. Patel, and J. C. Moraes, 1984: Observations of radiation exchange above and below Amazonian forest. *Q. J. Roy. Meteor. Soc.*, 110, 1163-1169.

Slingo, J. M., 1987: The development and verification of a cloud prediction scheme for the ECMWF model, *Q. J. R. Meteorol. Soc*., 113, 899–927.

Smith, G. L., Z. P. Szewczyk, D. A. Rutan, and B. L. Robert, 2006: Comparison of measurements from satellite radiation budget instruments *J. Geophys. Res.,* 111, D04101, doi:10.1029/2005JD006307.

Song, J., 1998: Diurnal asymmetry in surface albedo. *Agr. Forest. Meteorol.,* 92, 181-189.

Stackhouse, P. W., S. J. Cox, S. K. Grupta, J. C. Mikovitz, and M. Chiacchio, 2003: The WCRP/GEWEX Surface Radiation Budget Data set: A 1 degree resolution, 12 year flux climatology.

Stackhouse, P. W., S. K. Grupta, S. J. Cox, M. Chiacchio, and J. C. Mikovitz, 2000. The WCRP/GEWEX Surface Radiation Budget Project release 2: An assessment of surface fluxes a 1 degree resolution. In IRS 2000: *Current problems in atmospheric radiation*, W. L. Smith and Y. M. Timofeyev, Eds., *International Radiation Symposium*, St. Petersburg, Russia, July 24-29.

Sud, Y. C., G. K. Walker, J.-H. Kim, G. E. Liston, P. J. Sellers, and W. K.-M. Lau, 1996: Biogeophysical consequences of a tropical deforestation scenario: A GCM simulation study. *J. Climate,* 9, 3225–3247.

Suttles, J. T., R. N. Green, P. Minnis, G. L. Smith, W. F. Staylor, B. A. Wielicki, I. J. Walker, D. F. Young, V. R. Taylor, and L. L. Stowe, 1988: Angular *radiation models for Earth atmosphere system.* Volume I – Shortwave radiation. NASA Reference Publication 1184. 147pp.

Verstraete, M. M., 1987: Radiation transfer in plant canopies: Transmission of direct solar radiation and the role of leaf orientation. *J. Geophys. Res.*, 92:10985-10995.

Voldoire, A. and J. F. Royer, 2004: Tropical deforestation and climate variability. *Clim. Dyn.*, 22, 857-874.

Wei, X., A. N. Hahmann, R. E. Dickinson, Z. L. Yang, X. B. Zeng, K. J. Schaudt, C. B. Schaaf, and N. Strugnell, 2001: Comparison of albedo computed by land surface models and evaluation against remotely sensed data. *J. Geophys. Res.,* 106, 20687-20702.

Werth, D. and R. Avissar, 2002: The local and global effects of Amazon deforestation, *J. Geophys. Res*., 107, doi:10.1029/2001JD000717.

Wielicki, B. A. and R. N. Green, 1989: Cloud identification for ERBE radiative flux retrieval. *J. Appl. Meteorol.*, 28, 1133-1146.

Wright, I. R., C. A. Nobre, J. Tomasella, H. R. Rocha, J. m. Roberts, E. Vertamatti, A. D. Culf, R. C. S. Avalá, and M. G. Hodnett, 1996: Towards a GCM surface parameterization for Amazonia. In: Gash, J.H.C., Nobre, C.A., Roberts, J.M., Victoria, R.L. (Eds.), *Amazonian Deforestation and Climate*, 1st ed. John Wiley and Sons, Chichester, 473-504.

Xue, K., N. Liou, and A. Kasahara, 1990: Investigation of the biogeophysical feedback on the African climate using a two-dimensional model. *J. Climate,* 3, 337–352.

Yanagi, S. N. M. and M. H. Costa, 2006. Modeling radiative transfer in tropical rainforest canopies: Sensitivity of simulated albedo to canopy Architectural and Optical Parameters. Submitted to *Acta Amazonica*.

Zao, M., A. J. Pitman, and T. N. Chase, 2001: The impact of land cover change on the atmospheric circulation. *Clim. Dynam.,* 17, 467-477.

Zeng, N. and J. D. Neelin, 1999: A land-atmosphere interaction theory for the tropical deforestation problem. *J. Climate*, 12, 857-872.

Zeng, N., R. E. Dickinson, and X. Zeng, 1996: Climatic impact of Amazon deforestation—A mechanistic model study. *J. Climate,* 9, 859–883.

Zhang, H., K. McGuffie, and Henderson-Sellers, A., 1996: Impacts of tropical deforestation, part II, The role of large-scale dynamics, *J. Climate*, 9, 2498– 2521.

Zhou, L., R. E. Dickinson, Y. Tian, X. Zeng, Y. Dai, Z. –L. Yang, C. B. Schaaf, F. Gao,; Y. Jin, A. Strahler, R. B. Myneni, H. Yu, W. Wu, and M. Shaikh, 2003: Comparison of seasonal and spatial variations of albedos from Moderate Resolution Imaging Spectroradiometer (MODIS) and Common Land Model. *J. Geophys. Res.,* 108, doi: 10.1029/2002JD003326